Fakultät für Medizin

Pulse-chase imaging of neuronal mitochondria

Barbara Gailer

Vollständiger Abdruck der von der Fakultät für Medizin der Technischen Universität München zur Erlangung des akademischen Grades einer **Doktorin der Medizin (Dr. med.)** genehmigten Dissertation.

Vorsitz: Prof. Dr. Ernst J. Rummeny

Prüfende der Dissertation:

1. Prof. Dr. Thomas Misgeld
2. Prof. Dr. Bernhard Hemmer

Die Dissertation wurde am 31.05.2022 bei der Technischen Universität München eingereicht und durch die promotionsführende Einrichtung Fakultät für Medizin am 13.12.2022 angenommen.

Zusammenfassung

Neuronale Funktionen, wie zum Beispiel die zentrale Aufgabe der Erregungsübertragung, sind sehr energieintensiv. Daher sind Nervenzellen ganz besonders auf mitochondriale ATP-Produktion angewiesen. Jedoch stellt ihre ausgedehnte Zellarchitektur mit langen Axonen und verzweigten Dendriten eine besondere Herausforderung dar: um die gesamte Zelle mit funktionierenden Organellen zu versorgen, müssen Mitochondrien große Distanzen überwinden, da der Großteil an mitochondrialen Proteinen und Organellen vermutlich im Zellkörper produziert wird. Die Aufrechterhaltung eines gesunden mitochondrialen Pools wird durch ein komplexes Zusammenspiel aus axonalem Transport, mitochondrialen Fusionen und Teilungen, sowie Biogenese- und Abbauprozessen ermöglicht. All diese Prozesse sind unverzichtbar für neuronale Integrität. Jedoch ist es noch unklar, wie die Zelle diese Abläufe koordiniert und die Organellen in antero- und retrogradem Transport verteilt.

Das Ziel meiner Doktorarbeit war es, eine neue Methode zu entwickeln, um die Verteilungsmuster von Mitochondrien in Motoneuronen zu erforschen. Dazu wurden photo-aktivierbare Proteine genutzt: diese Moleküle ändern ihre Fluoreszenz durch Photo-aktivierung mit ultraviolettem Licht. Bisher wurde die Anwendbarkeit der Proteine für „in vivo“ Experimente in transgenen Mäusen noch nicht vollständig erforscht.

Daher untersuchte ich transgene Mäuse, die spezifisch in neuronalen Mitochondrien verschiedene photo-aktivierbare Proteine (paGFP, Kaede und Dendra) exprimieren. Im ersten Abschnitt dieser Arbeit charakterisierte ich die fluoreszenten Eigenschaften der Proteine mittels Weitfeld-Mikroskopie eines Nerv-Muskel-Explantats. Meine Ergebnisse zeigten, dass Thy1-mito-paGFP und Thy1-mito-Dendra besser für „live imaging“ geeignet sind, da sie signifikant mehr Kontrast nach Photo-aktivierung produzieren als Thy1-mito-Kaede. Im zweiten Abschnitt der Arbeit nutzte ich die Thy1-mito-Dendra Linie, um sogenannte „pulse-chase“ Experimente in Nerv-Muskel-Explantaten durchzuführen: ich photo-aktivierte Mitochondrien und verfolgte deren Verteilung in Axonen und Synapsen. Mittels dieser Technik konnte ich zeigen, dass Mitochondrien sehr selten innerhalb von Axonen oder nach Eintritt in die Synapse umkehren. Diese Ergebnisse legen nahe, dass kurzfristige Rezirkulation eine untergeordnete Rolle in der Zusammensetzung von retrogradem mitochondrialen Transport spielt.

Summary

Neurons require high levels of energy for synaptic transmission and depend vitally on mitochondrial ATP-production. Yet, their complex geometry with long axons and multi-branched dendrites complicates mitochondrial supply: the majority of organelles is presumably generated in the soma, still all mitochondria require constant rejuvenation irrespective of their distance to the cell body. A complex interplay of axonal transport, fusion and fission as well as biogenesis and degradation processes guarantees the maintenance of healthy mitochondria and is essential for neuronal integrity. However, it is poorly understood, how neurons orchestrate the distribution of organelles and which mechanisms underlie the steady stream of antero- and retrograde mitochondrial transport.

The aim of this thesis was, to investigate the patterns of mitochondrial delivery in motoneurons with a new approach, using photo-transformable fluorescent proteins. These proteins change their fluorescence upon exposure with UV-light and offer a unique labeling tool kit. Yet, their in vivo performance in transgenic mice has not been thoroughly explored. In this work, I characterized transgenic mice with the expression of three different photo-transformable proteins (paGFP, Kaede and Dendra) in mitochondria controlled by neuron-specific Thy1 promotor elements. In a first step I compared their fluorescent characteristics in an acute thoracic nerve-muscle explant. My results revealed, that Thy1-mito-Dendra and Thy1-mito-paGFP are favorable for imaging, because they produce significantly more contrast after photo-activation than Thy1-mito-Kaede.

In the second part of this work I established pulse-chase imaging experiments in motoneurons of nerve-muscle explants, to disambiguate the fate of mitochondria in retrograde transport: I photo-labeled a fraction of organelles using Thy1-mito-Dendra and tracked their distribution in axons and synapses. With this technique I could show that mitochondrial turn-arounds in axons and immediate recirculation at synapses are rare. These results suggest that short-term recirculation does not contribute to the pool of retrogradely moving mitochondria.

Table of Content

1 Introduction

Neurons are highly polarized, asymmetric cells, harboring distinct functional compartments: signals are received in the somatodendritic region and carried as action potentials to the synaptic terminals in long axons (Fig. 1.1). This complex architecture can be easily visualized regarding the structure of human motoneurons: their somata are located in the spinal cord and receive input from central neurons. At the same time their axons transmit action potentials to the neuromuscular junctions of our muscles. Axons targeted to very distant muscles, for example of fingers or toes, can extend up to one meter.

Considering these spatial challenges, the cell faces a logistic problem. Axons and especially synaptic sites with their typically high energy demand have to be supplied with adenosine triphosphate (ATP), which is mostly provided by mitochondrial respiration (Rangaraju et al. 2014). However, the majority of mitochondria is proposed to be generated in the soma of the cell (Sheng and Cai 2012): hence neurons depend on axonal transport, to distribute mitochondria for local energy production (Harris et al. 2012) and "to maintain a healthy pool of organelles throughout their extended architecture" (Schwarz 2013, Misgeld and Schwarz 2017) (Fig. 1.1). In the last years antero- and retrograde mitochondrial movement in neurons has been investigated extensively (Misgeld and Schwarz 2017), still basic questions are not answered. Especially the function of retrograde transport and the orchestration of mitochondrial biogenesis and degradation are poorly understood.

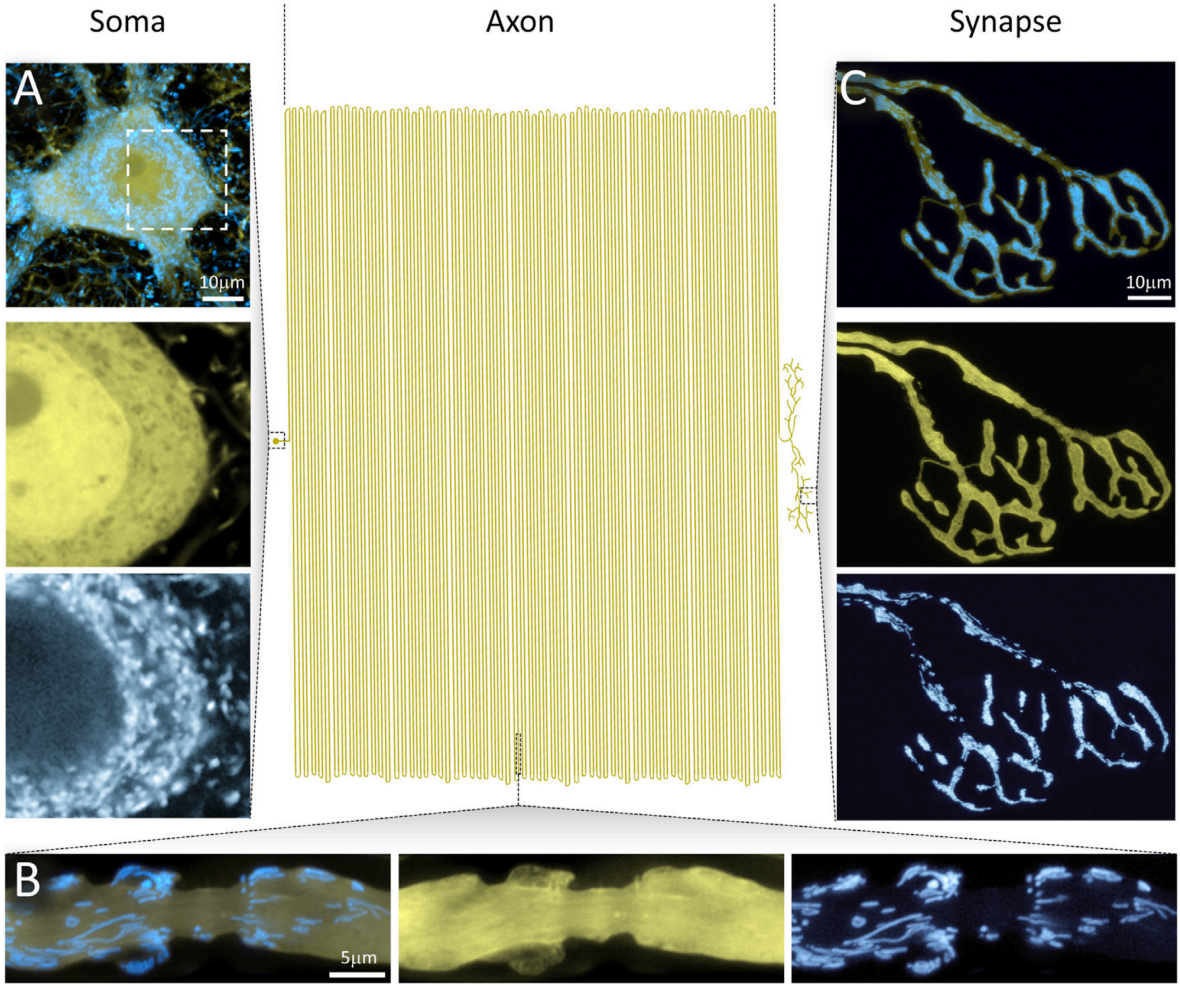

Fig. 1.1 Architecture of a mammalian motoneuron (from Misgeld and Schwarz 2017)

Schematic of a mouse motoneuron. Compared to the extended axonal process, the cell body is quite small. Still it has to supply all compartments, for example paranodes (B) or synapses (C), with organelles.

In this work I intended to study mitochondrial distribution and retrograde transport in motoneurons. To this end I provide transgenic mice with the expression of photo-transformable fluorescent proteins in neuronal mitochondria. These proteins change their spectral characteristics upon exposure to UV-light. With this technique mitochondrial subpopulations and single organelles can be labelled and tracked, to gain more information about mitochondrial delivery.

Below, I will review the state of knowledge of the mitochondrial life-cycle and organelle-trafficking. Then I will provide an overview on mitochondrial imaging and the characteristics of the different photo-transformable proteins used in this study.

1.1 Mitochondrial life-cycle

Mitochondria are essential organelles for the function and integrity of eukaryotic cells. As "powerhouse" of the cell they produce ATP via oxidative phosphorylation. Essential neuronal functions like neurotransmission or the firing of action potentials depend on mitochondrial ATP supply (Attwell and Laughlin 2001, Howarth et al. 2012). Yet mitochondria do not only provide energy but have multiple tasks: they are involved in fatty acid turn-over, regulate Ca^{2+}- signals and play a critical role in apoptosis (Nicholls and Budd 2000, Nunnari and Suomalainen 2012).

The complex mitochondrial biology makes it even more difficult to study and understand organelle transport in elaborated neurons. Mitochondria cannot be considered as individual autonomous organelles that are transported along microtubules. Extensive reticular mitochondria and single axonal organelles are present in neurons (Popov et al. 2005) and interact in a dynamic network. The organelles grow, move, exchange material by fusion and fission and undergo degradation (Plucińska and Misgeld 2016) (Fig. 1.2). These processes will be detailed below.

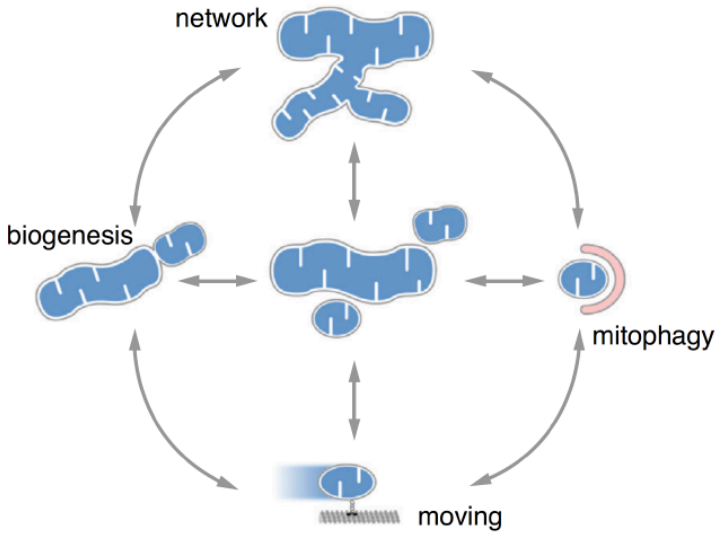

Fig. 1.2 Schematic of the mitochondrial life-cycle (modified from Plucinska and Misgeld, 2016)

Mitochondria form a network and undergo dynamic processes: biogenesis – transport - fusion/ fission – degradation. It is still unclear, where in neurons the single steps of the life-cycle take place.

Obviously, this dynamic life cycle is closely coupled to the organelles' axonal transport und distribution: mitochondrial homeostasis requires orchestrated transport between the locations of biogenesis, function and degradation.

1.1.1 Biogenesis

Mitochondrial biogenesis derives from growth and division of preexisting organelles, a “de novo synthesis” of mitochondria is not possible. The total mitochondrial proteome of 1500-2000 proteins (Pagliarini et al. 2008) is encoded both by nuclear and mitochondrial DNA (mtDNA). The 37 genes of the circular mtDNA are translated on the mitochondrial ribosome (Clayton 2003), whereas 99% of the mitochondrial proteins are encoded by nuclear genes and translated on cytosolic ribosomes (Fig. 1.3). Import machineries of the outer and inner membrane (TOM and TIM) facilitate post-translational import of the proteins into the organelle (Chacinska et al. 2009, Harbauer et al. 2014).

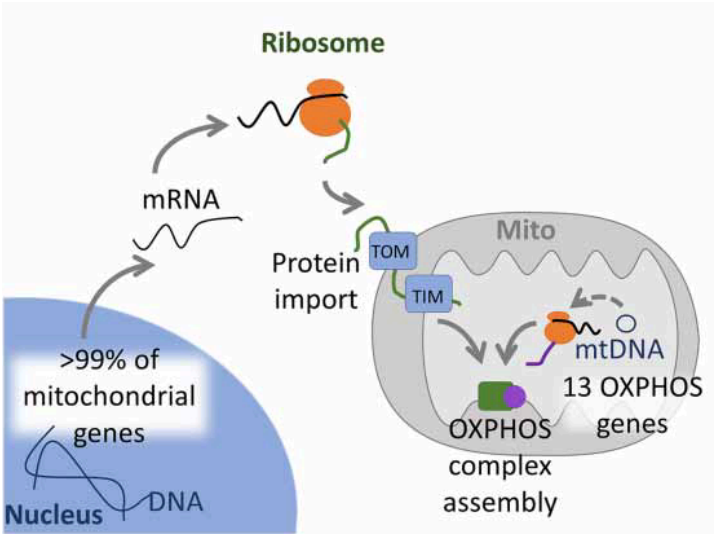

Fig. 1.3 Biogenesis of mitochondrial proteins (modified from Harbauer 2017)

Two protein synthesis machineries facilitate the expression of proteins of two genomes: proteins encoded in nuclear genes are translated on cytosolic ribosomes and transported into the organelle via TIM and TOM, whereas mitochondrial genes are transcribed and translated inside the organelle.

Although the steps of mitochondrial protein synthesis have been studied and characterized with great detail, it is not entirely clear where in the neuron this complex bigenomic biogenesis takes place. With 99 % of the mitochondrial proteins being encoded by nuclear DNA and translated on cytosolic ribosomes, the major part of mitochondrial biogenesis is supposed to take place in the soma of the neuron. Findings in cell culture which localize the main part of mtDNA replication in the perinuclear region support this assumption (Davis and Clayton 1996). Still, there is evidence for local axonal biogenesis of mitochondria: several studies have revealed local protein production in the axon (Koenig and Giuditta 1999), the existence of transcripts for nuclear-encoded mitochondrial proteins (Gioio et al. 2001, Aschrafi et al. 2016, Shigeoka et al. 2016) as well as mtDNA replication and mitochondrial fission within axons (Amiri and Hollenbeck 2008). A recent study showed, that axonal mitochondria can serve as “translational hotspots”: RNA granules trafficked on late endosome often pause on

mitochondria for local protein synthesis. Specifically Rab7a endosomes have been found to translate mRNAs encoding proteins for mitochondrial function and axonal viability (Cioni et al. 2019).

All in all the organelle supply of the long axoned peripheral neurons is complex: the cell has to coordinate biogenesis at the soma, transport to peripheral sites and homeostatic maintenance of all compartments. Local biogenesis could enable the neuron to respond quickly to organelle damage or increased demand of mitochondrial function and rejuvenate the pool of axonal mitochondria (Schwarz 2013, Misgeld and Schwarz 2017).

1.1.2 Fusion and Fission

Fusion and fission events are an important factor for mitochondrial homeostasis: these processes enable mitochondria to exchange material between the individual organelles (Schwarz 2013).

By fusion two mitochondrial segments are joined to a larger mitochondrion, and both membrane molecules and mitochondrial matrix are mixed (Busch et al. 2006). Key players in the process are GTPases of the dynamin related protein family: Mitofusin 1 and 2 (Chen et al. 2003, Koshiba et al. 2004), both located in the outer mitochondrial membrane, as well as OPA1 (Cipolat et al. 2004, Chen et al. 2005), associated with the inner mitochondrial membrane. Both complete and transient “kiss and run” fusions, where the mitochondria exchange material but keep their original form, were observed (Liu et al. 2009). Fusion facilitates the distribution of proteins or mtDNA among mitochondria and improves the coupling of mitochondrial respiration (Chen et al. 2005). The process has been shown to protect mitochondria during starvation (Rambold et al. 2011) and under stress-conditions (Tondera et al. 2009).

The opposite process, fission, is the separation of a daughter organelle from a mitochondrion or the mitochondrial reticulum. The GTPase Drp1 (Dynamin related protein) is a core component of the molecular machinery (Smirnova et al. 2001). During fission the enzyme locates to the mitochondrial membrane and facilitates scission via GTP hydrolysis (Praefcke and McMahon 2004). Fission is crucial to maintain a healthy mitochondrial population: studies have shown that the process enables both mitochondrial biogenesis and the isolation of dysfunctional mitochondria for autophagy (Twig et al. 2008, Burman et al. 2017, Kleele et al. 2021). In a recent publication Kleele et al. have characterized two different subgroups of fission, depending on the location of the fission event within the organelle: in cell culture “peripheral fission” isolates damaged mitochondrial components for mitophagy, whereas “midzone fission” promotes mitochondrial growth (Kleele et al. 2021).

The scission of smaller organelles is particularly important for the energy supply of complex neuronal cells: mutations in DRP1 in Drosophila result in a decrease of mitochondrial density at the pre-synaptic terminals as well as an impairment of neurotransmission during intense stimulation (Verstreken et al. 2005).

1.1.3 Degradation

Mitochondria are vulnerable to protein misfolding and DNA damages, because the organelles are exposed to high levels of reactive oxygen species (ROS), by-products of their energy production. Thus, the organelles depend on effective quality control and need to be degraded. The location of mitochondrial clearance is particularly important for our understanding of retrograde mitochondrial transport and delivery (see 1.2.3). It has been presumed, that mitochondria return to the soma for degradation, as the majority of lysosomes are located there. Yet findings in recent studies indicate that local clearance is likely to contribute to mitochondrial turnover (Misgeld and Schwarz 2017).

Several degradation pathways detailed below, both organelle and non-organelle specific, have been identified (Fig. 1.4).

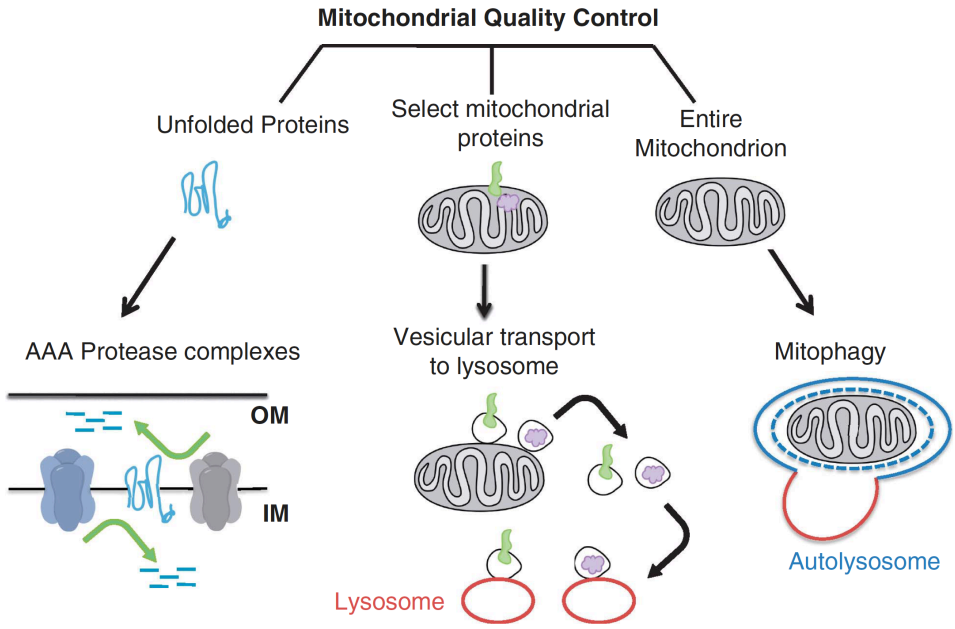

Fig. 1.4 Organelle-selective pathways of mitochondrial quality control (from Ashrafi and Schwarz 2013)

Damaged mitochondrial components can be degraded in different processes: single proteins can be removed by the AAA Protease complexes, and cargoes can be budded of as vesicles and targeted to lysosomes or peroxisomes. Whole or fragmented mitochondria are sequestered by an autophagic membrane and degraded by fusion to a lysosome.

Mitochondrial proteins can be removed individually: two AAA protease complexes in the inner mitochondrial membrane facilitate degradation of single misfolded proteins (Langer et al. 2001). This pathway is significant for proper mitochondrial quality control in neurons. A number of neurological disorders, like forms of hereditary spastic paraplegia (SPG7) or spinocerebellar ataxia (AFG3L2) are linked to mutations in the mitochondrial proteases (Levytskyy et al. 2016). The removal of individual proteins is probably active in all mitochondria irrespective of the localization (Misgeld and Schwarz 2017).

In a second degradation pathway mitochondria bud off mitochondria derived vesicles. Studies in cell culture found many subpopulations: the particles contain proportions of lipids and proteins and are delivered to peroxisomes (Neuspiel et al. 2008) or lysosomes (Soubannier et al. 2012). The vesicles can presumably be shed by mitochondria anywhere in the neuron, still further studies have to investigate the location of this degradation pathway.

The third pathway, mitophagy, an organelle selective form of autophagy, has been studied in detail during the last years. Two central proteins, PINK1 (Greene et al. 2003) and Parkin (Park et al. 2006) have been identified, and mutations of the correspondent genes have been found in hereditary forms of Parkinson's disease (Kitada et al. 1998, Valente et al. 2004). The mitochondrial kinase PINK1 has been characterized as a sensor for mitochondrial health. In damaged organelles the constant degradation of the protein is impaired and PINK1 is stabilized on the outer membrane (Jin et al. 2010, Narendra et al. 2010). In a complex cascade, including the recruitment of Parkin (Narendra et al. 2008, Matsuda et al. 2010) and the phosphorylation and ubiquitination of various proteins, the organelle is marked for autophagy. The organelle is engulfed by an autophagic membrane, the resulting autophagosome is trafficked along microtubules and fuses to a lysosome for degradation (Ashrafi and Schwarz 2013, Nguyen et al. 2016, Menzies et al. 2017). Lysosomes are abundant in the soma, yet local recruitment of Parkin to damaged organelles and the presence of lysosomes in axons suggest, that mitophagy can occur locally as well (Ashrafi et al. 2014, Maday and Holzbaur 2014).

In addition to these organelle-specific pathways, mitochondria can also be degraded via non-selective macroautophagy (Kissová et al. 2007, Evans and Holzbaur 2020): in this process portions of cytoplasm are engulfed by autophagosomes and sequestered by fusion to lysosomes. Bulk autophagy has been found to be particular important in response to starvation (Kuma et al. 2004) and development (Levine and Klionsky 2004), but there is also a relevant basal rate of turnover in quiescent cells (Komatsu et al. 2005, Hara et al. 2006). Macroautophagy was found to be more frequent in axon tips than in the soma or along the axon. The maturation into autophago-lysosomes occurs during retrograde translocation (Maday and Holzbaur 2014).

The findings suggest, that all these pathways play a part in mitochondrial turnover. Yet, we do not know to which extent the respective degradation mechanism contributes in intact neurons. Local clearance is probably an important component of mitochondrial quality control. The location could depend both on the respective pathway and the circumstances driving degradation. All these multilayer processes take an active part in maintaining mitostasis and have an impact on the organelles' transport rates.

1.2 Axonal transport of mitochondria

Axonal transport plays a central role in the extraordinary neuronal morphology providing a healthy pool of organelles and continuous ATP supply. Although the characteristics and molecular machinery of mitochondrial movement have been extensively studied, the mechanisms governing the distribution of "new" and "aged" mitochondrial material in antero- and retrograde transport have not been identified yet.

The majority of mitochondria are stationary in the soma and along the axon, whilst only a fraction (10-40%, variable in different studies) are moving in axons and dendrites (Pilling et al. 2006, Misgeld et al. 2007, Plucińska et al. 2012, Magrané et al. 2014). The organelles are transported bi-directionally and maintain the primary moving direction, complete reversals have rarely been observed (Morris and Hollenbeck 1993, Pilling et al. 2006, Misgeld et al. 2007). Strikingly, there is an obvious excess of anterograde mitochondria : approximately two third are moving in anterograde and one third moving in retrograde direction (Misgeld et al. 2007, Misgeld and Schwarz 2017). This discrepancy will be discussed in 4.2.1. The characteristic mitochondrial movement patterns are alternating phases of continuous "runs" and "pauses", and the resulting average velocity was detected quite variably between 0,25-1 µm/s in different studies (Misgeld and Schwarz 2017).

1.2.1 Mitochondrial transport machinery

Axonal transport is an active, bi-directional (antero- versus retrograde), ATP consuming process (Vale et al. 1985*a*). It requires a complex machinery of motor proteins, cytoskeletal tracks and adaptor proteins. This section provides a short overview of the mitochondrial transport machinery. The elaborate composition of motorproteins and various adaptor-, and docking proteins has been extensively reviewed (Sheng and Cai 2012, Maday et al. 2014).

Long-range movements

Long-distance movements are the predominant form of mitochondrial transport and have been studied in detail: members of the kinesin and dynein motorprotein family drive mitochondrial transport on microtubules (Vale et al. 1985*a*, Schnapp et al. 1986) (Fig. 1.5).

Microtubules: Microtubules are dynamic, cytoskeletal polymers and serve as tracks for long-distance mitochondrial transport (Grafstein and Forman 1980, Schnapp et al. 1986, Hollenbeck 1996). Polymers of α-β-tubulin-dimers form a polarized tube: the dynamic plus end can grow and shrink, while the minus end is stable (Desai and Mitchison 1997, Nogales 2000, Conde and Cáceres 2009). The arrangement of microtubules is important for the establishment of direction-specific transport. Axonal microtubules are uniformly parallel arranged with 95% percent of the plus-ends oriented towards the synapse, while in dendrites microtubules are shorter and grouped in arrays with mixed polarity (Burton and Paige 1981, Baas et al. 1988, Stepanova et al. 2003, Kleele et al. 2014).

Kinesin: Members of the Kinesin motorprotein family drive anterograde, plus-end directed axonal transport, providing energy via ATP hydrolysis (Vale et al. 1985*b*, *a*, Hirokawa et al. 1991). For anterograde mitochondrial transport the Kinesin-1-family (KIF5) has been identified as key motor (Hurd and Saxton 1996, Tanaka et al. 1998, Pilling et al. 2006). The KIF5 motors consists of a dimer of Kinesin heavy chains (KHC): the ATPase is located at the N-terminus, and cargoes bind at the C-terminal tail directly or via adaptor molecules (Hirokawa et al. 1989). An accessory dimer of Kinesin light chains (KLC) is often part of the complex (Hirokawa et al. 1989) and can influence the motility of the motor domain (Glater et al. 2006, Sun et al. 2011).

Dynein: Cytoplasmic Dynein 1 (abbreviated as “dynein”) is the primary motor for retrograde axonal transport (Schnapp and Reese 1989), and studies in Drosophila have confirmed specifically its role as key motor for retrograde mitochondrial movement (Pilling et al. 2006). The motordomain contains a dimer of two Dynein heavy chains with each 6 AAA+ ATPases. Additional dynein intermediate, light intermediate and light chains assemble and form a binding site for cargoes and regulatory proteins (Vallee et al. 2004).

The dynein activator, dynactin (Gill et al. 1991), is a multi-protein complex and essential for dynein function and retrograde transport (LaMonte et al. 2002, Moughamian and Holzbaur 2012*a*). By binding to dynein intermediate chains (Karki and Holzbaur 1995) and microtubules (Waterman-Storer et al.

1995, Culver-Hanlon et al. 2006), Dynactin enhances the processivity of the dynein/dynactin complex (King and Schroer 2000).

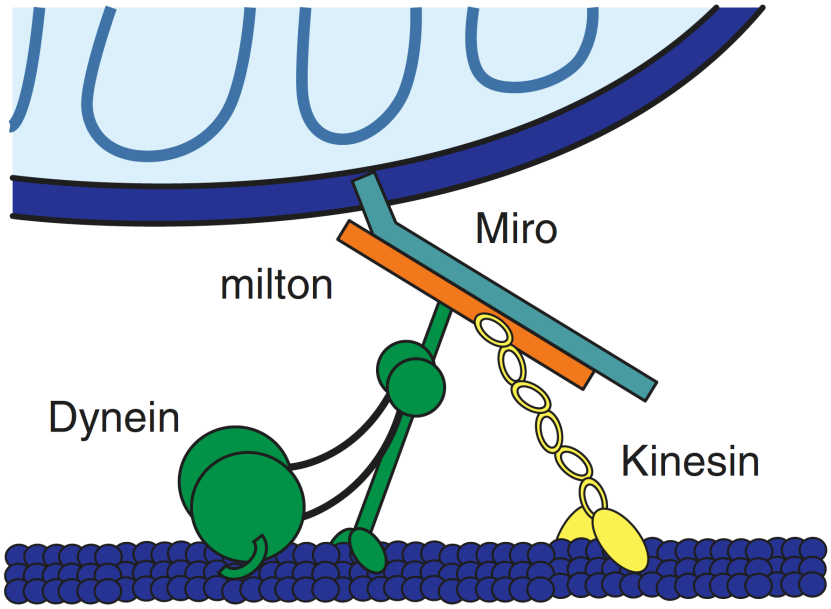

Fig. 1.5 The motor/adaptor complex of mitochondria (from Schwarz 2013)

Motor adaptors: In the last years several adaptor proteins were identified, amongst them the Milton/Miro complex: motorproteins (both KIF5 and Dynein) attach to mitochondria by assembling with the adaptor protein Trak1/2 (Milton in Drosophila) and the mitochondrial receptor Miro (Stowers et al. 2002, Guo et al. 2005, Fransson et al. 2006, Glater et al. 2006, van Spronsen et al. 2013) (Fig. 1.5). Studies confirm the significance of the Milton/Miro complex for mitochondrial transport: both depletion of Milton and Miro result in impaired bidirectional transport (Guo et al. 2005, Russo et al. 2009, Brickley and Stephenson 2011). Miro is critical not only for the movement of mitochondria itself but also for transport regulation – see 1.2.2.

Short range movements

Mitochondria can also be transported on actin-filaments: the role of these short-range movements, driven by Myosin-motors is less understood (Morris and Hollenbeck 1995, Bridgman 2004). Actin filaments are required for mitochondrial anchoring (Chada and Hollenbeck 2004, Gutnick et al. 2019) and short-distance movements are involved in mitochondrial positioning: studies in melanosomes and Drosophila showed that Myosin disrupts protracted microtubule-based transport and tethers the organelles to actin filaments (Gross et al. 2002, Pathak et al. 2010). Recent studies

showed that Miro is critical for actin-based transport as well: in fibroblasts Miro recruits Myosin XIX to mitochondria for coupling the organelles to the actin cytoskeleton (López-Doménech et al. 2018). Yet the role of Myosin XIX in neurons is not fully understood and the interaction between Myosins and the Miro/Trak complex need further investigation.

1.2.2 Regulation of mitochondrial transport

Among various regulatory mechanisms the mitochondrial membrane receptor Miro has been identified as a central element in mitochondrial delivery. The protein is crucial for the Ca^{2+}-dependent positioning of organelles and coordinates organelle dynamics during mitophagy (Schwarz 2013).

Intracellular Ca^{2+}/ synaptic activity

Elevated levels of Ca^{2+} arise from physiological stimuli like action potentials or the activation of glutamate receptors (Rintoul et al. 2003, Yi et al. 2004) and are typically found at sites of high energy demand. Thus the cell has to recruit mitochondria to provide Ca^{2+}-buffering and ATP-production: the mitochondrial membrane receptor Miro is a RhoGTPase with 2 Ca^{2+}-EF hands (Fransson et al. 2006) and arrests mitochondrial trafficking dependent on cytosolic Ca^{2+}-levels (Saotome et al. 2008, MacAskill et al. 2009, Wang and Schwarz 2009). Syntaphilin, an axonal docking protein (Kang et al. 2008), was identified as important component in Ca^{2+}-dependent positioning of mitochondria. The protein competes with Trak2 for binding KIF5, inhibits its motor activity and anchors mitochondria to microtubules. Miro-Ca^{2+} sensing favors the Syntaphilin-KIF5 binding and disruption of the motor-adaptor complex (Chen and Sheng 2013).

Mitochondrial damage

Mitophagy and mitochondrial dynamics are interconnected: by activation of the PINK/Parkin-pathway both Miro (Wang et al. 2011) and Mitofusins (Poole et al. 2010) are degraded. The resulting arrest of transport and fusion could be an early step of quarantine for damaged organelles and produce a population of stationary damaged mitochondria (Schwarz 2013). Yet an overall arrest of damaged organelles during transport would be inconsistent with the main location of degradation organelles in the soma. Does the severity of the mitochondrial damage decide, whether the organelles are arrested and how they are degraded? These findings show, that the complexity of mitochondrial trafficking is still poorly understood.

1.2.3 Mitochondrial delivery in neurons

The basic principles governing mitochondrial distribution are not identified yet. Still, substantial progress has been made in understanding the impact of anterograde transport: the delivery of healthy mitochondria from the cell body to axon terminals is essential for axonal outgrowth and regeneration (Morris and Hollenbeck 1993, Spillane et al. 2013, Han et al. 2016). In comparison, the function of retrograde transport is less understood and many questions are not answered: are antero- and retrograde populations physiologically and functionally distinct? Which mitochondria return back to the soma?

Different models have evolved to explain mitochondrial delivery and the "fate" of retrograde mitochondria. A common presumption is that aged and damaged mitochondria are transported back to the soma for degradation: some studies, treating mitochondria with drugs that disrupt mitochondrial physiology, detected increased retrograde transport and mitophagy in the soma (Miller and Sheetz 2004, Cai et al. 2012, Lin et al. 2017). In addition, analyses of mitochondrial movement in cultured neurons treated with a matrix potential indicator showed that lower mitochondrial potentials correlate with retrograde movement (Miller and Sheetz 2004, Lin et al. 2017). However, other studies did not detect a connection of membrane potential to transported populations (Verburg and Hollenbeck 2008, Suzuki et al. 2018). A recent in vivo study in zebrafish found, that organelles in retrograde transport are not degraded but redistributed throughout the cell (Mandal et al. 2021). Hence to date there is no direct evidence for the return of mitochondria to the soma for clearance or repair.

But why else would the cell transport organelles in the retrograde direction? A study of synaptic vesicle distribution in neurons with serially arranged "en passant" boutons proposed a different model for cargo-delivery (Wong et al. 2012): the authors showed, that dense core vesicles (DCV) circulate in the neuron and are captured sporadically by the synaptic boutons (Fig. 1.6). This "conveyor belt model" is analogous to the model of a running sushi restaurant (Moughamian and Holzbaur 2012*b*): continuous circulation and occasional capture allow an even distribution of the synaptic components/ sushi plates.

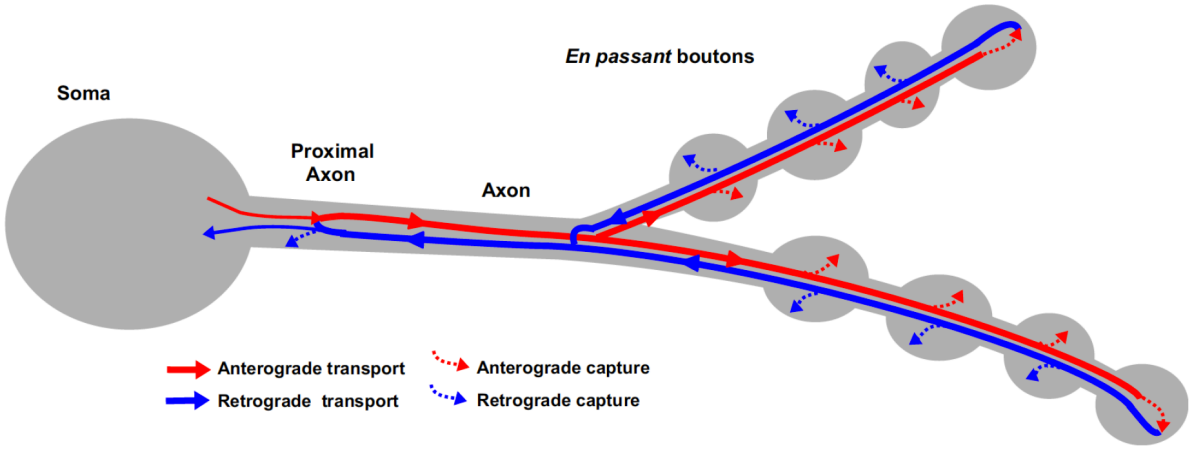

Fig. 1.6 Conveyor-belt model of neuropeptide delivery (modified from Wong et al. 2012)

Anterograde vesicles typically bypass the proximal boutons and accumulate at the most distal bouton. Excess vesicles are then transported retrograde and reverse again for anterograde transport instead of reentering the soma. During circulation DCVs are captured at a low probability at the synaptic boutons.

Hence, we have to consider at least three different, maybe coexisting possibilities for the fate of mitochondria in retrograde transport. First, aged or damaged mitochondria could return in retrograde direction towards the soma for degradation. Second, mitochondria could be transported retrogradely for redistribution, presumably after replenishment by fusion or protein import. Third, organelles could frequently recirculate and only sporadically enter synapses. This third possibility, the “conveyor-belt delivery”, has not been tested for mitochondrial distribution at all. Transgenic mice with a mitochondrial expression of photo-transformable proteins (see 1.3) promise to be useful tools to test this model, monitor mitochondrial movements for recirculation and disambiguate the fate of retrograde organelles.

1.3 Imaging neuronal mitochondria

The extended neuronal architecture and the complexity of the mitochondrial network make it difficult to observe and decipher organelle trafficking: this task has challenged researchers since the 1950s (Weiss and Hiscoe 1948, Droz and Leblond 1962, Miani 1963). In these last years a wide range of tools and techniques has evolved to visualize axonal transport (Fig. 1.7) (Surana et al. 2020).

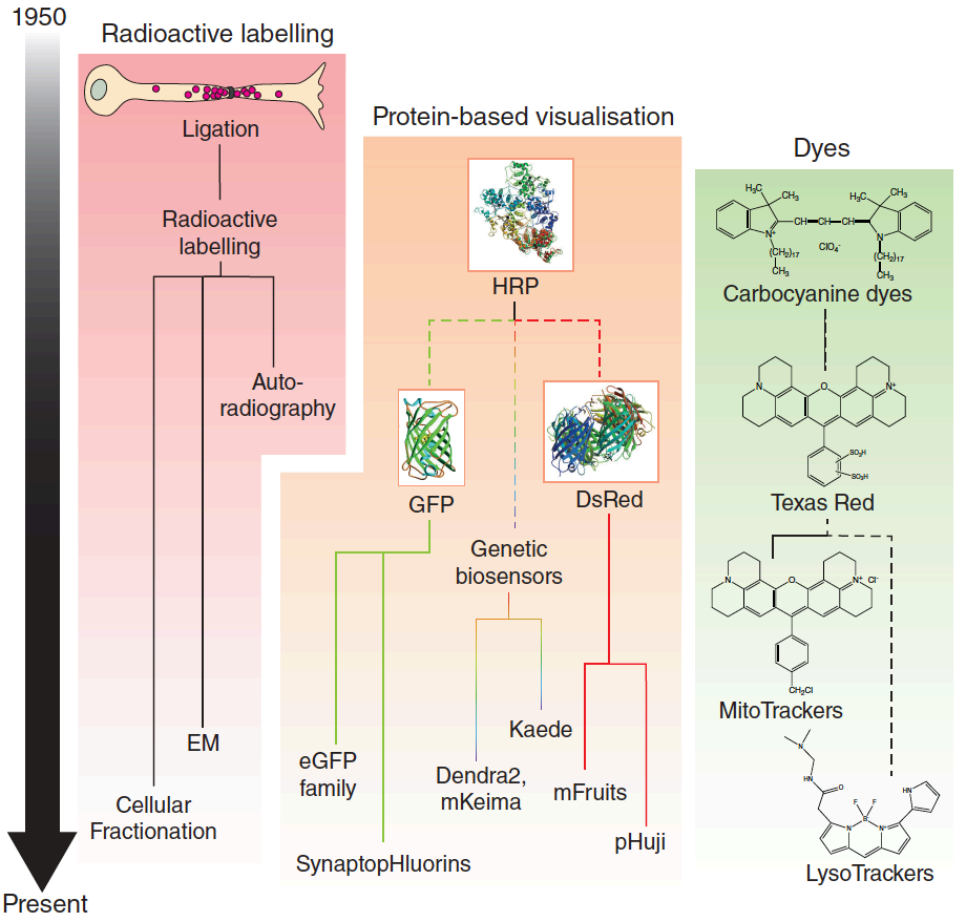

Fig. 1.7 Evolution of the axonal transport toolkit (modified from Surana et al. 2020)

In early studies radioactive precursors were used to label biomolecules (red box). HRP (horse radish peroxidase), an early protein based tool was superseded by the broad range of fluorescent proteins (e.g. eGFP and mFruits family). Functional sensors (pH-sensors: SynaptoHluorins, pHuji) and photo-transformable proteins (Dendra2, mKeima, Kaede) have become available (orange box). In addition a variety of molecular dyes, including the organelle specific Mitotrackers has been engineered (green box).

Already studies in the 1960s used the pulse chase approach to study the transport of proteins or phospholipids (Miani 1963, Ochs et al. 1969): after injection of a radiolabeled precursor transport rates were quantified by detecting the newly synthesized molecules in different segments of the axons (Fig. 1.7, red box). In early experiments single organelles were visualized in invertebrate neurons by using the Nomarski differential interference contrast microscopy (Cooper and Smith 1974). In further studies in cell culture specific dyes, accumulating in mitochondria based on their membrane potential (MitoTrackers, Fig. 1.7 green box) were established for organelle labelling (Morris and Hollenbeck 1995, Miller and Sheetz 2004).

Yet the discovery and engineering of the fluorescent proteins GFP (Shimomura et al. 1962, Chalfie et al. 1994, Zhang et al. 2002) and DsRed (Gross et al. 2002) have facilitated the rapid advancement in the studies of axonal and mitochondrial transport: fluorescent proteins were specifically targeted to neuronal mitochondria and expressed in transgenic animals. This enabled scientists to study mitochondrial dynamics in vivo amongst others in Drosophila (Pilling et al. 2006), mice (Misgeld et al. 2007) and zebrafish (Plucińska et al. 2012). Since then a variety of fluorescent proteins has been published, covering the spectrum from the ultraviolet to the far red regions (Fig. 1.7, orange box) (Day and Davidson 2009). In addition several fluorescent sensors, including pH indicators (Miesenböck et al. 1998), ROS – (Dooley et al. 2004, Hanson et al. 2004) and Ca^{2+}-sensors (Allen et al. 1999, Palmer et al. 2006), were generated and opened up the possibilities of functional imaging.

Another family of specialized fluorescent probes emerged in the last years: photo-transformable proteins switch their spectral properties upon exposure with light of a specific wavelength (Patterson and Lippincott-Schwartz 2002) and promise to be useful tools in the studies of mitochondrial delivery. Considering the constant antero- and retrograde transport, a stable fluorescent labelling of the complete mitochondrial population makes it difficult to observe a subgroup of mitochondria or screen the organelles for recirculation. In contrast, transgenic mice with an expression of photo-transformable proteins in neuronal mitochondrial (Magrané et al. 2012, Marinkovic et al. 2012, Pham et al. 2012, Bolea et al. 2014) facilitate the design of pulse chase studies: by photo-transformation of the respective proteins single mitochondria or specific subpopulations can be labelled (pulse) and tracked (chase).

1.4 Photo-transformable proteins for pulse-chase imaging

Photo-transformable proteins can be classified in two different categories: photo-convertible proteins switch their fluorescent color, for example from green to red fluorescence. In contrast photo-activatable proteins exhibit a non-fluorescent native state, which is activated for example to green fluorescence. In this work, the general term photo-transformation is used for all these proteins, whereas photo-conversion or photo-activation will only be used for the characteristics outlined above. Three photo-transformable proteins were expressed in murine neuronal mitochondria to study mitochondrial trafficking in motoneurons. The proteins' different properties promised to facilitate the design of multifaceted transport experiments. This section provides an overview of their fluorescent characteristics.

1.4.1 Photo-activatable GFP (paGFP)

PaGFP is a variant of the green fluorescent protein (wild-type GFP) from Aequoria victoria (Patterson and Lippincott-Schwartz 2002). The fluorescence (excitation 488 nm) of GFP can be slightly (2.6-fold) enhanced by UV-exposure due to a shift in the absorbance peaks. PaGFP was generated as an optimized photoactivatable version: in the native state of paGFP only little fluorescence can be detected upon exposure with 488 nm light. After photo-activation (413 nm light) fluorescence increased > 60-fold in cell culture (Patterson and Lippincott-Schwartz 2002). Due to its "dark" ground state imaging paGFP requires an additional permanent organelle labelling: in this study the expression of the monomeric red fluorescent protein tagRFP (Merzlyak et al. 2007) was used to visualize mitochondrial background.

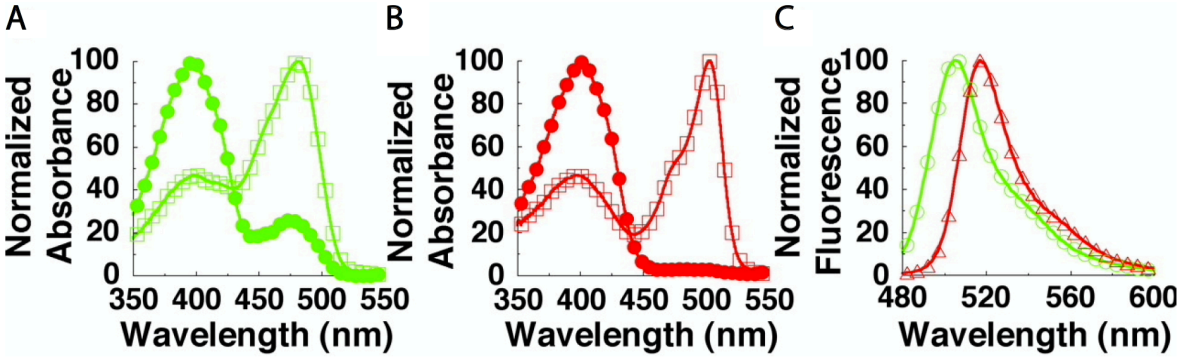

Fig. 1.8 Absorbance and emission spectra of EGFP and paGFP (modified from Patterson and Lippincott-Schwartz, 2002)

A: native (circles) and photo-activated (squares) absorbance spectra of EGFP. B: native (circles) and photo-activated (squares) absorbance spectra of paGFP. C: Emission spectra under excitation at 475nm of photo-activated EGFP (green) and paGFP (red).

1.4.2 Kaede

Kaede is a fluorescent protein from a coral, Trachyphyllia geoffroyi: the tetrameric protein emits green fluorescence in the native state, but is converted to red fluorescence by exposure to UV or violet light (350-400nm) (Ando et al. 2002). Experiments in cell culture revealed an up to 2000-fold increase in fluorescence contrast after photo-conversion. The photo-switch is irreversible and cannot be induced by the excitation wavelengths for imaging the native (480nm) and photo-converted fluorescence (540nm) (Fig. 1.9) (Ando et al. 2002).

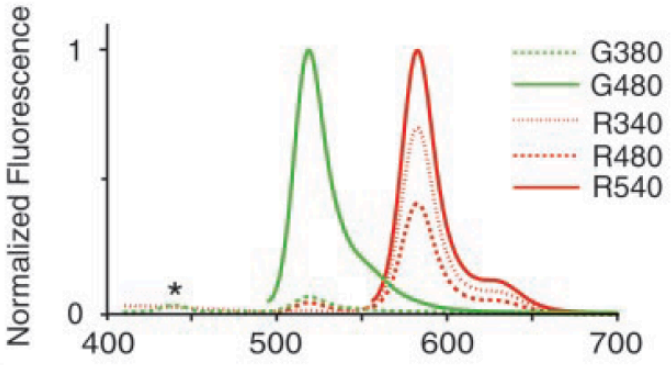

Fig. 1.9 Emission spectra of the native (green) and photo-converted (red) state of Kaede (modified from Ando et al. 2002)

*G380, G480 (green): emission spectra of the native state at excitation at 380 and 480nm. R340, R480, R540 (red): emission spectra of the photo-converted state at the respective wavelengths. * marks a small peak in G380 at 440nm caused by water raman.*

1.4.3 Dendra

Dendra, a monomeric variant of the fluorescent protein dendGFP from the octocoral Dendronephtypha sp. is another green-to-red photo-convertible protein (Fig. 1.10). In cell culture an up to 4500-fold photo-conversion contrast between the native and activated state can be achieved by photo-switch (Gurskaya et al. 2006). Photo-conversion is irreversible.

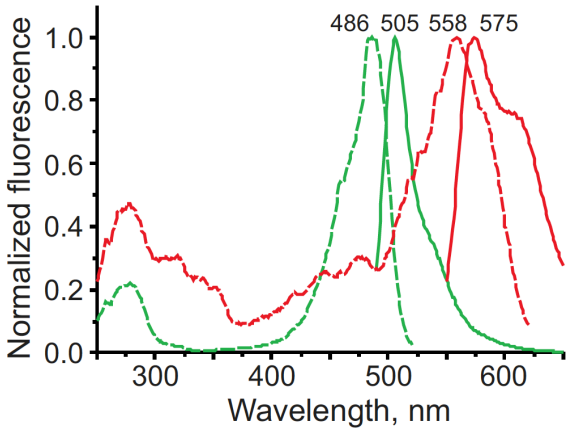

Fig. 1.10 Excitation and emission spectra of the native (green) and photo-converted (red) state of Dendra (modified from Gurskaya et al., 2006)

Excitation spectra are indicated by dashed lines, emission spectra are indicated by solid lines.

Unlike Kaede, Dendra can be photo-converted both by UV-violet (405nm) and blue light (450-490nm). Exposure to low intensity blue light, e.g. during imaging, did not provoke photo-conversion (Gurskaya et al. 2006). As UV-light can be phototoxic to biological systems, photo-switch with blue light could reduce the risk of phototoxicity.

2 Experimental Aims

The aim of this work was to decipher the fate and origin of anterogradely and retrogradely moving mitochondria in mouse motor axons using an optical pulse-chase approach. Particularly I wanted to accomplish the following tasks:

1) Characterization of mouse lines with Thy1-driven expression of different photo-transformable proteins in mitochondria.

2) Determination of the properties of photo-transformation and imaging of the different transgenic lines in the thoracic nerve-muscle explant.

3) Establishment of pulse-chase experiments in the nerve-muscle explant to monitor the movements of single organelles or cohorts of mitochondria. A focus was set on the relationship between antero- and retrograde transport and the question, whether mitochondria circulate in motoneurons and only sporadically enter synapses.

3 Materials and Methods

3.1 Animals

All animal experiments were performed in accordance with the regulation by the local authorities (Government of Upper Bavaria). All experiments were performed on adult mice (> 6 weeks), and mice from both sexes were included into the study.

Transgenic mice expressing the mitochondrial targeting sequence (mito-tag; subunit VIII of the human cytochrome c oxidase) (Caroni 1997, Feng et al. 2000, Misgeld et al. 2007) fused to the respective fluorescent protein at the C-terminus (mito-XFP) under control of the Thy1 promotor were generated by standard pronuclear injections (Thy1-mito-XFP, see Table 2) (Marinković et al. 2015*a*). The novel mouse lines Thy1-mito-paGFP and Thy1-mito-tagRFP were generated for this study, the other mouse lines were provided by collaboration partners. Mouse lines were used for experiments as listed in Table 1 . For details on references and generation as well as screening, see Table 2.

Experiment	**Mouse lines**
Screening	Thy1-mito-paGFP founders Thy1-mito-tagRFP founders Thy1-mito-Kaede Thy1-mitoDendra 3, 4
Creation of dose-response graphs ex vivo	Thy1-mito-paGFP N877 x Thy1-mito-tagRFP H Thy1-mito-Kaede Thy1-mito-Dendra 4
Pulse chase imaging ex vivo	Thy1-mito-Dendra 3
Transport control measurements ex vivo	Thy1-mito-CFP C

Table 1 Mouse lines and experiments in this study

Line	References	Generated by	Screened by
Photo-convertible fluorescent proteins			
Thy1-mito-Kaede	Ando et al. 2000 Marinkovic et al. 2012	L. Godinho, J. Song Lichtman Lab, Harvard Transgenesis facility Harvard	J. Song
Thy1-mito-Dendra 2 lines (3 and 4)	Gurskaya et al. 2006 Magrane et al. 2012, 14	M. Lakadamyali Lichtman Lab, Harvard Transgenesis facility Harvard	M. Lakadamyali
Photo-activatable fluorescent protein			
Thy1-mito-paGFP 11 founders N832, N834, N843, N847, N858, N873, N874, N877, N884, N901, N904, N909, N923	Patterson et al. 2002	M. Leischner-Brill Misgeld Lab MPI Dresden (R. Naumann)	B. Gailer
Stable fluorescent proteins			
Thy1-mito-CFP line C	Misgeld et al. 2007 Jackson Laboratory (Stock Nr. 007940)	Lichtman Lab, Harvard Transgenesis facility Harvard	T. Misgeld, M. Kerschensteiner
Thy1-mito-tag RFP 3 founders A, B, H	Merzlyak et al. 2007 Breckwoldt et al. 2014	M. Leischner-Brill Misgeld Lab MPI Dresden (R. Naumann)	B. Gailer

Table 2 Generation and references of transgenic mouse lines

3.2 Genotyping

Genomic DNA was extracted from tail biopsies using a one-step lysis. PCR was performed using standard protocols. Mouse tail lysis, PCR master mix and primers are detailed below:

Lysis of tails:

Reagent	**Quantity**	**PCR program (KAPA)**
Gitocher (see 2.10)	15 µl	55°C 5h
10% Triton *(Roth)*	7,5 µl	
ß-Mercaptoethanol *(Sigma Aldrich M6250)*	1,5 µl	
ProteinkaseK *(Sigma Aldrich P2308)*	0,75l	95°C 5min
H_2O	125,25 µl	4°C ∞
Total	150 µl/ Tube	

PCR mix

Reagent	**Quantity**	**PCR program**
Kapa fast ready *(Peqlab, 07-KK5101-03)*	10 µl	95°c for 5 min
forward primer	1 µl	95°C 10 sec
reverse primer	1 µl	58°C 10 sec
Tail lysis	1 µl	72°C 10 sec
H2O	7 µl	4°C ~
Total	20 µl	

Primers for PCR

mouse line	**Primer** (10pmol/µl)	**primer sequence**		**PCR product** (base pairs)
Thy1-mito-Kaede	Mito-Kaede-F	for	5´-GCT GCT GCT GCG GGG CTT GAC AGG-3´	370
	Mito-Kaede-R	rev	5´-AAA CGC CCC CGT CCT CGA ACA TCA GG-3´	
Thy1-mito-Dendra	MitoDendra-F	for	5´-CGC CAA GAT CCA TTC GTT-3´	230
	MitoDendra-R	rev	5´-TGG TCA GGA TGT CGT AGC TG-3´	
Thy1-mito-paGFP	Mito-F	for	5´-CGC CAA GAT CCA TTC GTT-3´	181
	EYFP-R	rev	5´-GAA CTT CAG GGT CAG CTT GC-3´	
Thy1-mito-tagRFP	Mito-F	for	5´-CGC CAA GAT CCA TTC GTT-3´	254
	RFP-R	rev	5´-TTC TGC TGC CGT ACA TGA AG-3	
Thy1-mito-CFP	Mito-F	for	5´-CGC CAA GAT CCA TTC GTT-3´	181
	EYFP-R	rev	5´-GAA CTT CAG GGT CAG CTT GC-3´	

DNA electrophoresis was performed on an agarose gel (Sigma, A9539, for preparation see 3.10) in a horizontal gel chamber (DNA Pocket Block-UV; Biozym Diagnostik). The agarose gel was loaded with 15 µl of the PCR reaction mix, 2 µl of 6 x loading Buffer (Millipore; 69046-3) and 8 µl Quick-Load® 1 kb DNA Ladder (New England Biolabs, N0468L). Electrophoresis was driven by application of 90 mV in 1x TAE buffer (Carl Roth, CL86.1). DNA bands were visualized under UV-light (312 nm) and documented using Genoplex (VWR).

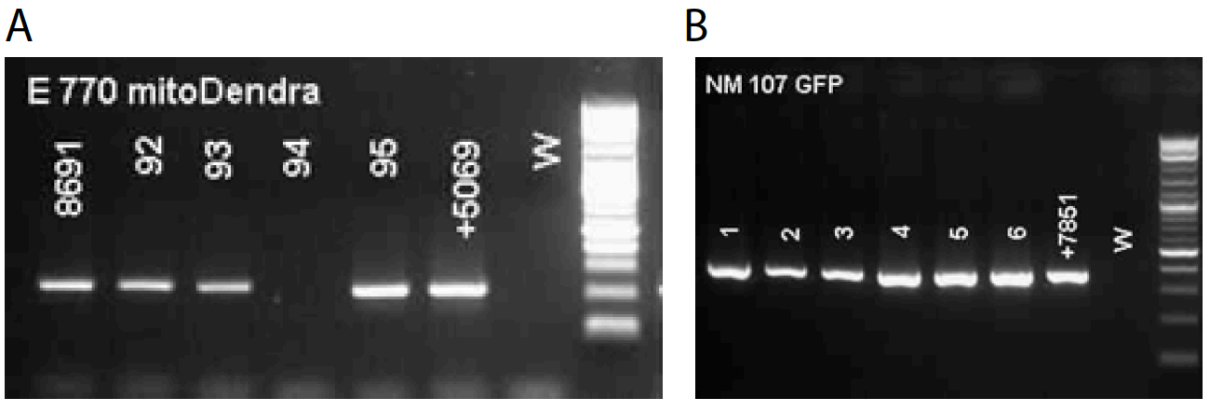

Fig. 3.1 Genotyping example of Thy1-mito-Dendra and Thy1-mito-paGFP

*Visualization of PCR products after electrophoresis. (**A**: Thy1-mito-Dendra, **B**: Thy1-mito-paGFP). Numbers on the gel refer to the earmark of tested animals. "W" labels the lane with the water control. DNA ladder on the very right. Positive controls were from animal number 5069 for Dendra (230 bp) and 7851 for GFP (181 bp).*

3.3 Immunostaining

Mice were lethally anaesthetized with isoflurane (Abbot) and transcardially perfused with 4 % paraformaldehyde (PFA) in 0.01 M phosphate buffered saline (PBS, see 2.10) using a pump (Ismatec ISM796B). The perfusion was started with 1x PBS at ~5 ml/min for about 1 min to remove blood, followed by about 25 ml of 4 % PFA. After removing the skin of the animal, the tissue was fixed in 4% PFA overnight, then stored in 1x PBS.

The thorax containing the triangularis sterni muscle was removed prior to perfusion and immersion fixed in 4% PFA for 2 h, then kept in 1x PBS. For immunostaining, the triangularis sterni muscle was separated from the anterior thoracic wall with a sharp needle.

Tissue was sectioned either at the cryostate or vibratome. For cryostate sections, the spinal cord with attached dorsal root ganglia (DRG), and the eyes were dissected and dehydrated in 30 % w/v sucrose (Carl Roth 4661.1) in 1x PBS. Tissue was embedded in cryomolds in "Tissue Tek" (Sakura) and snap-frozen in 2-methyl-butane (Sigma, M32631) on dry ice. Sections were cut with a Leica CM 1850 UV cryostate and mounted on "superfrost" slides (VWR, 631-0114). The spinal cord was cut at 50 µm thickness horizontally, the eye at 50 µm sagittal. Slides were stored at -20° C.

For vibratome sections, the skull was removed after post-fixation and brains were embedded in agarose (2% gel (Seakem 50004) in 1x PBS) and sectioned with a vibratome (Leica VT1200), sagittal at 100 µm thickness.

Considering the diverse properties and fluorescent emission of the photo-transformable proteins (see 1.4) different immunostainings had to be conducted to screen the transgenic lines. The mouse lines and the corresponding dyes/antibodies as well as the standardized protocol are listed below.

Thy1-mito-Kaede/ Thy1-mito-Dendra lines

Brain, spinal cord, retina:	Neurotrace 640/660 (Invitrogen N21483), diluted 1:500 in blocking solution (see 2.10)
Triangularis sterni muscle:	α-bungarotoxin, Alexa Fluor 647 conjugate (Invitrogen, B-35450) diluted 1:50 in 1x PBS

Thy1-mito-paGFP lines

Brain, spinal cord, retina:	rabbit anti-GFP antibody (Abcam ab290; 1:1000); secondary goat anti-rabbit antibody Alexa Fluor 488 (Invitrogen A11034; 1:1000)
	Neurotrace 640/660 (Invitrogen N21483; 1:500
Triangularis sterni muscle:	rabbit anti-GFP antibody (Abcam ab290; 1:1000); secondary goat anti-rabbit antibody Alexa Fluor 488 (Invitrogen A11034; 1:1000)
	α-bungarotoxin, Alexa Fluor 594 (Invitrogen, B-13432; 1:50)

Thy1-mito-tagRFP lines

Brain, spinal cord, retina:	Neurotrace 435/455 (Invitrogen N21479; 1:1000)
Triangularis sterni muscle:	α-bungarotoxin, Alexa Fluor 488 (Invitrogen, B-13422; 1:50)

For the different stainings, sections were incubated in blocking solution (see 3.10) for 60 min at room temperature, followed by an incubation in Neurotrace/ α-bungarotoxin/ anti-GFP in blocking solution over night at 4°C on shaker (for dilutions see above). Sections were washed three times in PBS, 1 h each wash. For the GFP immunostaining sections were then incubated in the secondary antibody diluted in blocking solution for 60 min at room temperature on shaker in the dark and washed again in PBS, three times, 60 min each in the dark.

After immunostaining the tissue was mounted in Vectashield (Biozol, H1000) on glass slides (Menzel).

3.4 Confocal microscopy

Image stacks were recorded using an Olympus FV1000 confocal microscope equipped with x20/0.8 N.A. and x60/0.8 N.A oil immersion objectives, as well as x10/0.4 N.A. and x4/0.13 N.A. air objectives. ImageJ/Fiji (Schindelin et al. 2012) was used to generate maximum intensity projections of the confocal image stacks, which were further edited in Adobe Photoshop. The different channels of the image were pseudo-colored. Several images had to be non-linearly gamma adjusted to make dim objects visible. Overview-images were stitched in Adobe Photoshop.

3.5 Ex vivo-imaging of mitochondria in the thoracic nerve-muscle explant

The acute thoracic nerve-muscle explant containing the triangularis sterni muscle, a flat, superficial muscle covering the inner surface of the anterior thoracic wall, is a well-established tool to study motor axons and NMJs (McArdle et al. 1981, Bishop et al. 2004, Misgeld et al. 2007, Brill et al. 2013, 2016). The preparation of the explant was performed following a protocol published previously (Kerschensteiner et al. 2008, Marinković et al. 2015*b*). After the mouse was lethally anaesthetized with isoflurane (Abbott), the skin covering the thorax was removed. To isolate the anterior thoracic wall, the abdominal wall was opened parallel to the ribs, the diaphragm was removed and the ribs were cut close to the vertebral column. After dissection the explants were permanently kept in 95% O_2/ 5% CO_2-bubbled 1x Ringer solution (see 2.10). The thoracic wall was mounted on a Sylgard-coated 3.5 cm dish with minutien pins (Fine Science Tools). For imaging, the explant was kept in a heating ring (Warner Instruments, 64-0110 DH35) with a slow and steady flow of pre-warmed (via in-line heater; Warner Instruments, SC-20) and bubbled Ringer solution at stable temperatures between 32 and 35°C.

Photo-transformation and imaging of mitochondria was performed with an Olympus BX51WL epifluorescent microscope equipped with x20/0.5 N.A. and x100/ 1.0 N.A. water immersion dipping cone objectives, an automated filter wheel (Sutter) and a CCD camera (Retiga EXi, Qimaging). All components were controlled by µManager, an open source software (Edelstein et al. 2010). Besides standard filter sets, following additional sets were used (all filters by AHF Analysentechnik): ET 46-001 (CFP) for experiments with Thy1-mito-CFP C, ET 46-008 (Texas Red) for experiments with Thy-mito-tagRFP, Triple Set ET F89-006 for CFP/YFP/mRFP for experiments with Thy1-mito-Kaede, Thy1-mito-Dendra, Thy1-mito-paGFP-Thy1-mito-tagRFP.

To minimize photo-toxicity and bleaching, I used neutral density filters (10, 20, 25 and 50 %, all by AHF) for imaging. Time-lapse movies of mitochondrial transport were recorded at 1 Hz with an exposure time from 200-400ms using the x100/ 1.0 N.A. objective, unless indicated otherwise.

For photo-transformation a 405 nm LED light source (Thorlabs, LED405 E) was manually switched into the excitation light path by a LED driver (Thorlabs, LEDD1). In all experiments photo-switch/activation was performed with the x100/ 1.0 N.A objective, field stop closed.

To determine the stability of mitochondrial transport rates during the imaging sessions, a control experiment was performed with Thy1-mito-CFP C mice. Imaging points in the distal arbor of the nerve (after 3 branch points of the intercostal nerve, see Fig. 3.2) were chosen, then mitochondrial transport was recorded every hour for 5 min for overall 6 h.

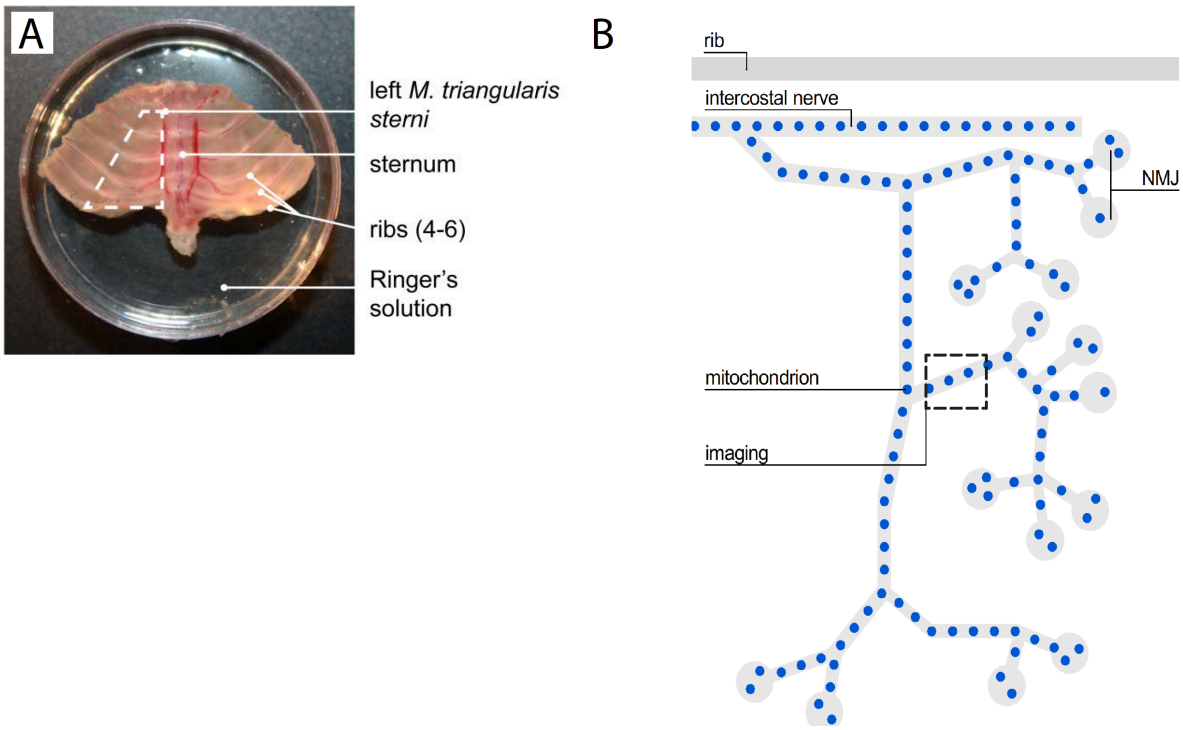

Fig. 3.2 Imaging mitochondria in motor neurons in the thoracic nerve-muscle explant

***A:** Murine thorax explant, pinned onto a Sylgard dish. Image provided by courtesy of M. Leischner-Brill. **B:** Schematic of the intercostal nerve in the nerve-muscle explant. Typical branch points and the imaging spot of the transport control measurements are labelled.*

3.6 Generation of dose-response-graphs of photo-transformation ex vivo

Properties of photo-transformation of the different proteins were characterized in superficial and flat NMJs in the acute nerve-muscle explant (described in 3.5): to determine the change in fluorescence, I alternately applied pulses of UV-light and acquired images of synapses (Fig. 3.3). Maximum four NMJs were photo-transformed per nerve-muscle explant. To avoid photo-

transformation by scattered light, distant NMJs were chosen (spaced by one rib, each arbor of an intercostal nerve).

Thy1-mito-Kaede, Thy1-mito-Dendra 4 and Thy1-mito-paGFP N877 crossed to Thy1-mito-tagRFP H were imaged at YFP 50%, 500ms, Red: 25%, 300ms for Thy1-mito-Kaede 22, YFP 25%, 300ms, Red: 25%, 300ms for Thy1-mito-Dendra 4 and YFP 25% 300ms, Red: 10% 300ms for Thy1-mito-paGFP N877-Thy1-mito-tagRFP H.

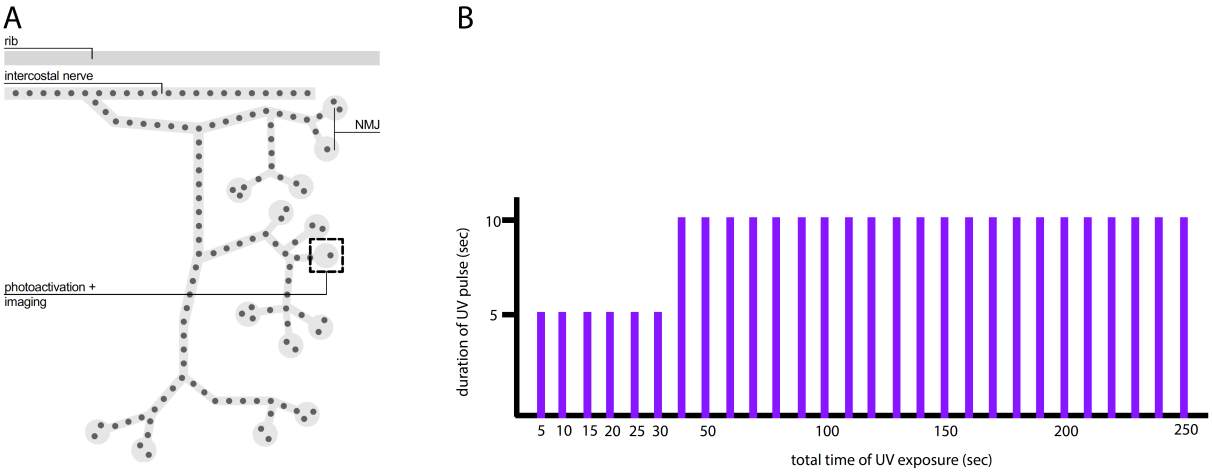

Fig. 3.3 Photo-transformation in the nerve-muscle explant

***A:** Schematic of the intercostal nerve in the nerve-muscle explant. NMJs were exposed to pulses of UV-light and imaged. **B:** Schematic of serial photo-transformation. UV-pulses are indicated by violet ticks. Initially pulses of 5 sec each were applied, pulses of 10 sec followed up to a total time of 250 sec UV-exposure.*

3.7 Pulse chase experiments in the nerve-muscle explant

Mitochondria were photo-transformed and imaged in the nerve-muscle explant (see 3.5) of Thy1-mito-Dendra 3 mice, to analyze anterograde and retrograde transport in different segments of the motor axon.

Pulse chase imaging in the axon: a superficial segment of an intercostal nerve`s proximal branch (between first and second branch point, Fig. 3.4,A) was photo-converted by applying 4-5 pulses of 405 nm light (30-45 sec exposure time) along the axon. Then transport was recorded at a more distally localized branch (typically after two branching points of the intercostal nerve).

Pulse chase imaging at the NMJ: a distal branch of the nerve (typically after the third branch point of the intercostal nerve, Fig. 3.4, B) was photo-converted with 4-5 pulses of 405 nm light (30-45 sec

exposure time) along the axon. Then the movements of anterogradely transported photo-switched mitochondria were traced: photo-converted organelles entering a NMJ were imaged for at least 30 min. Movies were recorded at 2 Hz.

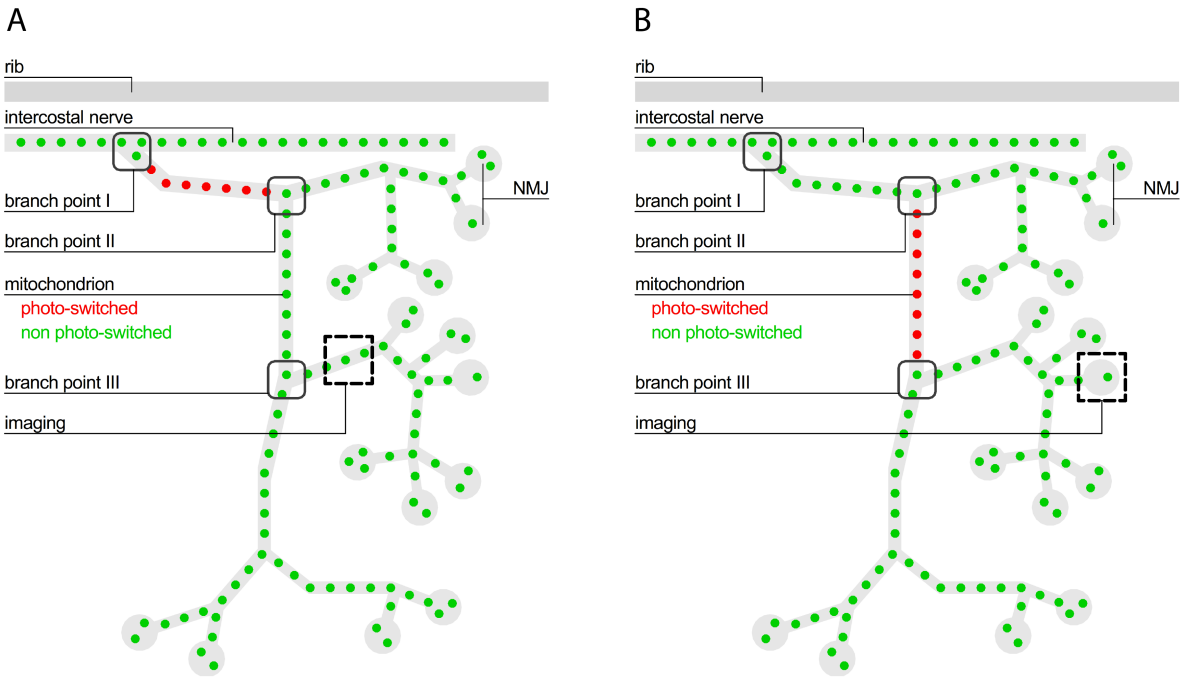

Fig. 3.4 Schematic of pulse chase experiments in acute nerve-muscle explants of Thy1-mito-Dendra

***A** shows the schematic of pulse imaging in the axon: after photo-conversion of mitochondria in the axon, the antero- and potentially retrograde flux of photo-switched (red) mitochondria was imaged. **B** shows the schematic of pulse imaging at the NMJ: after photo-conversion in the axon, single photo-switched mitochondria were imaged in the NMJ.*

3.8 Image processing and analysis

Measurement of mitochondrial shape: Different parameters of mitochondrial shape were determined in transport movies of mitochondria (nerve-muscle explant/adult Thy1-mito-Kaede mice/ widefield setup, x100/ 1.0 N.A. objective), recorded in a previous study (Marinkovic et al. 2012). Using Fiji, length and diameter of individual moving mitochondria were measured with the “line tool”, the area was outlined with the “freehand selection tool”. Each mitochondrion was measured in three different frames. The shape factor was calculated by dividing the length by the diameter, the volume was calculated by assuming a cylindrical shape: volume = length x $(\text{diameter}/2)^2$ x π. Moving mitochondrial volume was calculated with the formula: average volume x transport rate/min.

Dose-response graphs of photo-transformation: To create dose-response graphs for the photo-transformable proteins, intensity measurements of single images of a subsequently photo-transformed NMJ were performed using Fiji. A "Region of Interest" (ROI) of 140-144 pixels at a preferably superficial part with a high density of mitochondria was determined in every NMJ for the measurement. In this ROI the intensity was measured in the recorded images of the subsequent photo-transformation. In the case of drifting of the explant during the imaging, the ROI was repositioned manually to the selected spot. The intensity measurements were normalized to the background intensity, recorded at the respective NMJ before photo-transformation. R/G Ratio (mean red fluorescence: mean green fluorescence) was calculated before photo-switch and at full photoconversion (maximum of red fluorescence).

Transport rates: Transport rates of antero- and retrograde moving mitochondria were manually scored in time lapse movies of the nerve-muscle explant. Mitochondrial flux was defined as the number of fluorescent mitochondria per minute that crossed a vertical line placed along the axon.

Image representation: Confocal images were edited as described above (3.4). Figures were generated with Adobe Illustrator and ArchiCAD.

3.9 Statistics

Statistics were performed with Microsoft Excel and GraphPad Prism 8.0.0. Data were tested for normality with the D'Agostino-Pearson Test. Statistical significance was determined by using t-tests for data consistent with the Gaussian distribution, for not normally distributed data the Mann-Whitney and the Kruskal Wallis test as well as the Dunn's multiple comparison test were used. P-values < 0.05 were determined to be significant and labelled with *. Graphs indicate mean $\pm$ S.E.M. unless indicated otherwise.

3.10 Buffers and solutions

Gitocher Buffer

Reagent	Quantity	Concentration
Tris *(Roth, 4855.1)*	15 µl	1.43 mol/l
$(NH_4)_2SO_4$ *(Sigma-Aldrich, M3148)*	5µl	1.66 mol/l
$MgCl_2$	5 ml	0.65 mol/l
Gelatine *(Roth 4275.3)*	0.05	
H_2O	15 ml	
Total	50 ml	

Agarose Gel for electrophoresis

Reagent	Quantity
1x TAE buffer	50 ml
Agarose *(Seakem 50004)*	0.5 g
Gel Red nucleid acid stain *(VWR International, 730-2957)*	5 µl
Total	50 ml

Agarose was boiled shortly in 50 mL 1 × TAE buffer, then 5 µl Gel Red nucleid acid stain was added.

10x Phosphate Buffered Saline (PBS)

Reagent *(Source)*	Quantity	Concentration
NaH_2PO_4 *(Riedel de Haen 04270)*	2.56 g	18.6 mM
Na_2HPO_4 *(Sigma-Aldrich S3264)*	11.94 g	84.1 mM
NaCl	102.2 g	1750 mM
Total	1 l	

pH was adjusted to 7.4. All experiments were performed with 1xPBS.

Blocking Solution

Reagent	**Quantity**
Goat Serum *(Sigma Aldrich G9023)*	10 ml
Bovine serum albumin *(Sigma-Aldrich A3912)*	1 g
Triton-X *(Sigma-Aldrich T9284)*	0.5 ml
20% NaN_3 (Riedel de Haen 13412)	50 µl
1x PBS	up to 100 ml

10x Ringer's solution

Reagent	**Quantity**	**Concentration**
$NaHCO_3$ *(Sigma-Aldrich S6297)*	21.84 g	260 mM
$NaH_2PO_4*H_2O$ *(*Riedel de Haen 04270)	1.72 g	12.5 mM
KCl	1.86 g	25 mM
NaCl	73.05 mg	1.2 mM
H_2O	up to 1 l	
Total	1 l	

1x Ringer's solution

Reagent	**Quantity**	**Concentration**
1M $CaCl_2$ *(Sigma-Aldrich C1016)*	2 ml	2 mM
1M $MgCl_2$	1 ml	1 mM
H_2O	900 ml	
10x Ringer's Solution	100 ml	20 mM
Glucose *(Sigma-Aldrich 16301)*	3.6 g	
Total	1 l	

$CaCl_2$ and $MgCl_2$ are prepared monthly. 1x Ringer's Solution is produced on the day of the experiment, glucose is added before the experiment. The solution was bubbled with carbogen gas (95 % O_2 and 5 % CO_2) for at minimum 30 min before the start of the experiment.

4 Results

In this study I characterized transgenic mouse lines with the expression of different photo-transformable and stable fluorescent proteins in neuronal mitochondria. I used these mouse lines to study the patterns of mitochondrial distribution in motoneurons with live pulse chase imaging: after photo-transformation of a pulse of mitochondria, I imaged/ chased the organelles' distribution in motoneurons of the acute nerve-muscle explant.

4.1 Screening and characterization of Thy1 transgenic mouse lines

In the first part of this work I screened and characterized Thy1-mito-Kaede, - Dendra, -paGFP- and tagRFP-lines. Due to a random insertion of the transgene, the expression patterns of founder lines under the Thy1-promoter are highly variable: they differ both in the labelling of subpopulations as well as in the fraction of labelled cells within a subgroup (Feng et al. 2000).

In a first step mouse lines were selected for bright and neuron specific expression, especially in motoneurons in order to perform live imaging later on. Transgene expression was determined in fixed tissue and during live imaging in subsequent neuronal populations:

Live imaging:

thoracic nerve-muscle explant	*motoneurons*

Fixed tissue:

brain	*cortex (cortical layers)*
	cerebellum (mossy fibers, Purkinje cells, granule cells)
	hippocampus (dentate gyrus, cornu ammonis CA1-3)
retina	*bipolar cells, amacrine cells, retinal ganglion cells*
spinal cord	*motoneurons, dorsal root ganglia*
triangularis sterni muscle	*motoneurons*

The expression-patterns of the proteins were classified as listed below:

+	*expression in > 80% of the cells*
+/-	*subset expression in < 80% of cells*
sparse labelling	*expression in single neurons < 5% of cells*
-	*no expression*

In a second step, I obtained specific information about the proteins' properties during photo-transformation ex-vivo: synapses in the nerve-muscle explant of adult mice were exposed to an increasing number of pulses of UV-light to create dose-response graphs (Fig. 3.3). For live imaging, two characteristics of the photo-transformable proteins are especially important and had to be determined:

- *photo-efficiency (= time to reach maximal photo-transformation):* UV-light has been reported to negatively influence living tissue (Post et al. 2005). The selection of a photo-efficient protein is crucial, to minimize UV-exposition during in vivo imaging and avoid potential phototoxic damages.
- *contrast, produced by photo-transformation:* the fluorescence intensity of the photo-transformed proteins is relevant and low contrast complicates live imaging. Dim photo-transformed proteins are difficult to distinguish from the background and require higher light intensities for imaging, which rises the risk for phototoxic damages and bleaching.

4.1.1 Thy1-mito-paGFP /Thy1-mito-tagRFP mouse lines

Thy1-mito-paGFP

paGFP, a monomeric protein enhances its native fluorescence after photo-activation: its ground state is barely fluorescent, after photo-activation with UV-light the protein emits green fluorescence (Patterson and Lippincott-Schwartz 2002) . Thy1-mito-paGFP mice were generated at the beginning of this study (3.1). The pronuclear injections of the Thy1-mito-paGFP construct were successful and resulted in thirteen founders (N832, N834, N843, N847, N858, N873, N874, N877, N884, N901, N904, N909, N923). Founders were crossbred with wildtype animals and tested for germline transmission in the next generation. Two of these founders did not reproduce (N834, N901). Eleven out of thirteen lines were fertile and bred PCR-positive offspring, which was screened for mito-paGFP expression patterns. Expression patterns were determined in fixed tissue of brain, retina, spinal cord and triangularis sterni muscle, stained with anti-GFP antibodies (see 3.3). The expression level of the fluorescent protein was determined in motoneurons in the nerve-muscle explant after photo-activation with 405nm-light.

The lines presented various expression patterns in CNS and PNS (see Table 3). For imaging mitochondrial transport in the triangularis explant a broad labelling of motoneurons was required. Therefore eight lines with subset or sparse labelling in motoneurons (N858, N843, N873, N874, N847, N884, N904, N923) were excluded from further experiments in nerve-muscle explants. Three lines

(N832, N877, N909) presented labelling in nearly all motoneurons. In Thy1-mito-paGFP N832 a very bright expression of paGFP was detected. As in previous publications highly expressing homozygous MitoMouse-lines showed neurological alterations in adulthood (Misgeld et al. 2007), this mouse line was not used for experiments. The two remaining lines with a broad and bright labelling of motoneurons were selected for upcoming experiments: Thy1-mito-paGFP N877 (Fig. 4.1) and N909 (Fig. 4.2). In the CNS of these mice all layers of the cortex and hippocampus are labelled. In both Thy1-mito-paGFP N909 and Thy1-mito-paGFP N877 cerebellar Purkinje cells and mossy fibers are labelled.

Line	Spinal cord		Retina			Cortex	Cerebellum			Hippocampus				Expression Level
	MN	DRG	RG	AC	BC		GC	MF	PC	DG	CA1	CA2	CA3	
N832	+	+	+	+/-	-	+	+/-	+	+/-	+	+	-	-	very bright
N877	+	+	+	+/-	-	+	-	+	+	+	+	+	+	bright
N909	+	+/-	+	+/-	-	+	-	+/-	+	+	+	+	+	bright
N858	+/-	+/-	+	+/-	-	+/-	-	+	+/-	+	+	+	+	bright
N843	+/-	+/-	+	+/-	-	+/-	+	+	-	+	+	+	+	dim
N873	+/-	+/-	+	+/-	-	+/-	+	+	+	+	+/-	+/-	+/-	dim
N874	+/-	+/-	+	+/-	-	+/-	-	+	-	+	+/-	+/-	+/-	dim
N847	+/-	+/-	+	+/-	-	+/-	+	+	-	+	+	+	+	dim
N884	+/-	+/-	+	+/-	-	+/-	+	+	+/-	+	+/-	+/-	+/-	dim
N904	sparse labelling		-	-	-	sparse labelling								dim
N923	sparse labelling		-	-	-	sparse labelling								dim

Table 3 Expression of Thy1-mito-paGFP in transgenic mouse lines

+: expression in most cells; +/-: subset expression in < 80% of cells; sparse labelling: expression in single neurons <5%; -: no expression; AC: amacrine cells; BC: bipolar cells; CA: cornu ammonis; DG: dentate gyrus; DRG: dorsal root ganglion; GC: granule cells; L: cortical layer; MF: mossy fibers; MN: motor neurons; PC: Purkinje cells; RG: retinal ganglion cells. Mouse lines labelled with green were used for further experiments.

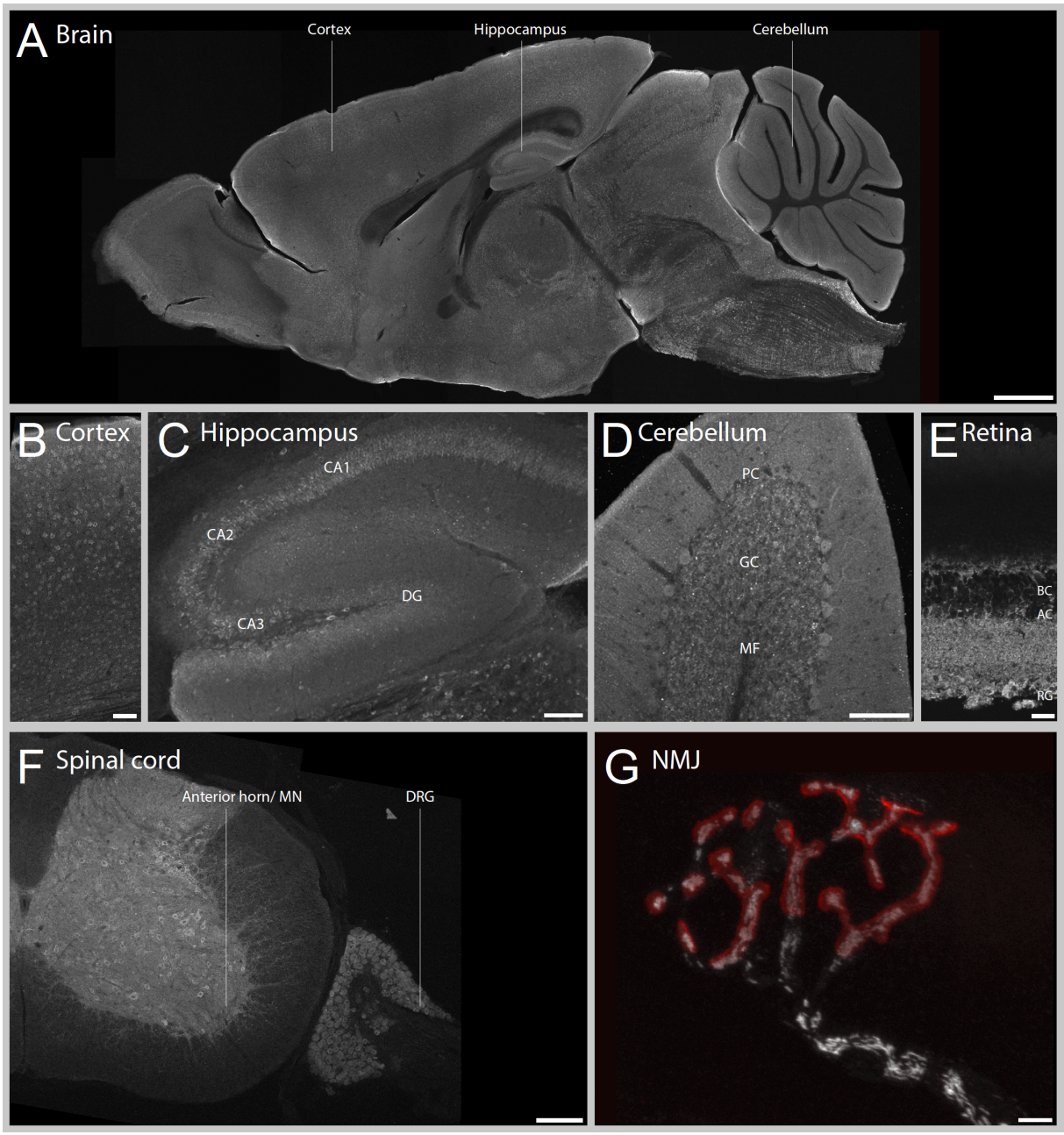

Fig. 4.1 Expression pattern of Thy1-mito-paGFP N877

***CNS - A**: sagittal brain section; **B**: cortex; **C**: hippocampus; DG: dentate gyrus, CA: cornu ammonis; **D**: cerebellum; PC: purkinje cells, GC: granular cells, MF: mossy fibers; **E**: retina; RG: retinal ganglion cells; AC: amacrine cells; BC: bipolar cells; **F**: horizontal spinal cord section; MN= motoneurons; DRG: dorsal root ganglion; A-F: antiGFP staining (gray-scale) **PNS - G**: neuromuscular junction in the triangularis sterni muscle; antiGFP staining (gray-scale); postsynaptic receptors stained with bungarotoxin (red). Scale bar in **A** 1 mm; in **B, C, D** 50 µm; in **E** 20 µm; in **F** 200 µm, in **G** 5 µm.*

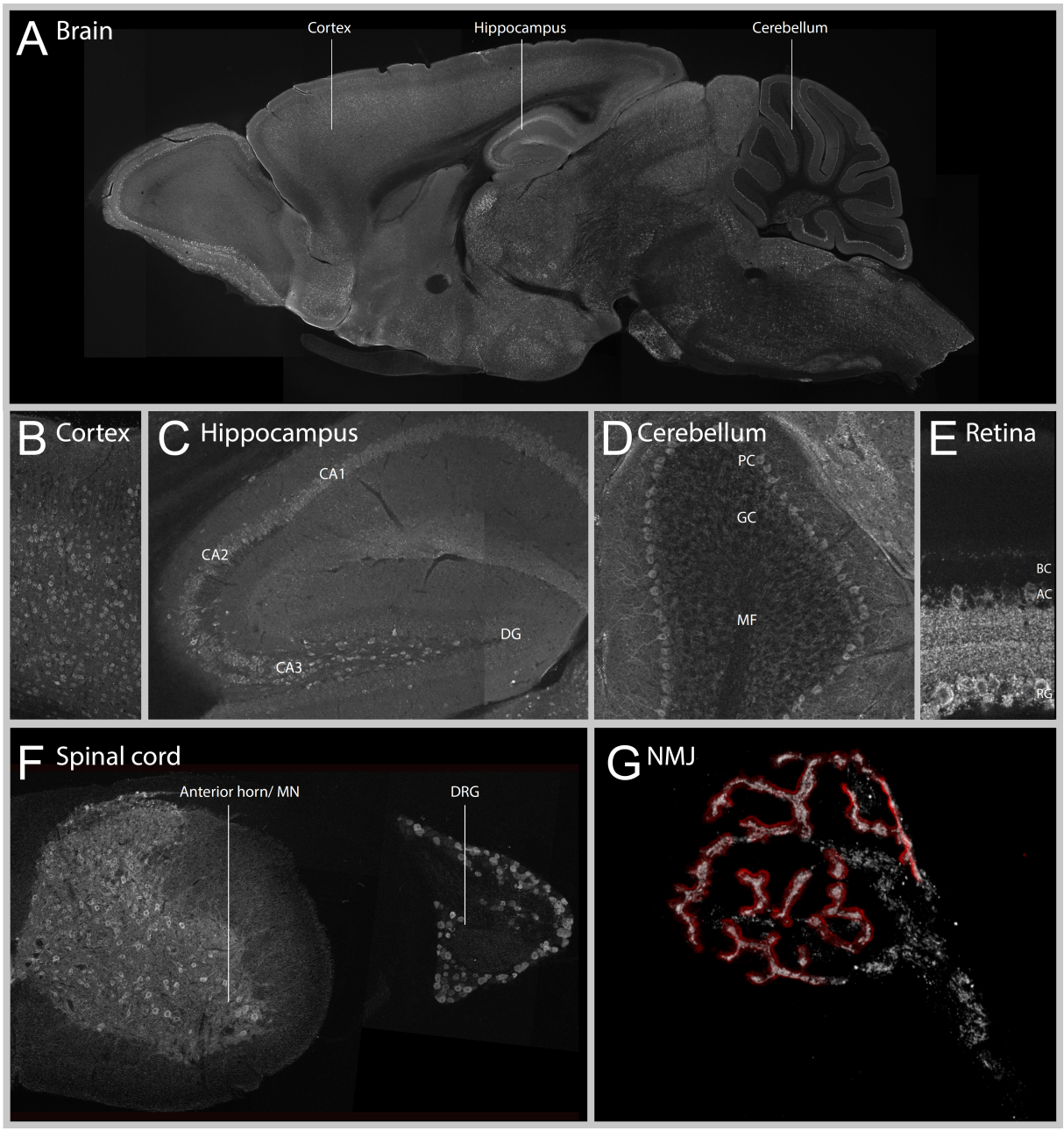

Fig. 4.2 Expression pattern of Thy1-mito-paGFP N909

***CNS - A**: sagittal brain section; **B**: cortex; **C**: hippocampus; DG: dentate gyrus, CA: cornu ammonis; **D**: cerebellum; PC: purkinje cells, GC: granular cells, MF: mossy fibers; **E**: retina; RG: retinal ganglion cells; AC: amacrine cells; BC: bipolar cells; **F**: horizontal spinal cord section; MN= motoneurons; DRG: dorsal root ganglion; A-F: antiGFP staining (gray-scale) **PNS - G**: neuromuscular junction in the triangularis sterni muscle; antiGFP staining (gray-scale); postsynaptic receptors stained with bungarotoxin (red). Scale bar in **A** 1 mm; in **B, C, D** 50 µm; in **E** 20 µm; in **F** 200 µm, in **G** 5 µm.*

Thy1-mito-tagRFP

Imaging of Thy1-mito-paGFP was expected to be difficult, because the fluorescence of its ground state is close to negligible. Therefore, I wanted to provide an auxiliary organelle labelling by crossbreeding Thy1-mito-paGFP with a "mitoMouse" with a permanent fluorescent labelling of mitochondria. Considering paGFP's spectral properties and its photo-activation by UV-light, a red fluorescent protein was selected for co-labelling. However, the naturally available fluorophores in the red part of the light spectrum are di- or tetrameric and cause mistargeting and aggregation (Chudakov et al. 2005). mFruits, monomeric variants of Dsred have been engineered, but are substantially less bright (Shaner et al. 2004, Wang et al. 2004). In contrast, tagRFP, modified from the GFP-like protein of a sea anemone, is a monomeric and bright red fluorescent protein (Merzlyak et al. 2007) and was therefore selected for the generation of transgenic mice.

Eight PCR-positive founders were obtained from the pronuclear injections of the Thy1-mito-tagRFP construct (which were named in alphabetical order A – H). Five of these founders (line C, D, E, F, G) bred only PCR-negative offspring, so no germline transmission occurred. In three lines (A, B, H) PCR positive offspring was screened (Table 4). Mouse line B presented a very bright and broad labelling in CNS and PNS. Again, this line was not used for experiments to avoid the possibility of neurological problems due to the high expression levels.

Mouse line H showed a broad spectrum of labelled neurons including motoneurons, cortical and hippocampal neurons and cerebellar Purkinje cells (Thy1-mito-tagRFP H, Fig. 4.3). This line was crossbred with Thy1-mito-paGFP N877 for transport experiments in the acute nerve-muscle explants. Generation and screening of the Thy1-mito-tagRFP H line was published in another study of our lab covering a multiparametric optical analysis of mitochondrial function in neurons (Breckwoldt et al. 2014). In this study the transgenic mouse line was combined with a mitochondrially targeted calcium sensor by adeno- associated virus (AAV)-mediated gene transfer (rAAV-mito-GCaMP-3). After laser axotomy in the nerve-muscle explant, organelle morphology and matrix calcium levels were observed: mitochondrial rounding and fragmentation started immediately after the axotomy and spread along the axon over the next few minutes, accompanied by an increase in matrix calcium.

Mouse line A presented a sparse, but bright labelling in motoneurons, cortex and cerebellum, as well as a broad labelling in hippocampal dentate gyrus and CA3 (Fig. 4.4). This line was maintained, as the sparse labelling in cortex and cerebellum could be useful for CNS-imaging in the future.

Line	Spinal cord		Retina			Cortex	Cerebellum			Hippocampus				Expression Level
	MN	DRG	RG	AC	BC		GC	MF	PC	DG	CA1	CA2	CA3	
B	+	+/-	+/-	-	-	+/-	+	+	-	+	+	+	+	very bright
H	+	+/-	+/-	+/-	-	+/-	-	+	+	-	-	+	+	bright
A	sparse labelling		-	-	-	+/-	-	+/-	-	+	+/-	-	+	bright

Table 4 Expression of Thy1-mito-tagRFP in transgenic mouse lines

+: expression in most cells; +/-: subset expression in < 80% of cells; -: no expression; AC: amacrine cells; BC: bipolar cells; CA: cornu ammonis; DG: dentate gyrus; DRG: dorsal root ganglion; GC: granule cells; L: cortical layer; MF: mossy fibers; MN: motor neurons; PC: Purkinje cells; RG: retinal ganglion cells. Mouse lines labelled with green were used for further experiments.

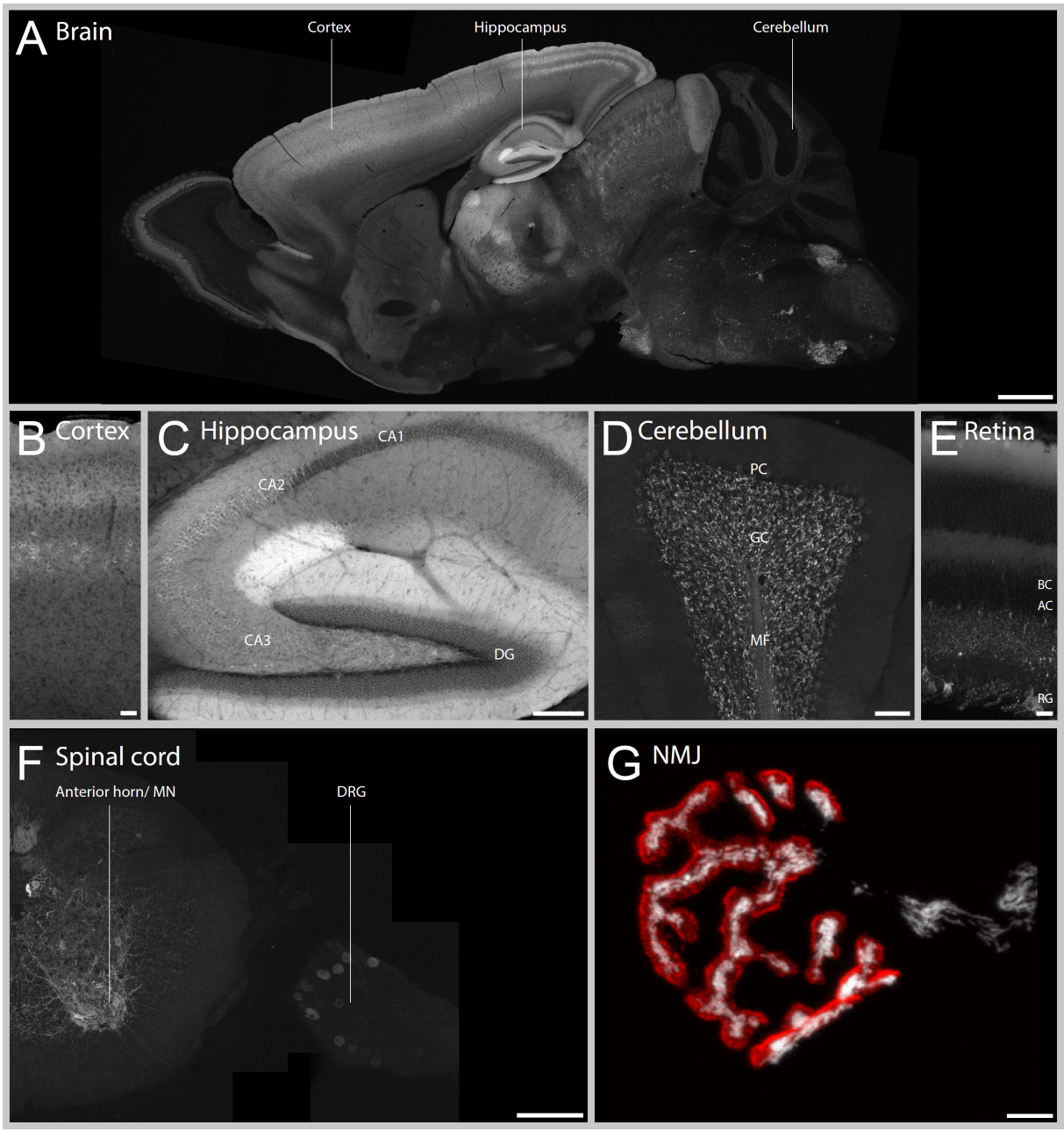

Fig. 4.3 Expression pattern of Thy1-mito-tagRFP H

***CNS - A**: sagittal brain section; **B**: cortex; **C**: hippocampus; DG: dentate gyrus, CA: cornu ammonis; **D**: cerebellum; PC: purkinje cells, GC: granular cells, MF: mossy fibers; **E**: retina; RG: retinal ganglion cells; AC: amacrine cells; BC: bipolar cells; **F**: horizontal spinal cord section; MN= motoneurons; DRG: dorsal root ganglion; A-F: tagRFP (gray-scale) **PNS - G**: neuromuscular junction in the triangularis sterni muscle; tagRFP (gray-scale); postsynaptic receptors stained with bungarotoxin (red). Scale bar in **A** 1 mm; in **B, C, D** 50 µm; in **E** 20 µm; in **F** 200 µm, in **G** 5 µm.*

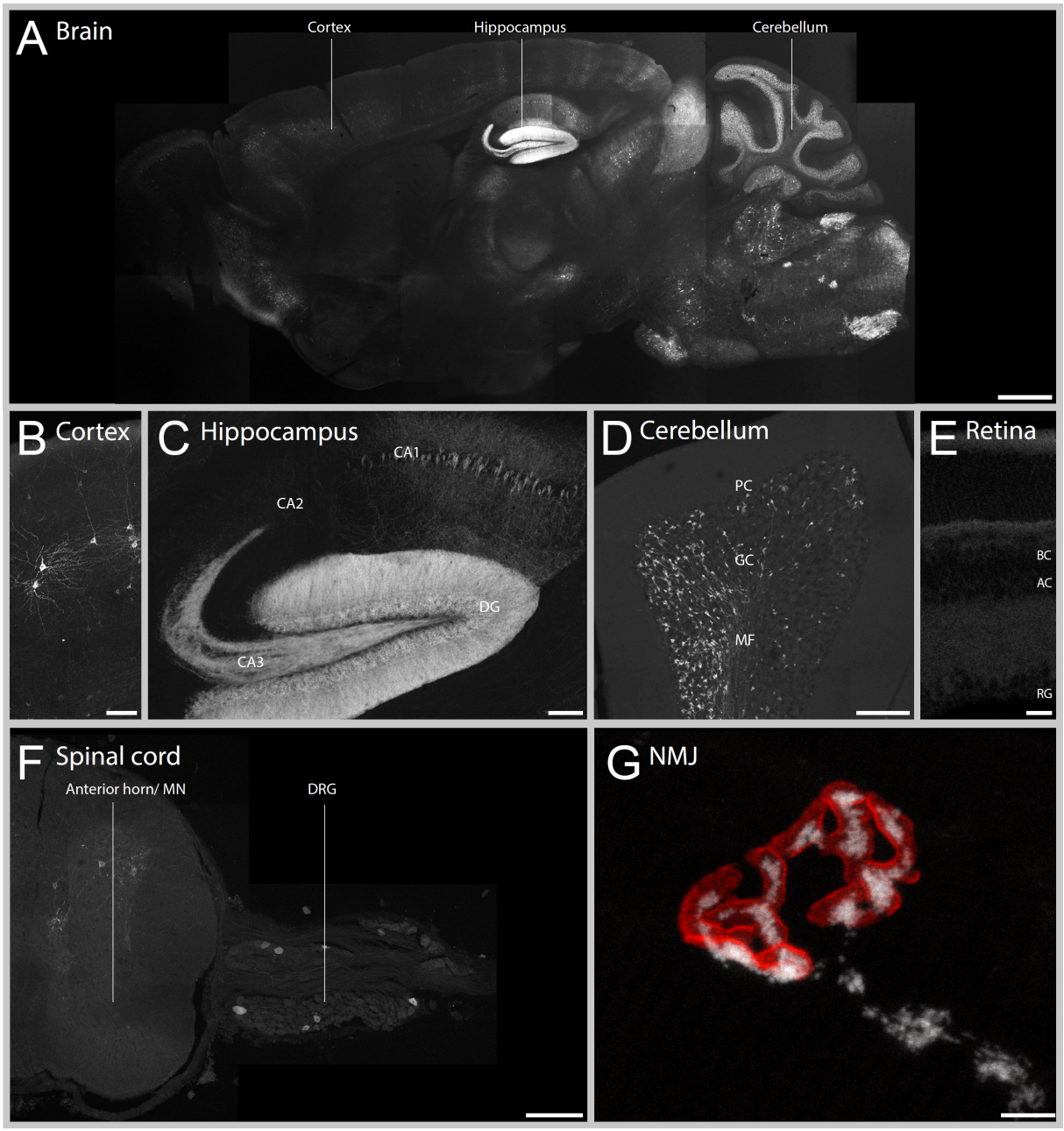

Fig. 4.4 Expression pattern of Thy1-mito-tagRFP A

***CNS - A**: sagittal brain section; **B**: cortex; **C**: hippocampus; DG: dentate gyrus, CA: cornu ammonis; **D**: cerebellum; PC: purkinje cells, GC: granular cells, MF: mossy fibers; **E**: retina; RG: retinal ganglion cells; AC: amacrine cells; BC: bipolar cells; **F**: horizontal spinal cord section; MN= motoneurons; DRG: dorsal root ganglion; A-F: tagRFP (gray-scale) **PNS - G**: neuromuscular junction in the triangularis sterni muscle; tagRFP (gray-scale); postsynaptic receptors stained with bungarotoxin (red). Scale bar in **A** 1 mm; in **B, C, D** 50 µm; in **E** 20 µm; in **F** 200 µm, in **G** 5 µm.*

Thy1-mito-paGFP x Thy1-mito-tagRFP

Thy1-mito-paGFP N877 was crossbred with Thy1-mito-tagRFP H to visualize mitochondrial background and ease photo-activation and imaging of mitochondrial transport in motoneurons. The double-transgenic mice were used to characterize the properties of photo-activation in synapses of the acute nerve-muscle explant (see Fig. 3.3, Fig. 4.5)

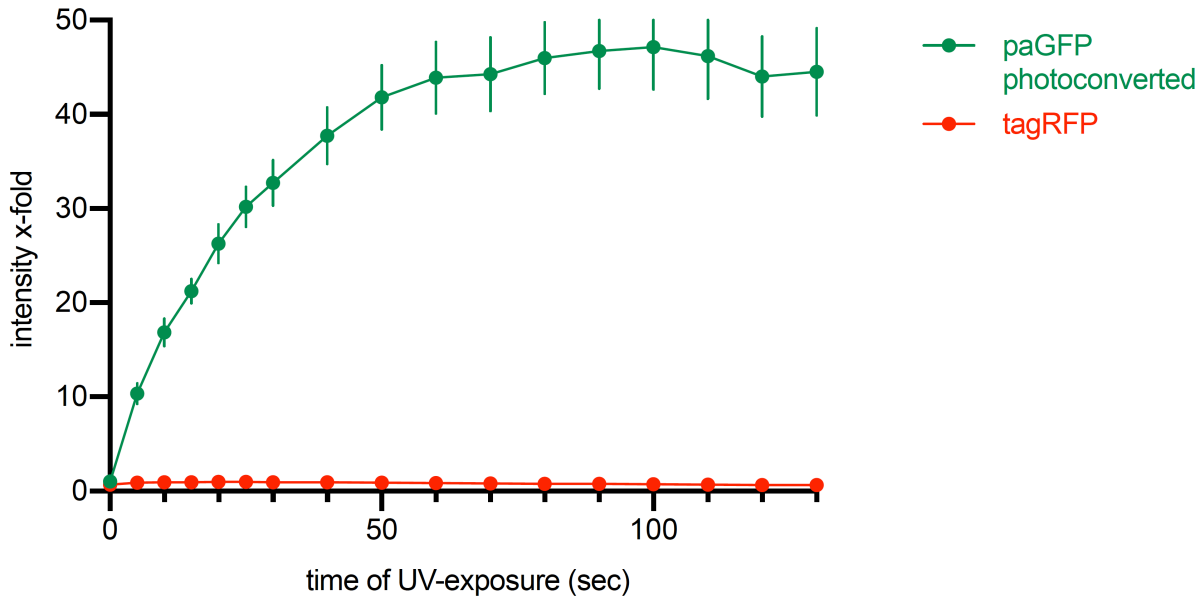

Fig. 4.5 Photo-activation characteristics of mito-paGF x mito-tagRFP ex vivo

The dose-response graph was created by subsequent exposure of NMJs to pulses of UV-light (405nm) in the nerve-muscle explant of Thy1-mito-paGFP N877 x Thy1-mito-tagRFP H mice (n=11, 4 animals). Some error bars are hidden by the data symbols.

In mito-paGFP fluorescence in photo-activated mitochondria monotonically increases over time and reaches an asymptotic value near 50, providing a ~ 47-fold increase in fluorescence. Complete photo-activation, measured by the maximum increase in fluorescence takes a relatively long time of 100 seconds. Concerning photo-efficiency and -toxicity this is a disadvantage for in vivo imaging.

4.1.2 Thy1-mito-Kaede mouse line

Kaede is a tetrameric photo-convertible protein: its native green fluorescence switches to red fluorescence by exposure to UV or violet light (350-400nm) (Ando et al. 2002). The Thy1-mito-Kaede mouse was generated by my principal investigator together with collaboration partners at Harvard University (see 3.1) and was prior to my thesis used to study mitochondrial axonal transport in motoneurons in a mouse model of ALS (Marinkovic et al. 2012). In Thy1-mito-Kaede almost all

motoneurons are labelled, so the line is suitable for imaging mitochondrial transport in the nerve-muscle explant. In this work I completed the initial characterization of expression patterns, as Marinkovic et al. only screened for expression in motoneurons. In the CNS, expression was detected in different compartments (Fig. 4.6, Table 5). In the hippocampal CA2 region as well in the cerebellar Purkinje cell layer most of the cells (> 80%) are labelled, whereas in the cortex only single cells expressing Thy1-mito-Kaede can be found. However, compared to Thy1-mito-Dendra (4.1.3) the overall expression level of the fluorescent protein Kaede is dim.

Line	Spinal cord		Retina			Cortex	Cerebellum			Hippocampus				Expression Level
	MN	DRG	RG	AC	BC		GC	MF	PC	DG	CA1	CA2	CA3	
Kaede	+	+	+/-	+/-	-	+/-	-	+	+	-	-	+	-	dim

Table 5 Expression of mito-Kaede in Thy1-mito-Kaede

+: expression in most cells; +/-: subset expression in < 80% of cells; AC: amacrine cells; BC: bipolar cells; CA: cornu ammonis; DG: dentate gyrus; DRG: dorsal root ganglion; GC: granule cells; L: cortical layer; MF: mossy fibers; MN: motor neurons; PC: Purkinje cells; RG: retinal ganglion cells

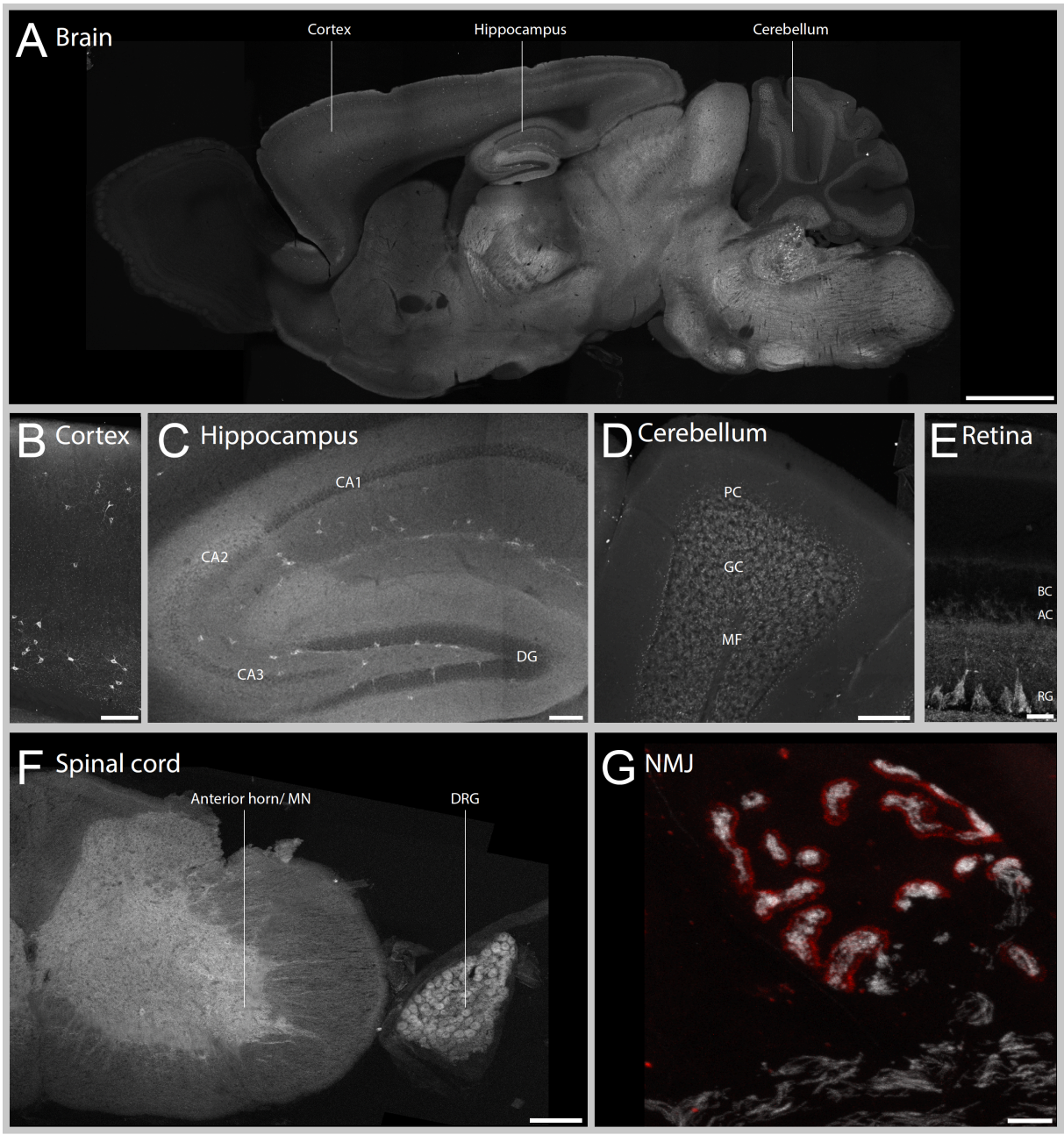

Fig. 4.6: Expression pattern of Thy1-mito-Kaede

***CNS - A**: sagittal brain section; **B**: cortex; **C**: hippocampus; DG: dentate gyrus, CA: cornu ammonis; **D**: cerebellum; PC: purkinje cells, GC: granular cells, MF: mossy fibers; **E**: retina; RG: retinal ganglion cells; AC: amacrine cells; BC: bipolar cells; **F**: horizontal spinal cord section; MN= motoneurons; DRG: dorsal root ganglion; A-F: Kaede (gray-scale) **PNS - G**: neuromuscular junction in the triangularis sterni muscle; Kaede (gray-scale); postsynaptic receptors stained with bungarotoxin (red)). Scale bar in **A** 1 mm; in **B, C, D** 50 µm; in **E** 20 µm; in **F** 200 µm, in **G** 5 µm.*

In the acute nerve-muscle explant mito-Kaede provides a fast photo-switch with maximal photo-conversion after 15 seconds of UV-exposure, further photo-conversion bleaches the protein. Mito-Kaede produces a maximum of 9-fold increase in red fluorescence and a 13-fold increase in the Red/Green Ratio.

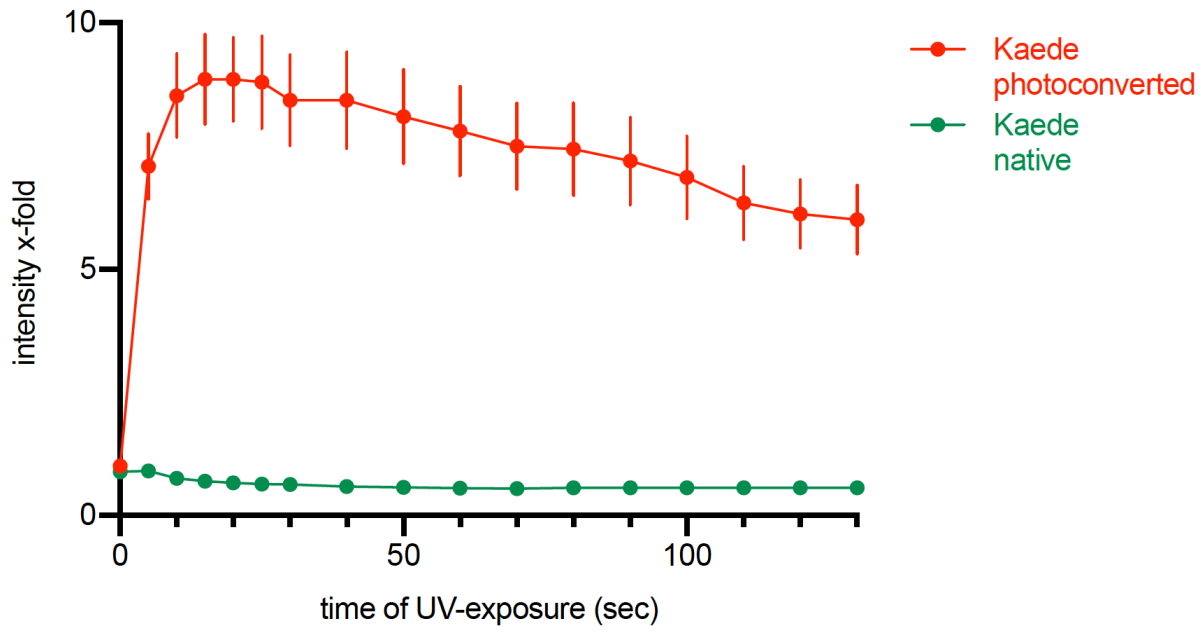

Fig. 4.7 Photo-conversion characteristics of mito-Kaede ex vivo

The dose-response graph was created by subsequent exposition of NMJs to pulses of UV-light (405nm) in the nerve-muscle explant of Thy1-mito-Kaede (n=12, 4 animals). Some error bars are hidden by the data symbols.

4.1.3 Thy1-mito-Dendra mouse lines

The monomeric protein Dendra can be photo-converted from green to red fluorescence both by ultraviolet and 488 nm light. Two Thy1-mito-Dendra lines (line 3 and 4) were as well generated by my principal investigator together with collaboration partners at Harvard University (see 3.1). The expression patterns of these lines were characterized and turned out to be rather similar amongst each other. In both lines, most motoneurons (>80 %) are labelled with a bright fluorescent signal. The lines differ slightly in the expression patterns of the CNS (Table 6). In Thy1-mito-Dendra 3 only mossy fibers express the photo-convertible protein in the cerebellum and a broad labelling of all cortical layers was found. In Thy1-mitoDendra 4 cerebellar Purkinje and mossy fibers as well as a subset of cortical layers are labelled. As the two lines are very similar, we decided to breed only one strain for

further experiments: Thy1-mito-Dendra 4 was chosen because its Purkinje cell labelling could be useful for cerebellar imaging in upcoming studies. (Fig. 4.8).

Line	Spinal cord		Retina			Cortex	Cerebellum			Hippocampus				Expression Level
	MN	DRG	RG	AC	BC		GC	MF	PC	DG	CA1	CA2	CA3	
3	+	+	+	+/-	-	+	-	+	-	-	-	+	-	bright
4	+	+	+	+/-	-	+/-	-	+	+	-	-	+	-	bright

Table 6 Expression of Thy1-mito-Dendra in transgenic mouse lines

+: expression in most cells; +/-: subset expression in < 80% of cells; AC: amacrine cells; BC: bipolar cells; CA: cornu ammonis; DG: dentate gyrus; DRG: dorsal root ganglion; GC: granule cells; L: cortical layer; MF: mossy fibers; MN: motor neurons; PC: Purkinje cells; RG: retinal ganglion cells. Mouse lines labelled with green were used for further experiments.

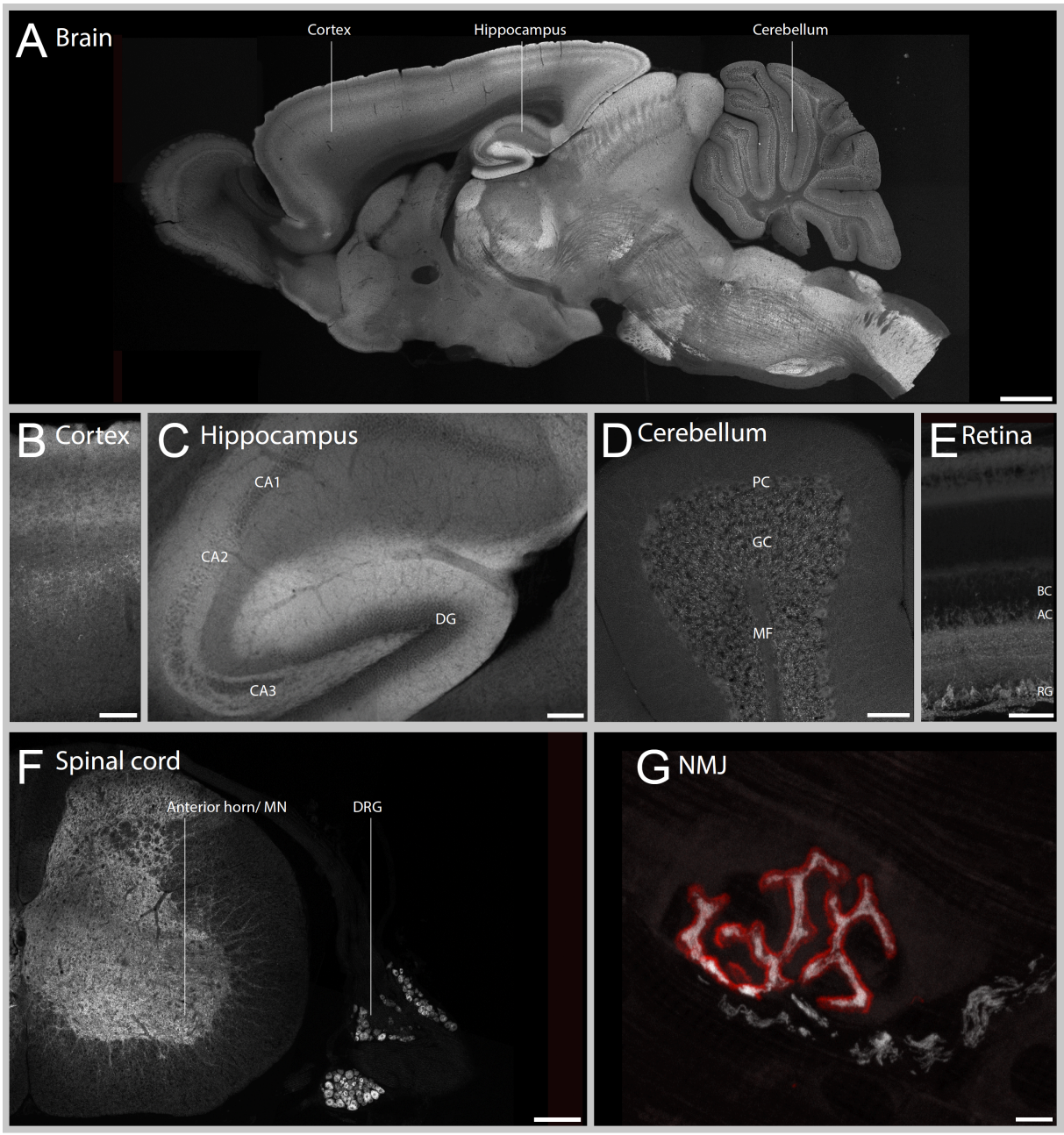

Fig. 4.8: Expression pattern of Thy1-mito-Dendra 4

***CNS - A**: sagittal brain section; **B**: cortex; **C**: hippocampus; DG: dentate gyrus, CA: cornu ammonis; **D**: cerebellum; PC: purkinje cells, GC: granular cells, MF: mossy fibers; **E**: retina; RG: retinal ganglion cells; AC: amacrine cells; BC: bipolar cells; **F**: horizontal spinal cord section; MN= motoneurons; DRG: dorsal root ganglion; A-F: Dendra (gray-scale) **PNS - G**: neuromuscular junction in the triangularis sterni muscle; Dendra (gray-scale); postsynaptic receptors stained with bungarotoxin (red). Scale bar in **A** 1 mm; in **B, C, D** 50 µm; in **E** 20 µm; in **F** 200 µm, in **G** 5 µm.*

In the nerve-muscle explant complete photo-conversion of mito-Dendra requires 40 seconds of UV-exposure. Just as mito-Kaede, further UV-exposure bleaches the protein. However, in comparison to mito-Kaede, mito-Dendra provides higher contrast: a 38-fold gain in red fluorescence and 42-fold increase in Red/Green Ratio was detected after photo-switch.

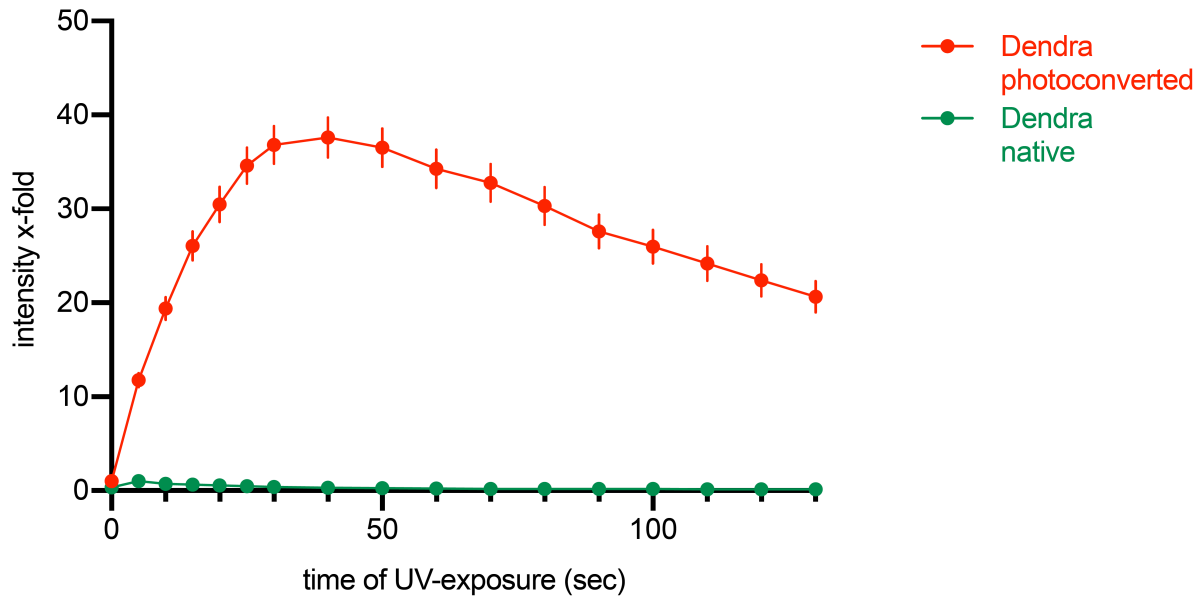

Fig. 4.9 Photo-conversion characteristics of mito-Dendra ex vivo

The dose-response graph was created by subsequent exposition of NMJs to pulses of UV-light (405nm) in the acute nerve-muscle explant of Thy1-mito-Dendra 4 (n=12, 3 animals). Some error bars are hidden by the data symbols.

4.1.4 Comparison of photo-transformation characteristics ex vivo

In order to select the most suitable line for studying axonal transport of mitochondria in motoneurons, we compared the photo-transformable proteins and their characteristics in the nerve muscle explant. The graph below (Fig. 4.10) summarizes intensity produced by photo-transformation vs UV-exposure of mito-Kaede, mito-Dendra and mito-paGFP. Mito-paGFP (47-fold increase in green fluorescence) produces more contrast than mito-Dendra (38-fold gain in red fluorescence). Both proteins are clearly better than mito-Kaede: in comparison to mito-Kaede, the increase in fluorescence is more than fourfold in mito-Dendra and more than fivefold in mito-paGFP.

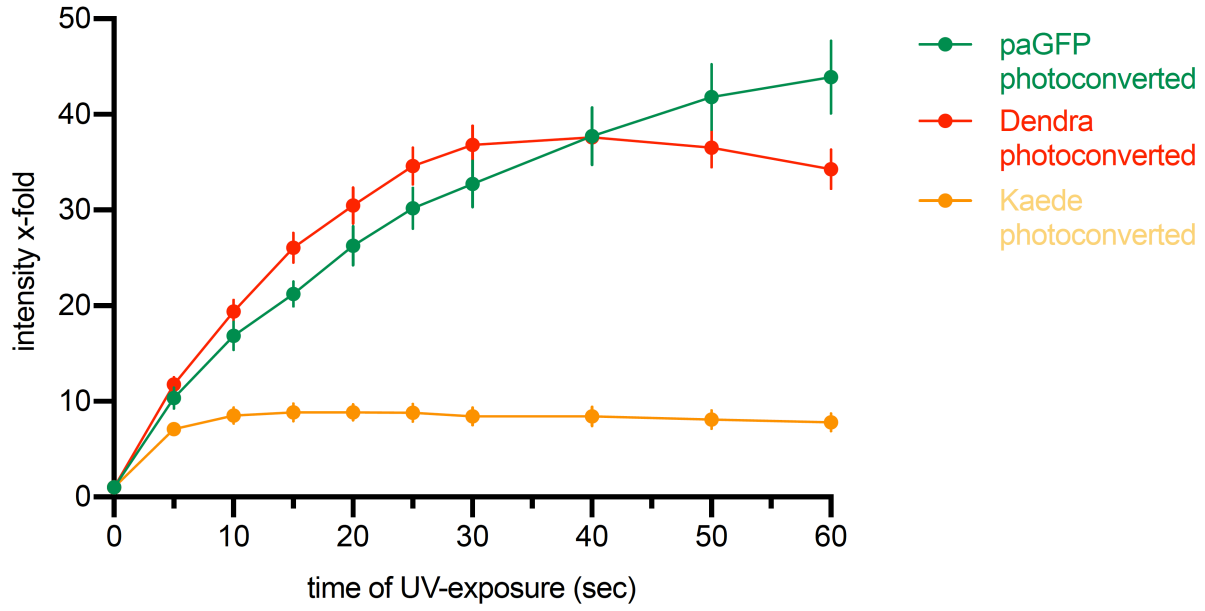

Fig. 4.10 Photo-transformation characteristics of mito-paGFP, mito-Kaede and mito-Dendra ex vivo

Comparison of photo-transformation graphs of the three proteins in the thoracic nerve-muscle explant: mito-Dendra and mito-paGFP produce higher contrast than mito-Kaede. Mito-paGFP requires more than double of the UV-exposition for maximal photo-transformation (100 sec) than mito-Dendra (40 sec), whereas Kaede produces maximal contrast after 15 seconds of photo-transformation. Some error bars are hidden by the data symbols.

However, these data have to be critically regarded considering phototoxicity and -efficiency. During live imaging the exposure of light, especially UV light, should be minimized, to avoid potentially phototoxic damages. Fig. 4.10 shows, that in the range of 0 - 40 seconds of UV-exposure, mito-Dendra provides a higher increase in fluorescence than mito-paGFP. Only at more than 40 seconds of UV-exposure mito-paGFP produces more contrast than mito-Dendra. Hence the full capacity of mito-paGFP requires a very long time of UV-exposure, risks phototoxic damages and is unlikely to be applied for live imaging.

mito-Kaede provides the fastest photo-transformation with maximal photo-conversion after 15 seconds. However, even after 15 seconds of UV-exposure, mito-Dendra and mito-paGFP, both not being fully photo-transformed, produce more contrast than mito-Kaede. Besides the poor contrast, the dim expression in the native state of Thy1-mito-Kaede is disadvantageous for imaging.

In conclusion, we favored Thy1-mito-Dendra and Thy1-mito-paGFP over Thy1-mito-Kaede for live imaging in the acute nerve-muscle explant. In terms of photo-efficiency and contrast Thy1-mito-Dendra is also slightly better than Thy1-mito-paGFP ex vivo. As Thy1-mito-paGFP is less prone to

bleaching this line has its advantage on long imaging sessions or when imaging with more light or laser (e.g. confocal microcopy) is needed.

Beyond the above characteristics, the difference of “photo-conversion” and “photo-activation” plays a fundamental role in the selection of the respective mouse lines: in photo-convertible mouse lines, e.g. Thy1-mito-Kaede and Thy1-mito-Dendra, mitochondria are single colored fluorescent either in native (‘green’) or photo-converted (‘red’) state. In contrast, organelles labelled with paGFP can only be displayed after photo-activation. In the double transgenic line Thy1-mito-paGFP x Thy1mito-tagRFP all mitochondria are ‘red’, and following photo-activation a fraction of the organelles is in addition ‘green/red’ (Fig. 4.11). This crossbreeding facilitates a stable labelling of all organelles as well as the possibility to photo-activate mitochondria and image these organelles simultaneously in both channels.

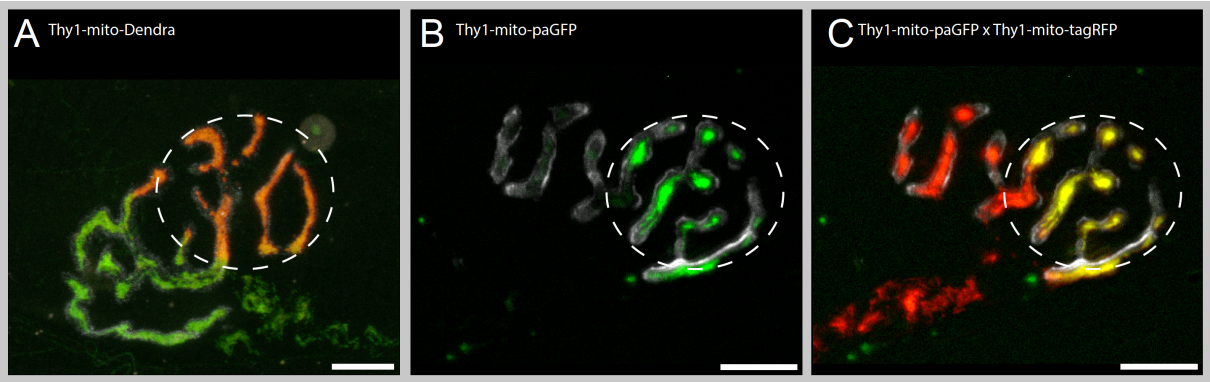

Fig. 4.11 “Photo-conversion” versus “photo-activation” in NMJs ex vivo

NMJs of different transgenic mouse lines were photo-transformed with UV-light (dashed circles) in acute nerve-muscle explants. In all pictures postsynaptic receptors are stained with bungarotoxin (grayscale).

***A)** Photo-conversion in Thy1-mito-Dendra: native (green), photo-converted (red). Organelles can be imaged either in the native or photo-converted state. **B)** Photo-activation in Thy1-mito-paGFP: native (not visible), photo-activated (green). Only photo-activated organelles are visible. **C)** Imaging in double transgenic mice (Thy1-mito-paGFP x Thy1-mito-tagRFP): tagRFP (red), paGFP activated (green). All organelles are labelled with mito-tagRFP, photo-activated mitochondria can be imaged simultaneously in red and green fluorescence (yellow= merge of red and green fluorescence). Scale bar 10 µm in all pictures. Figure B and C were provided by courtesy of N. Marahori.*

Due to its good contrast and fast photo-conversion I selected Thy1-mito-Dendra for the transport studies ex vivo (see 4.2.2).

4.2 Mitochondrial trafficking in motoneurons

In the second part of this work, the transgenic mouse lines were used to study the relationship of anterograde and retrograde axonal transport (4.2.1) and to analyze mitochondrial distribution within one motoneuron (4.2.2).

4.2.1 Mitochondrial size in antero- and retrograde transport

Various prior studies have measured transport rates in different models and species (see below). Although the rates differ, one striking characteristic is consistent: anterograde organelle flux exceeds retrograde flux. In all studies listed below the ratio anterograde to retrograde flux is ≥ 1.5.

Species/ preparation	**Ratio flux antero/flux retrograde**	**Reference**
Drosophila larva intersegmental nerve	1.5	(Pilling et al. 2006)
D. rerio Rohon Beard neurons	1.7	(Plucińska et al. 2012)
Mus musculus intercostal nerve	1.9	(Misgeld et al. 2007)
Mus musculus tibialis nerve	3.2	(Gilley et al. 2012)
Mus musculus sciatic nerve	2.7	(Bilsland et al. 2010)

Table 7 Anterograde to retrograde ratio of mitochondrial flux measured in different in vivo studies (modified from Misgeld and Schwarz, 2017)

Considering the complexity of the mitochondrial life-cycle, there are at least two different hypotheses to explain this bias in transport rates. First, fewer mitochondria could return due to an actual decrease in mitochondrial mass: organelles could be removed in the axonal arbor or in synapses. Second, mitochondria could fuse in distal axons, resulting in fewer, but larger organelles returning to the soma. To test this, I explored, whether the retrogradely moving mitochondrial populations differ not only in quantity but also in size. To this end I analyzed the organelles' shape in movies of mitochondrial transport in nerve-muscle explants of Thy1-mito-Kaede, that were recorded for a

previous study by Petar Marinković (Marinkovic et al. 2012): I quantified length, area and diameter of photo-converted anterograde and retrograde moving organelles, namely the ones moving out of the photo-converted area (Fig. 4.12). The contrast provided by photo-conversion eased the differentiation from the background. With my measurements I calculated mitochondrial volume and shape factor (= ratio length/diameter).

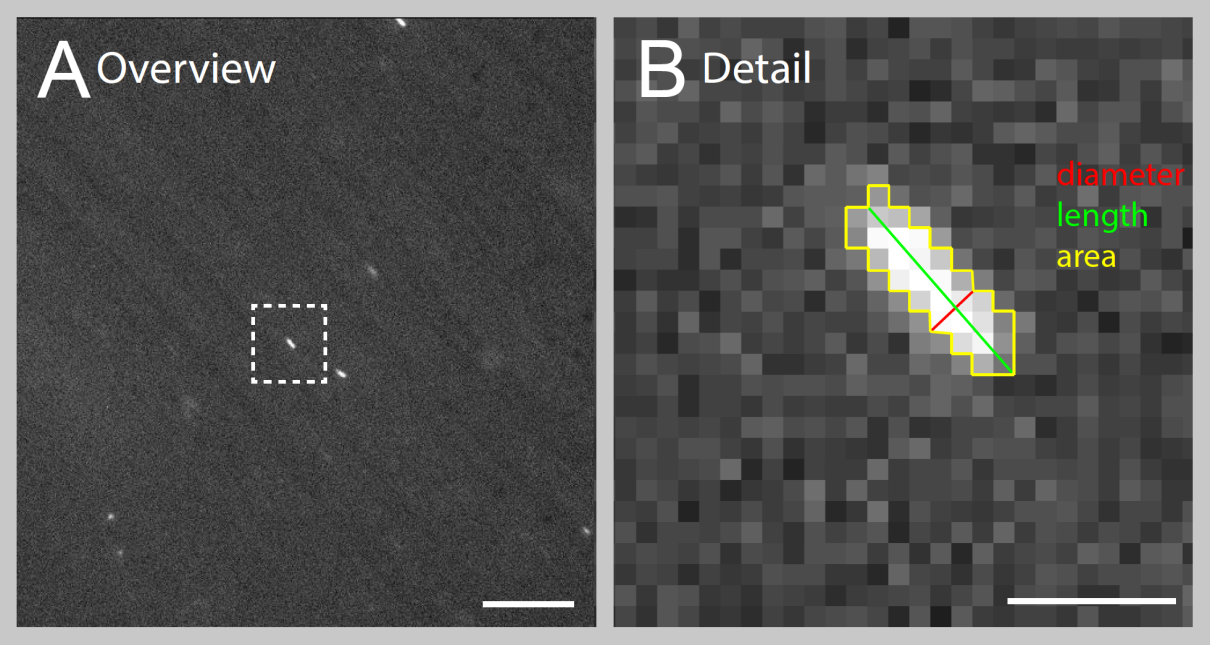

Fig. 4.12 Measurements of mitochondrial shape in nerve-muscle explants of Thy1-mito-Kaede

***A)** Photo-converted mitochondrion (in dashed rectangle) in an axon of the nerve-muscle explant (Thy1-mito-Kaede). Scale bar 10 µm. **B)** Zoom-in of the photo-converted mitochondrion. Diameter (red), length (green) and area (yellow) were measured. Scale bar 1 µm. Picture A and B were provided by courtesy of P. Marinković.*

In total mitochondrial size was determined in n= 127 mitochondria (six mice) in anterograde and n= 95 mitochondria (five mice) in retrograde transport (Fig. 4.13). In my dataset retrograde mitochondria are slightly, but significantly longer (anterograde 1.44 +/- 0.06 µm vs retrograde 1.62 +/- 0.08 µm). The organelles' diameter did not differ (anterograde 0.52 +/- 0.003 µm vs retrograde 0.52 +/- 0.01 µm). Consequently also the shape factor differed significantly (anterograde 2.74 +/- 0.12 vs retrograde 3.1 +/- 0.15). The measurements of mitochondrial area showed again that retrograde organelles are significantly larger (anterograde 0.54 +/- 0.03 μm^2 vs retrograde 0.63 +/- 0.03 μm^2).

However, when these results were used to calculate the volume of the organelles, no significant difference was detected (anterograde 0.32 +/- 0.02 μm^3 vs retrograde 0.36 +/- 0.02 μm^3).

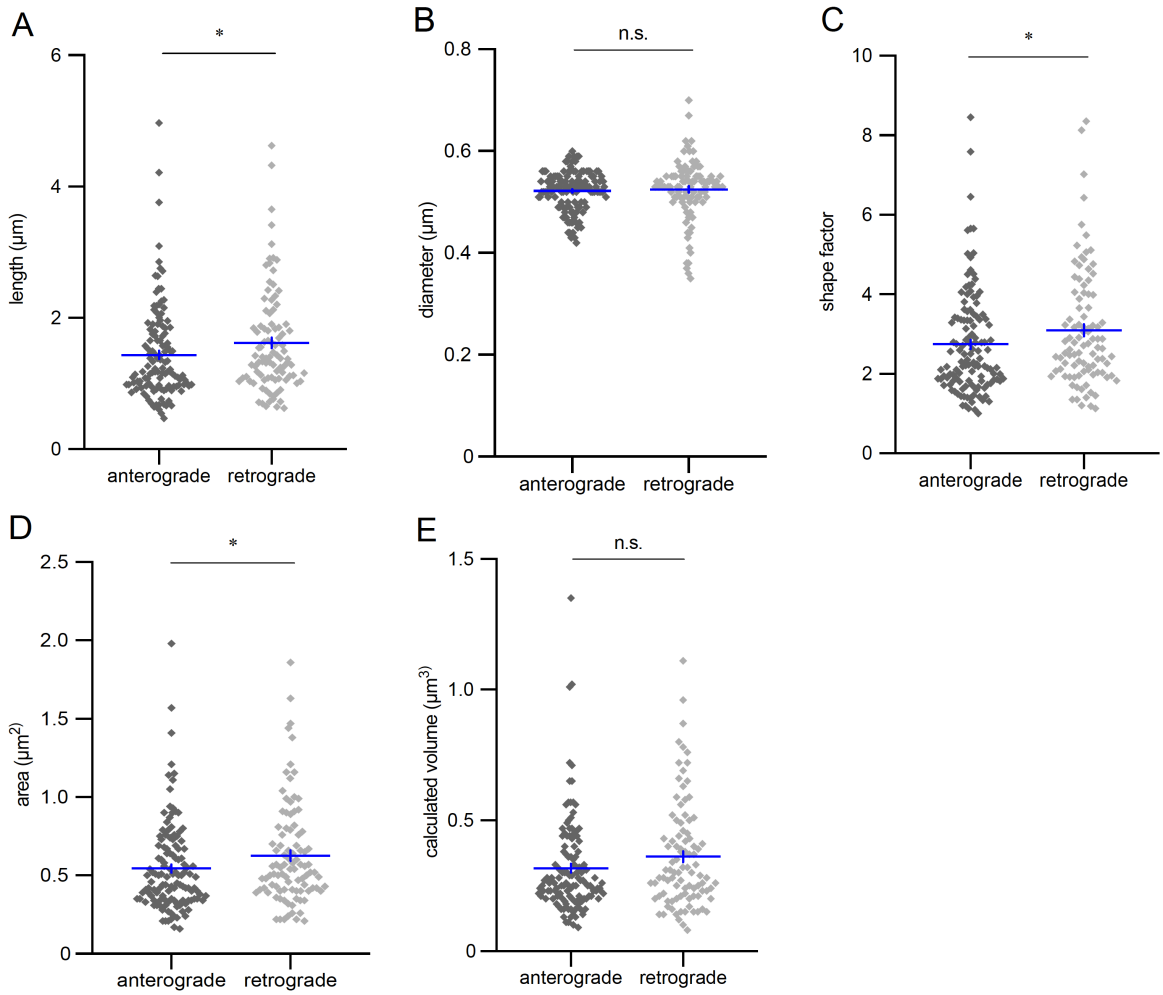

Fig. 4.13 Measurements of mitochondrial shape in the anterograde and retrograde moving population

*Length **(A)**, diameter **(B)** and area **(D)** were quantified in mitochondria imaged in the acute nerve-muscle explant. (anterograde n= 127, 6 mice; retrograde n= 95, 5 mice) Shape factor **(C)** and volume **(E)** was calculated as described in 3.8.* = P<0,05, n.s. = not significant.*

In conclusion, compared to the anterograde population length is 12 %, shape factor 13 % and area 17 % higher in the retrograde population. Can these differences compensate the bias in transport rates? In a next step I combined my data with the rates of organelle flux: moving mitochondrial volume was calculated by multiplying mitochondrial volume by mean transport rates of a previous study in the thoracic nerve-muscle explant (Misgeld et al. 2007). Despite the detected differences in shape the moving mitochondrial volume in anterograde transport still significantly exceeds retrograde moving volume (anterograde 1.87 +/- 0.09 µm^3/min vs retrograde 1.12 +/- 0.06 µm^3/min). Hence the

discrepancy in transport rates cannot be evened out by the detected differences in organelle "mass": a significant portion of mitochondrial mass might disappear in motor axon branches. The question, where and how this degradation takes place will be discussed in 5.3.

4.2.2 Pulse chase imaging of mitochondria in acute nerve-muscle explants

The overall life cycle regulation of mitochondria in motoneurons has not been elucidated. The transport of anterograde organelles has an evident rational: mitochondrial biogenesis occurs mainly in the soma (see 1.1.1), so mitochondria have to be transported and distributed throughout the cell. But what about the organelles in retrograde transport? We do not know, when and why mitochondria return to the soma. "Aged" organelles could return for degradation (Miller and Sheetz 2004) or redistribution after repair (Mandal et al. 2021) .Yet these theories have not been conclusively confirmed and there is growing evidence for local degradation (see 1.1.3) and biogenesis (see 1.1.1). Contrariwise mitochondria could also recirculate in the axon and only sporadically enter synapses if required. This "conveyor belt model" model has been proposed for the delivery of synaptic vesicles in Drosophila (Wong et al. 2012) (see 1.2.3).

In the next set of experiments I used Thy1-mito-Dendra transgenic mice, to observe mitochondrial delivery in motoneurons. Specifically I wanted to test the "conveyor belt model" for mitochondrial transport in motoneurons: do organelles recirculate and only sporadically enter synapses? The feature of photo-conversion was utilized to perform live pulse chase imaging in the acute nerve-muscle explant: a "pulse" of mitochondria was photo-converted and "chased" (=imaged) during transport in the neuron.

For the design of these experiments an important aspect had to be taken into account: during the preparation of the nerve-muscle explant, the cell bodies are dissected, so the explant has a limited lifespan (Kerschensteiner et al. 2008). Monitoring of potential recirculation requires prolonged imaging duration for several hours. To verify that the explant was stable for this long time window I performed control measurements of transport in the distal axon (Fig. 4.14, Panel A). Due to a significant drop in transport rates after 300 min, I limited my imaging time to 240 min (Fig. 4.14, Panel B).

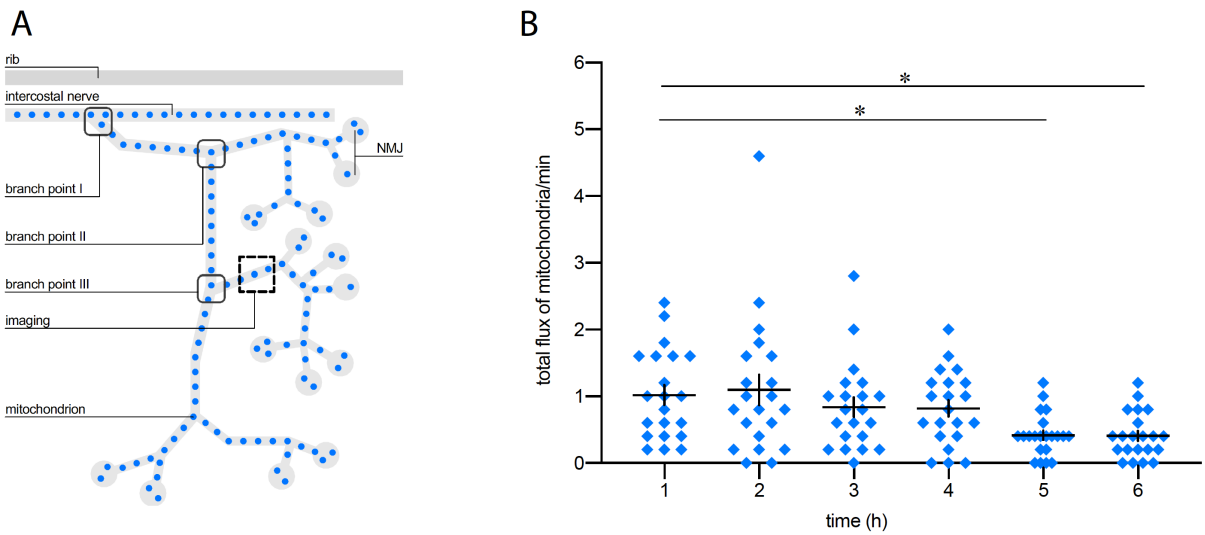

Fig. 4.14 Monitoring transport rates in the thoracic nerve-muscle explant in Thy1-mito-CFP C

A) *Schematic of the intercostal nerve in the nerve-muscle explant. Typical branch points and the imaging spot of the transport control measurements are labelled.* ***B)*** *Results of the control measurements of axonal transport in the distal part of the intercostal nerve in Thy1-mitoCFP C show a significant drop in the total transport after 5 hours. (n = 22 axons from 1 animal). * = p < 0,05.*

4.2.2.1 Pulse chase imaging in the axon

In the first experiment I monitored axonal mitochondria for recirculation: I photo-switched a segment of the fascicle and measured the transport of photo-converted mitochondria at a more distal imaging point (Fig. 4.15, Panel A). First the anterograde flux of the photo-converted population was imaged “passing by”. According to the “conveyor belt model” photo-switched mitochondria would recirculate and appear as retrograde moving mitochondria at the imaging point.

During the imaging time of the experiment only one percent of the photo-converted mitochondria returned. In three independent experiments, 1154 photo-converted mitochondria were recorded in anterograde transport, whereas in total 12 photo-converted organelles returned (Fig. 4.15, Panel B).

These results suggest that a negligible fraction of mitochondria turn around in the axon during our four hour imaging session. Although the data cannot exclude circulation of mitochondria at synapses, there seems to be no evidence for major mitochondrial exchange. However, due to the lifespan of the explant, I cannot exclude that more mitochondria are returning later on.

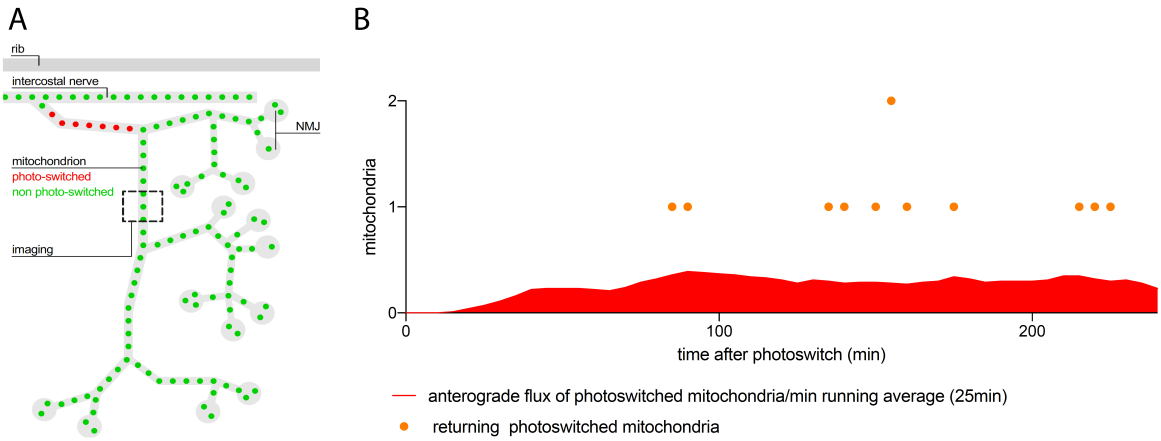

Fig. 4.15 Pulse chase imaging in axons of the nerve-muscle explant

***A)** Schematic of pulse imaging in the axon of Thy1-mito-Dendra-mice: after photo-conversion of mitochondria in the axon, the anterograde flux of photo-switched (red) mitochondria and potentially recirculating photo-switched mitochondria in the retrograde population were imaged. **B)** Results of the pulse chase imaging illustrating the flux of the photo-converted anterograde population (red) and the few individual returning photo-switched mitochondria (orange). (n=18 axons from 3 pulse chase experiments of 3 animals)*

4.2.2.2 Pulse chase imaging at synapses

In a second experiment pulse-chase imaging was performed, to observe the movements of single mitochondria at synapses. In a “conveyor belt model” mitochondria would frequently turn around before and at the NMJ.

After photo-conversion of a distal branch of the intercostal nerve in Thy1-mito-Dendra mice, imaging of photo-switched mitochondria was performed at synapses (Fig. 4.16, Panel A). In total four synapses of four different animals were observed: eight mitochondria could be imaged for an average time of 39 +/- 5min after entering the synapse. Every mitochondrion remained in the NMJ, no turn-arounds or immediate exits were recorded (Fig. 4.16, Panel B).

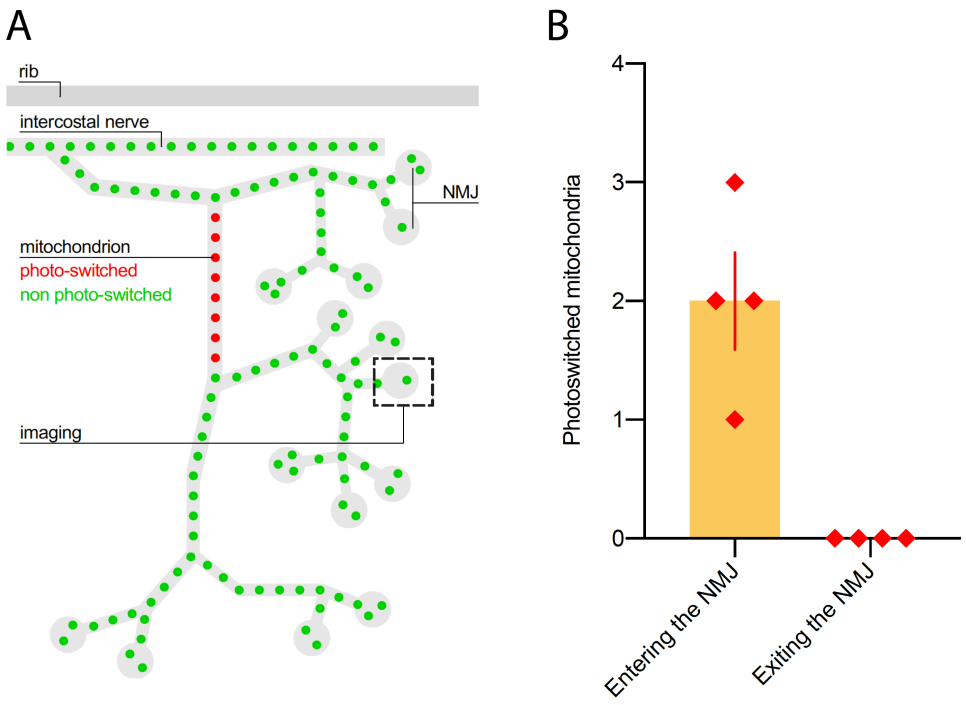

Fig. 4.16 Pulse chase imaging of mitochondria at synapses

A) *Schematic of pulse chase imaging at the NMJ in the thoracic nerve-muscle explant of Thy1-mito-Dendra-mice: after photo-conversion of mitochondria in the axon, single photo-switched organelles were imaged in synapses.* ***B)*** *Recordings of photo-converted mitochondria at the NMJ showed, that all mitochondria remained for 39 +/- 5 min after their entry in the NMJ. No immediate exits or turnovers were recorded. (n= 8 mitochondria from 4 NMJs from 4 animals)*

As only flat and superficially located NMJs offer good conditions for continuous imaging, many mitochondria could not be tracked. Due to the small sample size this experiment cannot make a definite statement concerning the “conveyor belt model”. Yet the results suggest, that short-term mitochondrial turn-overs after entry of the NMJ are rare.

Regarding my pulse-chase data we can conclude, that the delivery of mitochondria seems not to follow strictly the “conveyor-belt-model”. It is more likely, that the organelles join the pool of stationary mitochondria by fusion or anchoring in axons or synapses. When and if they return to the soma, has to be further investigated (see also 5.3).

5 Discussion

In this work I used the transgenic expression of different photo-transformable fluorescent proteins to study mitochondrial transport and size in an acute murine nerve-muscle explant. To this end, we generated novel mouse lines (Thy1-mito-paGFP and Thy1-mito-tagRFP) and compared their properties during live imaging with preexisting lines (Thy1-mito-Dendra and Thy1-mito-Kaede mouse (Marinkovic et al. 2012)). In a second step I established "pulse chase" imaging in the nerve-muscle explant: following cohorts of photo-transformed mitochondria, I demonstrated, that the organelles do not circulate in motor axon branches, but likely join the stationary pool of pre-existing mitochondria.

5.1 Photo-transformable proteins in the thoracic nerve-muscle explant

With this study I provide the first systematic characterization of several photo-transformable proteins during live imaging of murine neuronal mitochondria. The proteins' fluorescent properties have been studied in cell culture (Lukyanov et al. 2005) and in a comparative study of photo-transformable proteins (amongst them Kaede and paGFP) in an in vivo chick embryo model (Stark and Kulesa 2007). Since 2012 also three different mouse lines with the expression of photo-convertible proteins (Kaede and Dendra) in mitochondria have been published (Magrané et al. 2012, 2014, Marinkovic et al. 2012, Pham et al. 2012) (Table 8).

Line	Reference	Expression	Live imaging	Mode of imaging/ *photo-activation*
Thy1-mito-Kaede	Marinkovic et al. 2012	Neuronal mitochondria	Acute explants of intercostal, saphenous and tibialis nerve	Widefield setup *405 nm LED light (5 sec)*
Thy1.2-mito-Dendra2	Magrané et al. 2012/2014, Bolea et al. 2014	Neuronal mitochondria	In vivo imaging of sciatic and femoralis nerve, soleus muscle (NMJs)	Confocal microscope *488 nm Laser (7,5 mW) for 1 min*

Line	Reference	Expression	Live imaging	Mode of imaging/ *photo-activation*
PhAM^{floxed} **PhAM^{excised}**	Pham et al. 2012	**floxed:** conditional mitochondrial expression **excised:** ubiquitous mitochondrial expression	Live mouse sperm Myofibers, Cardiomyocytes M. extensorum digitorum longus explant Cerebellar slices	Confocal microscope *405 nm Laser (4 %) 90 bleaching iterations*

Table 8 Up-to-date published mouse lines expressing photo-convertible proteins in mitochondria: imaging and photo-switch modes.

However, these studies (Magrané et al. 2012, 2014, Marinkovic et al. 2012, Pham et al. 2012) used diverse in vivo preparations and did not determine or compare the properties of photo-transformation and imaging. Hence there is few knowledge considering live imaging of neuronal mitochondria. In my dataset I characterized the proteins' fluorescence properties during imaging in the acute nerve-muscle explant with a focus on contrast and photo-efficiency. My results revealed, that both mito-paGFP and mito-Dendra produce a considerably higher increase in fluorescence after photo-transformation than mito-Kaede (see Fig. 4.10). Strikingly, some of my findings are consistent with the previously published data in vitro and in vivo, whereas other observations differ relevantly (Table 9):

Kaede provides the fastest photo-transformation in all preparations (Ando et al. 2002, Stark and Kulesa 2007). Also paGFP's comparably slow, monotonically increase in fluorescence during photo-activation is reproducible (Patterson and Lippincott-Schwartz 2002, Stark and Kulesa 2007). However, compared to cell culture and the chick embryo model I detected a generally lower increase in contrast in all proteins ex vivo (Table 9). One observation was striking: Kaede provides the highest increase in contrast in vitro, whereas in the nerve-muscle explant both mito-Dendra and mito-paGFP are clearly superior.

Protein/ Model/ Reference	Activating light	Duration of photo-activation	Increase in intensity
paGFP			
In vitro (COS7 cells) Patterson and Lippincott-Schwartz, 2002	413nm laser light (4000 W/cm^2)	1 sec	>60 fold
In vivo chick embryo model Starck and Kulesa, 2007	405nm laser (44W/µm)	7,5 min	200 fold
Live imaging: acute nerve-muscle explant (Thy1-mito-paGFP N877)	405nm LED light (23 W/cm^2)	100 sec	47 fold
Kaede			
In vitro (HeLa cells) Ando et al., 2002	400nm (Xenon lamp, 1,6 W/cm^2)	50 sec	800 fold
In vivo chick embryo model Starck and Kulesa, 2007	405nm laser (44W/µm)	25 sec	N/D
Live imaging: acute nerve-muscle explant (Thy1-mito-Kaede)	405nm LED light (23 W/cm^2)	15 sec	9 fold
Dendra			
In vitro (HelLa cells) Gurskaya et al., 2006	488nm laser light (1,4 W/cm^2)	2-5 sec	150-300 fold
Live imaging: acute nerve-muscle explant (Thy1-mito-Dendra 4)	405nm LED light (23 W/cm^2)	40 sec	38 fold

Table 9 Comparison of photo-transformable proteins in vitro and in vivo

Properties of paGFP, Kaede and Dendra in vitro and during live imaging of chick embryos and in murine neuronal mitochondria. N/D not determined. Results of my study are labelled with green. N. Marahori performed the measurement of the "power at sample" at our setup and kindly provided the data.

Still, there is no definite reason for mito-Kaede's unfavorable properties in the nerve-muscle-explant, as the data are difficult to compare in many respects:

- The proteins are obviously expressed and imaged in diverse tissue and preparations: in my live dataset the proteins are expressed in transgenic mice in neuronal mitochondria. In contrast in

the chick embryo model the proteins were transferred to cells via electroporation and the in vitro data results represent the proteins' expression in different cell cultures. We cannot exclude, that the transgenic expression and the cellular and sub-cellular surroundings variably affect the proteins' fluorescent properties.

- The preparation of the nerve-muscle explant has to be taken into consideration. Although I tried to minimize the exposition of light during the dissection of the nerve-muscle explant, a basal photo-transformation could be a reason for the by comparison reduced increase in fluorescence after photo-transformation.
- The mode of photo-transformation varies: only in my dataset photo-transformation was consistently performed with a 405 nm LED light. In the other studies diverse wavelengths and sources of light were used for photo-transformation (Table 9).

In any case, the differences observed between these studies emphasize the importance of my findings: especially for live imaging, the knowledge of the fluorescent properties in the specific preparation is required to choose the mouse line/ photo-transformable protein suitable for the experiment and optimize imaging and photo-switch conditions.

Regarding my data, also the mode of photo-transformation has to be critically discussed. In my experiments photo-transformation was performed with UV-light. Exposure to these wavelengths has been shown to negatively influence cell division in whole mount Drosophila embryos (Post et al. 2005), hence we have to consider potential phototoxic damages. Although previous studies (Marinkovic et al. 2012, Magrané et al. 2014) did not observe a disturbance in transport after photo-conversion, further studies, assigning a threshold dose of UV-light for intact mitochondrial transport during live imaging, are required.

However, there are possibilities to avoid the use of UV-light, which have not been tested in this study. Post et al. showed, that in contrast to UV-light, exposition of 488 nm light did not compromise cell division in Drosophila embryos. Dendra can be photo-switched by 488 nm light, so further data are required to evaluate this technique during live imaging.

Two-photon laser scanning microscopy uses pulsed lasers in the near infrared wavelength and is another important option for photo-transformation. In contrast to widefield or confocal microscopy, multiphoton excitation occurs only at the beam focus and offers diverse advantages. The relatively deep optical penetration and reduced ability to cause nonspecific phototoxicity make it ideal for live imaging (Helmchen and Denk 2005). With this technique, a three-dimensionally defined volume can be photo-transformed, which allows a spatially confined labeling of tissue.

Successful photo-transformation by a two photon laser has been reported for paGFP (Post et al. 2005, Schneider et al. 2005) and Kaede (Watanabe et al. 2007).The technique has been used in diversity of studies, covering live imaging of cells (Watanabe et al. 2007, Smith et al. 2011), zebrafish (Clanton et al. 2011, Dal Maschio et al. 2017), Drosophila (Post et al. 2005) and mice (Chtanova et al. 2014). To date the two-photon photo-transformation of Dendra has not been studied. Two-photon-imaging might be another option for live imaging of photo-transformable proteins and conditions of photo-transformation and imaging should be evaluated in further studies.

5.2 Mitochondrial size in antero- and retrograde transport

Misgeld and Schwarz (2017) have reviewed in detail, that the discrepancy in antero- and retrograde axonal transport has been observed in almost all in vivo studies across various species and neuronal populations (see Table 7). An explanation for this bias could be that mitochondria fuse in distal axons and if whole organelles are initiating their retrograde journey, they would be fewer and larger. In this context the size of the single organelles becomes important and was determined in this work. My dataset covers mitochondrial length, diameter and area, measured in the nerve-muscle explant of Thy1-mito-Kaede mice. These measurements were used to calculate shape factor, mitochondrial volume and transported mitochondrial volume. My results revealed, that retrograde mitochondria are slightly but significantly larger, concerning length and area, in addition the shape factor of the retrograde population is significantly higher (see 4.2.1). Regarding the diameter and the calculated volume I did not detect a significant difference in the two populations. Still, the larger retrograde mitochondria do not balance the bias in transport rates: significantly more mitochondrial volume is transported anterogradely.

Several previous studies addressed the size of mitochondria in transportation: a common observation was, that retrograde mitochondria are slightly, yet not always significantly larger (Table 10). In an early study in lobster motor axons as well as in the first study in the murine thoracic nerve-muscle explant retrograde mitochondria were longer, yet the statistical significance of this difference has not been addressed (Forman et al. 1987, Misgeld et al. 2007). Anyway, my measurements of mitochondrial length resemble the results of the earlier study in the same model (Misgeld et al. 2007), emphasizing its reproducibility. Other studies in Drosophila and zebrafish did detect a slight, yet not significant shift of higher length and volume towards retrograde mitochondria (Pilling et al. 2006, Plucińska et al. 2012).

Species/ preparation	Length (µm)	Volume (µm³)	Reference
Homarus americanus leg nerve	ant: 5.5 ret: 6.9	-	(Forman et al. 1987)
Drosophila larva intersegmental nerve	ant: 0.91 ret: 1.08	-	(Pilling et al. 2006)
D. rerio Rohon Beard neurons	-	ant: 0.21 ret: 0.23	(Plucińska et al. 2012)
Mus musculus intercostal nerve	ant: 1.47 ret: 1.69	-	(Misgeld et al. 2007)
Mus musculus intercostal nerve (Thy1-mito-Kaede)	ant: 1.44 ret: 1.62	ant: 0.32 ret: 0.36	This study

Table 10 Mitochondrial size in antero- and retrograde transport (modified from Misgeld and Schwarz 2017)

ant= anterograde, ret= retrograde. Results of my study are labelled with green.

However, for the interpretation of these data it is crucial to consider the resolution of light or fluorescence microscopy and the organelle size. According to the Abbe Diffraction Limit (d= λ/2NA) the resolution limit of imaging photo-converted Kaede is at 270 nm. Yet, studies using electron microscopy reveal, that also smaller organelles exist: an analysis of murine hippocampal mitochondria showed, that 11 % of non-somatic mitochondria were smaller then 200 nm, 39 % measured between 200-400 nm (Mukherjee et al. 2016). Hence it is likely that in my results very small organelles are not correctly represented. It has to be questioned, whether the detected differences between anterograde and retrograde organelle shape are correct and could possibly derive from altered organelle quality or fusion processes or arise from the described measuring inaccuracy.

The required resolution exceeds the resolution capacity of conventional light- and fluorescence microscopy. Of course, electron microscopy can provide resolution at nanometers and ultrastructural characterization of organelles (Perkins and Frey 2000). Yet, this technique cannot be used to image live specimens and hence stationary and moving mitochondria cannot be distinguished. Although correlated light electron microscopy (Bishop et al. 2011) allows the re-identification of single organelles in electron microscopy, it is hardly feasible, to collect a large sample size of mitochondrial shape parameters with this complex and time-consuming technique. The difficulty of live imaging in

nanometer resolution may be overcome by the novel fluorescence microscopy methods: super-resolution techniques including the patterned-illumination-based methods (e.g. STED, RESOLFT) and single-molecule-switching-based methods (e.g. STORM, PALM) provide a spatial resolution from 10 to 70 nm in biological systems (Sigal et al. 2018). Mitochondria have been imaged in live cells at a resolution of 30 nm with STORM microcopy (Shim et al. 2012). Nanometer-resolution imaging in tissues remains challenging, but further improvements could provide insights on mitochondrial morphology changes in anterograde- and retrogradely moving mitochondria.

Despite the minor measuring inaccuracies, my dataset clearly confirms the hitherto observed bias in transported mitochondrial volume between anterograde and retrograde direction: significantly more mitochondrial volume is transported in the anterograde direction. Which mechanisms could cause this discrepancy? We have to assume, that mitochondrial material is either degraded locally or transported retrogradely in for example vesicles or lysosomes, that are not detected as mitochondrial transport. This complex interaction of transport and quality control will be revisited in 5.3.

5.3 Retrograde transport and mitochondrial trafficking

For our understanding of mitochondrial delivery it is crucial, to decode the composition of retrograde transport: which mitochondria return to the soma and what is their fate?

With my pulse-chase experiments, I tried to decipher if immediate recirculation of organelles could play a role in the composition of the retrograde mitochondrial pool. Following photo-conversion and organelle tracking in the thoracic nerve-muscle explant, I detected one percent of mitochondria recirculating within the axon (Fig. 4.15) and no turn-arounds at neuromuscular synapses (Fig. 4.16). However, we have to consider the limitations of these datasets: a critical point of the pulse chase imaging in the axon is the imaging window in axotomized motor axons. Previous publications limited the imaging duration in the acute nerve-muscle explant to two hours (Kerschensteiner et al. 2008). I performed imaging for up to four hours, as my transport control experiments in the distal axon showed stable transport rates (Fig. 4.14). The most distant NMJs of the nerve are located in an estimated distance of 50 to 60 µm from the photo-transformation spot. Assuming velocities as in previous publications, anterograde mitochondria travel at peak velocities of 1.02 µm/s, retrograde organelles at 1.41 µm/s (Misgeld et al. 2007). Hence peripheral recirculation should be detected in my experimental setting, if the mitochondria do not pause for longer intervals at axons or synapses before they turn around. Still, a more complex setting such as an in vivo preparation, e.g. the sciatic nerve

(Misgeld et al. 2007) could facilitate even longer observation periods.

Considering the pulse chase data at synapses the low sample size owing to the difficult tracking of organelles into NMJs is critical (see 4.2.2.1). In my experiments mitochondria were photo-converted in axons and then tracked, until they entered a synapse. An alternative, "inverse" experiment could make it easier, to observe mitochondria at synapses: after photo-conversion of a synapse, the spectral characteristics of entering and exiting organelles can be observed at the entry point. (Fig. 5.1). With this design, one could choose a synapse that is convenient for imaging and avoid the protracted and partly ineffective tracking of mitochondria, until they enter a synapse.

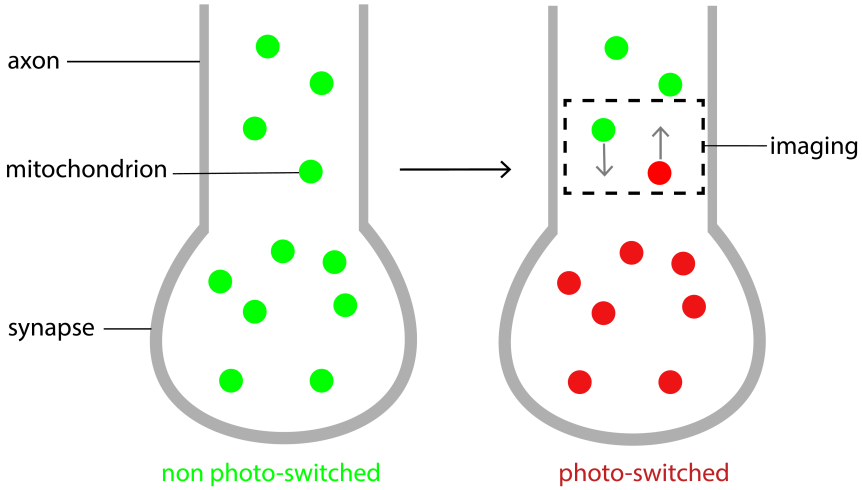

Fig. 5.1 Schematic of a potential photo-conversion experiment at synapses

After photo-conversion of the synaptic mitochondria, imaging is performed at the entry point of the synapse: the spectral characteristics of organelles entering and exiting the synapse can be tracked. Non photo-converted (green) mitochondria can be observed after the entry of the synapse, to monitor potential short-term recirculation.

But which conclusions can be drawn from my findings? My data on mitochondrial delivery show that short-term-recirculating organelles do not play a major role in the mitochondrial pool of retrograde transport. Anyway, the fate of retrograde mitochondria is still ambiguous and we have to take account of different, maybe coexisting possibilities:

- Dysfunctional mitochondria could return towards the soma for degradation (Miller and Sheetz 2004, Cai et al. 2012, Lin et al. 2017).
- Organelles could be redistributed, probably after replenishment through either protein import or fusion with newly synthesized mitochondria (Mandal et al. 2021).

- Recirculation might still be possible: I found, that anterogradely delivered mitochondria remained in the axon's periphery for > 4 hours and at synapses for > 39 min. The organelles could explore synaptic sites for longer than these time intervals and recirculate afterwards.

Mitochondrial local biogenesis, fusion and fission as well as diverse and multilocated degradation mechanisms add another layer of complexity on understanding if young or old, freshly fused or divided mitochondria are moving. There is convincing evidence for local biogenesis of mitochondrial proteins in vitro (Aschrafi et al. 2016) as well as in Xenopus retinal ganglion cells in vivo (Shigeoka et al. 2016, Cioni et al. 2019). A portion of peripheral mitochondria could be maintained and rejuvenated by local protein synthesis, so that not all organelles have to be transported back to the soma. However, it is not clear, to what extent somatic and peripheral protein synthesis contribute to mitochondrial biogenesis.

Fusion and fission events may have a share in the local maintenance of the peripheral mitochondrial pool: dysfunctional mitochondria can fuse with healthy organelles and subsequently undergo fission to distribute components. These dynamic events could also help to isolate damaged mitochondrial material (Youle and van der Bliek 2012) and reduce the number of organelles, that are transported back to the soma.

Lastly mitochondrial delivery cannot be decoded without understanding the complex degradation machinery. Several local mechanisms could account for the detected excess of anterograde mitochondrial volume: there is evidence for local mitophagy (Ashrafi et al. 2014) and the consequential arrest of mitochondrial movement by degradation of Miro (Wang et al. 2011). Presumably, also degradation by mitochondrial proteases and shedding of MDVs can occur anywhere in a cell (see 1.1.3). We also have to consider a basal rate of macroautophagy: mitochondrial fragments are transported retrogradely within autophagosomes or lysosomes. Due to the pH-dependent quenching of fluorescent proteins it is unlikely, that these fragments are detected as mitochondrial flux. Irrespective to the localization, we still do not know, to what extent these different pathways contribute to mitochondrial degradation in intact neurons and how organelles are "selected" for these pathways.

Of course, these observations of local quality control and rejuvenation do not exclude, that other damaged organelles could be transported retrogradely for degradation (Lin et al. 2017) or redistribution (Mandal et al. 2021).

In conclusion hitherto findings suggest, that in the mitochondrial life-cycle the organelles do not have to obligatorily return to the soma. Retrograde mitochondrial transport is critical for the mitochondrial maintenance and homeostasis in motoneurons (Mandal et al. 2021), but it is likely not

only a disposal mechanism for organelle removal and degradation. Presumably the mitochondrial population in retrograde transport is not uniform and organelles are transported towards the soma for different reasons and destinations. The approach, to count mitochondria as they come and go, might be too simple to give consideration to the complexity of mitochondrial trafficking. Further studies are needed to understand the closely intertwined ensemble of mitochondrial movement, biogenesis, fusion/fission and degradation.

5.4 Further possible applications

Alterations in mitochondrial transport have been shown to be important pathological events in numerous neurological disorders, like amyotrophic lateral sclerosis, Parkinson's or Alzheimer's' Disease (De Vos et al. 2008, Millecamps and Julien 2013, Mandal and Drerup 2019). Transgenic mouse lines with the expression of photo-transformable proteins in neuronal mitochondria are a valuable tool to study not only the physiological delivery of organelles but also possible alterations of transport in models of neurodegenerative diseases. To this end especially "multiparametric analyses", combining the observation of mitochondrial transport and functional state (Breckwoldt et al. 2014), are promising: the transgenic or viral expression of a variety of functional sensors, like pH-, ROS- or Ca^{2+}-sensors (Gökerküçük et al. 2020) can be combined with the expression of photo-transformable proteins to simultaneously investigate movement and the bioenergetic status of single organelles or mitochondrial subpopulations.

In addition the mouse lines facilitate diverse possibilities considering microscopy techniques (widefield-, confocal-, and to some extent two-photon microscopy) and different preparations: this study has only used the acute nerve-muscle explant, but also in vivo imaging of peripheral (Misgeld et al. 2007) or central motoneurons (Kerschensteiner et al. 2005, Nikić et al. 2011) could be promising. The combination of these powerful tools will hopefully contribute to further understand and decipher the complexity of neuronal mitochondrial transport in sickness and health.

6 List of Abbreviations

ALS	amyotrophic lateral sclerosis
ATP	adenosine triphosphate
bp	base pair
Ca^{2+}	Calcium ions
CFP	cyan fluorescent protein
cm	centimeter
CNS	central nervous system
DCV	dense core vesicles
DNA	deoxyribonucleic acid
GFP	green fluorescent protein
h	hour
m	meter
ml	milliliter
min	minute
mtDNA	mitochondrial DNA
n	sample size
nm	nanometer
NMJ	neuromuscular junction
PBS	phosphate buffered saline
PFA	paraformaldehyde
RNA	ribonucleic acid
ROS	reactive oxygen species
sec	second
µl	microliter
µm	micrometer
UV	ultra violet
W	Watt

7 Index of Figures and Tables

8 Publications

Breckwoldt, M.O.; Pfister, F.M.J.; Bradley, P.M.; Marinković, P.; Williams, P.R.; Brill, M.S.; Plomer, B.; Schmalz, A.; St Clair, D.K.; Naumann, R.; Griesbeck, O.; Schwarzländer, M.; Godinho, L.; Bareyre, F.M.; Dick, T.P.; Kerschensteiner, M.; Misgeld, T. 2014. **Multiparametric optical analysis of mitochondrial redox signals during neuronal physiology and pathology in vivo**. *Nature Medicine* 20: 555–560.

Paper in preparation:

Marahori N.A. Gailer B., Iatroudi A., Kleele T., Schifferer M., Avramopoulos P., Stefan Engelhardt S., Lakadamyali M.,Brill M.S., Misgeld T. **An optineurin-dependent retrograde transit filter in distal axons mediates mitochondrial quality control in synapses**

9 Acknowledgments

To begin with, I would like to express my gratitude to my supervisor Prof. Thomas Misgeld. Thank you for your support and inspiring enthusiasm for science – the time in your lab has been a significant step in my personal and professional development. In addition I want to thank Monika Leischner-Brill for your outstanding supervision, all the encouragement and the patient proofreading of this work.

Thanks to all my colleagues in the lab for scientific support, interesting talks as well as a lot of fun during and beyond work: Bogdan, Cathy, Gabi, Grace, Laura, Leanne, Marina, Michael, Moni, Natalia, Petar, Peter and Phil. Special thanks to Tatjana Kleele for your friendship and the continuous encouragement on this long journey.

Further I would like to express my gratitude to the exceptional technical staff at the Institute of Neuronal Cell Biology, in particular Manuela Budak, Nebahat Budak, Yvonne Hufnagel, Monika Schetterer, Kristina Wullimann and Sarah Bechtold.

This work would not have been completed without the continuous support of my wonderful family and friends – thank you! Special thanks go to my sister Theresa for proofreading the thesis and polishing up my English. I am deeply grateful to my husband Stefan – for technical support, encouragement during the final phase and for all your love.

Finally I would like to dedicate this work to my parents, Eva and Alois. I am deeply grateful for your support, patience and unconditional love!

10 References

Allen, G.J.; Kwak, J.M.; Chu, S.P.; Llopis, J.; Tsien, R.Y.; Harper, J.F.; Schroeder, J.I.: Cameleon calcium indicator reports cytoplasmic calcium dynamics in Arabidopsis guard cells. The Plant Journal: For Cell and Molecular Biology 1999; 19: 735–747.

Amiri, M.; Hollenbeck, P.J.: Mitochondrial biogenesis in the axons of vertebrate peripheral neurons. Developmental Neurobiology 2008; 68: 1348–1361.

Ando, R.; Hama, H.; Yamamoto-Hino, M.; Mizuno, H.; Miyawaki, A.: An optical marker based on the UV-induced green-to-red photoconversion of a fluorescent protein. Proceedings of the National Academy of Sciences of the United States of America 2002; 99: 12651–12656.

Aschrafi, A.; Kar, A.N.; Gale, J.R.; Elkahloun, A.G.; Vargas, J.N.S.; Sales, N.; Wilson, G.; Tompkins, M.; Gioio, A.E.; Kaplan, B.B:. A heterogeneous population of nuclear-encoded mitochondrial mRNAs is present in the axons of primary sympathetic neurons. Mitochondrion 2016; 30: 18–23.

Ashrafi, G.; Schwarz, T.L.: The pathways of mitophagy for quality control and clearance of mitochondria. Cell Death and Differentiation 2013; 20: 31–42.

Ashrafi, G.; Schlehe, J.S.; LaVoie, M.J.; Schwarz, T.L.: Mitophagy of damaged mitochondria occurs locally in distal neuronal axons and requires PINK1 and Parkin. The Journal of Cell Biology 2014; 206: 655–670.

Attwell, D.; Laughlin, S.B.: An energy budget for signaling in the grey matter of the brain. Journal of Cerebral Blood Flow and Metabolism: Official Journal of the International Society of Cerebral Blood Flow and Metabolism 2001; 21: 1133–1145.

Baas, P.W.; Deitch, J.S.; Black, M.M.; Banker, G.A.: Polarity orientation of microtubules in hippocampal neurons: uniformity in the axon and nonuniformity in the dendrite. Proceedings of the National Academy of Sciences of the United States of America 1988; 85: 8335–8339.

Bilsland, L.G.; Sahai, E.; Kelly, G.; Golding, M.; Greensmith, L.; Schiavo, G.: Deficits in axonal transport precede ALS symptoms in vivo. Proceedings of the National Academy of Sciences of the United States of America 2010; 107: 20523–20528.

Bishop, D.; Nikić, I.; Brinkoetter, M.; Knecht, S.; Potz, S.; Kerschensteiner, M.; Misgeld, T.: Near-infrared branding efficiently correlates light and electron microscopy. Nature Methods 2011; 8: 568–570.

Bishop, D.L.; Misgeld, T.; Walsh, M.K.; Gan, W.-B.; Lichtman, J.W.: Axon branch removal at developing synapses by axosome shedding. Neuron 2004; 44: 651–661.

Bolea, I.; Gan, W.-B.; Manfedi, G.; Magrané, J.: Imaging of mitochondrial dynamics in motor and sensory axons of living mice. Methods in Enzymology 2014; 547: 97–110.

Breckwoldt, M.O.; Pfister, F.M.J.; Bradley, P.M.; Marinković, P.; Williams, P.R.; Brill, M.S.; Plomer, B.; Schmalz, A.; St Clair, D.K.; Naumann, R.; Griesbeck, O.; Schwarzländer, M.; Godinho, L.; Bareyre, F.M.; Dick, T.P.; Kerschensteiner, M.; Misgeld, T.: Multiparametric optical analysis of mitochondrial redox signals during neuronal physiology and pathology in vivo. Nature Medicine 2014; 20: 555–560.

Brickley, K.; Stephenson, F.A.: Trafficking kinesin protein (TRAK)-mediated transport of mitochondria in axons of hippocampal neurons. The Journal of Biological Chemistry 2011; 286: 18079–18092.

Bridgman, P.C.: Myosin-dependent transport in neurons. Journal of Neurobiology 2004; 58: 164–174.

Brill, M.S.; Marinković, P.; Misgeld, T.: Sequential photo-bleaching to delineate single Schwann cells at the neuromuscular junction. Journal of Visualized Experiments: JoVE 2013; e4460.

Brill, M.S.; Kleele, T.; Ruschkies, L.; Wang, M.; Marahori, N.A.; Reuter, M.S.; Hausrat, T.J.; Weigand, E.; Fisher, M.; Ahles, A.; Engelhardt, S.; Bishop, D.L.; Kneussel, M.; Misgeld, T.: Branch-Specific Microtubule Destabilization Mediates Axon Branch Loss during Neuromuscular Synapse Elimination. Neuron 2016; 92: 845–856.

Burman, J.L.; Pickles, S.; Wang, C.; Sekine, S.; Vargas, J.N.S.; Zhang, Z.; Youle, A.M.; Nezich, C.L.; Wu, X.; Hammer, J.A.; Youle, R.J.: Mitochondrial fission facilitates the selective mitophagy of protein aggregates. The Journal of Cell Biology 2017; 216: 3231–3247.

Burton, P.R.; Paige, J.L.: Polarity of axoplasmic microtubules in the olfactory nerve of the frog. Proceedings of the National Academy of Sciences of the United States of America 1981; 78: 3269–3273.

Busch, K.B.; Bereiter-Hahn, J.; Wittig, I.; Schagger, H.; Jendrach, M.: Mitochondrial dynamics generate equal distribution but patchwork localization of respiratory Complex I. Molecular Membrane Biology 2006; 23: 509–520.

Cai, Q.; Zakaria, H.M.; Simone, A.; Sheng, Z.-H.: Spatial parkin translocation and degradation of damaged mitochondria via mitophagy in live cortical neurons. Current biology 2012; CB 22: 545–552.

Caroni, P.: Overexpression of growth-associated proteins in the neurons of adult transgenic mice. Journal of Neuroscience Methods 1997; 71: 3–9.

Chacinska, A.; Koehler, C.M.; Milenkovic, D.; Lithgow, T.; Pfanner, N.: Importing mitochondrial proteins: machineries and mechanisms. Cell 2009; 138: 628–644.

Chada, S.R.; Hollenbeck, P.J.: Nerve growth factor signaling regulates motility and docking of axonal mitochondria. Current biology 2004; CB 14: 1272–1276.

Chalfie, M.; Tu, Y.; Euskirchen, G.; Ward, W.W.; Prasher, D.C.: Green fluorescent protein as a marker for gene expression. Science (New York, N.Y.) 1994; 263: 802–805.

Chen, H.; Chomyn, A.; Chan, D.C.: Disruption of fusion results in mitochondrial heterogeneity and dysfunction. The Journal of Biological Chemistry 2005; 280: 26185–26192.

Chen, H.; Detmer, S.A.; Ewald, A.J.; Griffin, E.E.; Fraser, S.E.; Chan, D.C.: Mitofusins Mfn1 and Mfn2 coordinately regulate mitochondrial fusion and are essential for embryonic development. The Journal of Cell Biology 2003; 160: 189–200.

Chen, Y.; Sheng, Z.-H.: Kinesin-1-syntaphilin coupling mediates activity-dependent regulation of axonal mitochondrial transport. The Journal of Cell Biology 2013; 202: 351–364.

Chtanova, T.; Hampton, H.R.; Waterhouse, L.A.; Wood, K.; Tomura, M.; Miwa, Y.; Mackay, C.R.; Brink, R.; Phan, T.G.: Real-time interactive two-photon photoconversion of recirculating lymphocytes for discontinuous cell tracking in live adult mice. Journal of Biophotonics 2014; 7: 425–433.

Chudakov, D.M.; Lukyanov, S.; Lukyanov, K.A.: Fluorescent proteins as a toolkit for in vivo imaging. Trends in Biotechnology 2005; 23: 605–613.

Cioni, J.-M.; Lin, J.Q.; Holtermann, A.V.; Koppers, M.; Jakobs, M.A.H.; Azizi, A.; Turner-Bridger, B.; Shigeoka, T.; Franze, K.; Harris, W.A.; Holt, C.E.: Late Endosomes Act as mRNA Translation Platforms and Sustain Mitochondria in Axons. Cell 2019; 176: 56-72.e15.

Cipolat, S.; Martins de Brito, O.; Dal Zilio, B.; Scorrano, L.: OPA1 requires mitofusin 1 to promote mitochondrial fusion. Proceedings of the National Academy of Sciences of the United States of America 2004; 101: 15927–15932.

Clanton, J.A.; Shestopalov, I.; Chen, J.K.; Gamse, J.T.: Lineage labeling of zebrafish cells with laser uncagable fluorescein dextran. Journal of Visualized Experiments; JoVE 2014.

Clayton, D.A.: Mitochondrial DNA replication: what we know. IUBMB life 2003; 55: 213–217.

Conde, C.; Cáceres, A.: Microtubule assembly, organization and dynamics in axons and dendrites. Nature Reviews. Neuroscience 2009; 10: 319–332.

Cooper, P.D.; Smith, R.S.: The movement of optically detectable organelles in myelinated axons of Xenopus laevis. The Journal of Physiology 1974; 242: 77–97.

Culver-Hanlon, T.L.; Lex, S.A.; Stephens, A.D.; Quintyne, N.J.; King, S.J.: A microtubule-binding domain in dynactin increases dynein processivity by skating along microtubules. Nature Cell Biology 2006; 8: 264–270.

Dal Maschio, M.; Donovan, J.C.; Helmbrecht, T.O.; Baier, H.: Linking Neurons to Network Function and Behavior by Two-Photon Holographic Optogenetics and Volumetric Imaging. Neuron 2017; 94: 774-789.e5.

Davis, A.F.; Clayton, D.A.: In situ localization of mitochondrial DNA replication in intact mammalian cells. The Journal of Cell Biology 1996; 135: 883–893.

Day, R.N.; Davidson, M.W.: The fluorescent protein palette: tools for cellular imaging. Chemical Society Reviews 2009; 38: 2887–2921.

De Vos, K.J.; Grierson, A.J.; Ackerley, S.; Miller, C.C.J.: Role of axonal transport in neurodegenerative diseases. Annual Review of Neuroscience 2008; 31: 151–173.

Desai, A.; Mitchison, T.J.: Microtubule polymerization dynamics. Annual Review of Cell and Developmental Biology 1997; 13: 83–117.

Dooley, C.T.; Dore, T.M.; Hanson, G.T.; Jackson, W.C.; Remington, S.J.; Tsien, R.Y.: Imaging dynamic redox changes in mammalian cells with green fluorescent protein indicators. The Journal of Biological Chemistry 2004; 279: 22284–22293.

Droz, B.; Leblond, C.P.: Migration of proteins along the axons of the sciatic nerve. Science (New York, N.Y.) 1962; 137: 1047–1048.

Edelstein, A.; Amodaj, N.; Hoover, K.; Vale, R.; Stuurman, N.: Computer control of microscopes using μManager. Current Protocols in Molecular Biology 2010; Chapter 14: Unit14.20.

Evans, C.S.; Holzbaur, E.L.F.: Quality Control in Neurons: Mitophagy and Other Selective Autophagy Mechanisms. Journal of Molecular Biology 2020; 432: 240–260.

Feng, G.; Mellor, R.H.; Bernstein, M.; Keller-Peck, C.; Nguyen, Q.T.; Wallace, M.; Nerbonne, J.M.; Lichtman, J.W.; Sanes, J.R.: Imaging neuronal subsets in transgenic mice expressing multiple spectral variants of GFP. Neuron 2000; 28: 41–51.

Forman, D.S.; Lynch, K.J.; Smith, R.S.: Organelle dynamics in lobster axons: anterograde, retrograde and stationary mitochondria. Brain Research 1987; 412: 96–106.

Fransson, S.; Ruusala, A.; Aspenström, P.: The atypical Rho GTPases Miro-1 and Miro-2 have essential roles in mitochondrial trafficking. Biochemical and Biophysical Research Communications 2006; 344: 500–510.

Gill, S.R.; Schroer, T.A.; Szilak, I.; Steuer, E.R.; Sheetz, M.P.; Cleveland, D.W.: Dynactin, a conserved, ubiquitously expressed component of an activator of vesicle motility mediated by cytoplasmic dynein. The Journal of Cell Biology 1991; 115: 1639–1650.

Gilley, J.; Seereeram, A.; Ando, K.; Mosely, S.; Andrews, S.; Kerschensteiner, M.; Misgeld, T.; Brion, J.-P.; Anderton, B.; Hanger, D.P.; Coleman, M.P.: Age-dependent axonal transport and locomotor changes and tau hypophosphorylation in a “P301L” tau knockin mouse. Neurobiology of Aging 2012; 33: 621.e1-621.e15.

Gioio, A.E.; Eyman, M.; Zhang, H.; Lavina, Z.S.; Giuditta, A.; Kaplan, B.B.: Local synthesis of nuclear-encoded mitochondrial proteins in the presynaptic nerve terminal. Journal of Neuroscience Research 2001; 64: 447–453.

Glater, E.E.; Megeath, L.J.; Stowers, R.S.; Schwarz, T.L.: Axonal transport of mitochondria requires milton to recruit kinesin heavy chain and is light chain independent. The Journal of Cell Biology 2006; 173: 545–557.

Gökerküçük, E.B.; Tramier, M.; Bertolin, G.: Imaging Mitochondrial Functions: from Fluorescent Dyes to Genetically-Encoded Sensors. Genes 2020; 11.

Grafstein, B.; Forman, D.S.: Intracellular transport in neurons. Physiological Reviews 1980; 60: 1167–1283.

Greene, J.C.; Whitworth, A.J.; Kuo, I.; Andrews, L.A.; Feany, M.B.; Pallanck, L.J.: Mitochondrial pathology and apoptotic muscle degeneration in Drosophila parkin mutants. Proceedings of the National Academy of Sciences of the United States of America 2003; 100: 4078–4083.

Gross, S.P.; Tuma, M.C.; Deacon, S.W.; Serpinskaya, A.S.; Reilein, A.R.; Gelfand, V.I.: Interactions and regulation of molecular motors in Xenopus melanophores. The Journal of Cell Biology 2002; 156: 855–865.

Guo, X.; Macleod, G.T.; Wellington, A.; Hu, F.; Panchumarthi, S.; Schoenfield, M.; Marin, L.; Charlton, M.P.; Atwood, H.L.; Zinsmaier, K.E.: The GTPase dMiro is required for axonal transport of mitochondria to Drosophila synapses. Neuron 2005; 47: 379–393.

Gurskaya, N.G.; Verkhusha, V.V.; Shcheglov, A.S.; Staroverov, D.B.; Chepurnykh, T.V.; Fradkov, A.F.; Lukyanov, S.; Lukyanov, K.A.: Engineering of a monomeric green-to-red photoactivatable fluorescent protein induced by blue light. Nature Biotechnology 2006; 24: 461–465.

Gutnick, A.; Banghart, M.R.; West, E.R.; Schwarz, T.L.: The light-sensitive dimerizer zapalog reveals distinct modes of immobilization for axonal mitochondria. Nature Cell Biology 2019; 21: 768–777.

Han, S.M.; Baig, H.S.; Hammarlund, M.: Mitochondria Localize to Injured Axons to Support Regeneration. Neuron 2016; 92: 1308–1323.

Hanson, G.T.; Aggeler, R.; Oglesbee, D.; Cannon, M.; Capaldi, R.A.; Tsien, R.Y.; Remington, S.J.: Investigating mitochondrial redox potential with redox-sensitive green fluorescent protein indicators. The Journal of Biological Chemistry 2004; 279: 13044–13053.

Hara, T.; Nakamura, K.; Matsui, M.; Yamamoto, A.; Nakahara, Y.; Suzuki-Migishima, R.; Yokoyama, M.; Mishima, K.; Saito, I.; Okano, H.; Mizushima, N.: Suppression of basal autophagy in neural cells causes neurodegenerative disease in mice. Nature 2006; 441: 885–889.

Harbauer, A.B.; Zahedi, R.P.; Sickmann, A.; Pfanner, N.; Meisinger, C.: The protein import machinery of mitochondria-a regulatory hub in metabolism, stress, and disease. Cell Metabolism 2014; 19: 357–372.

Harris, J.J.; Jolivet, R.; Attwell, D.: Synaptic energy use and supply. Neuron 2012; 75: 762–777.

Helmchen, F.; Denk, W.: Deep tissue two-photon microscopy. Nature Methods 2005; 2: 932–940.

Hirokawa, N.; Pfister, K.K.; Yorifuji, H.; Wagner, M.C.; Brady, S.T.; Bloom, G.S.: Submolecular domains of bovine brain kinesin identified by electron microscopy and monoclonal antibody decoration. Cell 1989; 56: 867–878.

Hirokawa, N.; Sato-Yoshitake, R.; Kobayashi, N.; Pfister, K.K.; Bloom, G.S.; Brady, S.T.: Kinesin associates with anterogradely transported membranous organelles in vivo. The Journal of Cell Biology 1991; 114: 295–302.

Hollenbeck, P.J.: The pattern and mechanism of mitochondrial transport in axons. Frontiers in Bioscience: A Journal and Virtual Library 1996; 1: d91-102.

Howarth, C.; Gleeson, P.; Attwell, D.: Updated energy budgets for neural computation in the neocortex and cerebellum. Journal of Cerebral Blood Flow and Metabolism: Official Journal of the International Society of Cerebral Blood Flow and Metabolism 2012; 32: 1222–1232.

Hurd, D.D.; Saxton, W.M.: Kinesin mutations cause motor neuron disease phenotypes by disrupting fast axonal transport in Drosophila. Genetics 1996; 144: 1075–1085.

Jin, S.M.; Lazarou, M.; Wang, C.; Kane, L.A.; Narendra, D.P.; Youle, R.J.: Mitochondrial membrane potential regulates PINK1 import and proteolytic destabilization by PARL. The Journal of Cell Biology 2010; 191: 933–942.

Kang, J.-S.; Tian, J.-H.; Pan, P.-Y.; Zald, P.; Li, C.; Deng, C.; Sheng, Z.-H.: Docking of axonal mitochondria by syntaphilin controls their mobility and affects short-term facilitation. Cell 2008; 132: 137–148.

Karki, S.; Holzbaur, E.L.: Affinity chromatography demonstrates a direct binding between cytoplasmic dynein and the dynactin complex. The Journal of Biological Chemistry 1995; 270: 28806–28811.

Kerschensteiner, M.; Schwab, M.E.; Lichtman, J.W.; Misgeld, T.: In vivo imaging of axonal degeneration and regeneration in the injured spinal cord. Nature Medicine 2005; 11: 572–577.

Kerschensteiner, M.; Reuter, M.S.; Lichtman, J.W.; Misgeld, T.: Ex vivo imaging of motor axon dynamics in murine triangularis sterni explants. Nature Protocols 2008; 3: 1645–1653.

King, S.J.; Schroer, T.A.: Dynactin increases the processivity of the cytoplasmic dynein motor. Nature Cell Biology 2000; 2: 20–24.

Kissová, I.; Salin, B.; Schaeffer, J.; Bhatia, S.; Manon, S.; Camougrand, N.: Selective and non-selective autophagic degradation of mitochondria in yeast. Autophagy 2007; 3: 329–336.

Kitada, T.; Asakawa, S.; Hattori, N.; Matsumine, H.; Yamamura, Y.; Minoshima, S.; Yokochi, M.; Mizuno, Y.; Shimizu, N.: Mutations in the parkin gene cause autosomal recessive juvenile parkinsonism. Nature 1998; 392: 605–608.

Kleele, T.; Rey, T.; Winter, J.; Zaganelli, S.; Mahecic, D.; Perreten Lambert, H.; Ruberto, F.P.; Nemir, M.; Wai, T.; Pedrazzini, T.; Manley, S.: Distinct fission signatures predict mitochondrial degradation or biogenesis. Nature 2021; 593: 435–439.

Kleele, T.; Marinković, P.; Williams, P.R.; Stern, S.; Weigand, E.E.; Engerer, P.; Naumann, R.; Hartmann, J.; Karl, R.M.; Bradke, F.; Bishop, D.; Herms, J.; Konnerth, A.; Kerschensteiner, M.; Godinho, L.; Misgeld, T.: An assay to image neuronal microtubule dynamics in mice. Nature Communications 2014; 5: 4827.

Koenig, E.; Giuditta, A.: Protein-synthesizing machinery in the axon compartment. Neuroscience 1999; 89: 5–15.

Komatsu, M.; Waguri, S.; Ueno, T.; Iwata, J.; Murata, S.; Tanida, I.; Ezaki, J.; Mizushima, N.; Ohsumi, Y.; Uchiyama, Y.; Kominami, E.; Tanaka, K.; Chiba, T.: Impairment of starvation-induced and constitutive autophagy in Atg7-deficient mice. The Journal of Cell Biology 2005; 169: 425–434.

Koshiba, T.; Detmer, S.A.; Kaiser, J.T.; Chen, H.; McCaffery, J.M.; Chan, D.C.: Structural basis of mitochondrial tethering by mitofusin complexes. Science (New York, N.Y.) 2004; 305: 858–862.

Kuma, A.; Hatano, M.; Matsui, M.; Yamamoto, A.; Nakaya, H.; Yoshimori, T.; Ohsumi, Y.; Tokuhisa, T.; Mizushima, N.: The role of autophagy during the early neonatal starvation period. Nature 2004; 432: 1032–1036.

LaMonte, B.H.; Wallace, K.E.; Holloway, B.A.; Shelly, S.S.; Ascaño, J.; Tokito, M.; Van Winkle, T.; Howland, D.S.; Holzbaur, E.L.F.: Disruption of dynein/dynactin inhibits axonal transport in motor neurons causing late-onset progressive degeneration. Neuron 2002; 34: 715–727.

Langer, T.; Käser, M.; Klanner, C.; Leonhard, K.: AAA proteases of mitochondria: quality control of membrane proteins and regulatory functions during mitochondrial biogenesis. Biochemical Society Transactions 2001; 29: 431–436.

Levine, B.; Klionsky, D.J.:Development by self-digestion: molecular mechanisms and biological functions of autophagy. Developmental Cell 2004; 6: 463–477.

Levytskyy, R.M.; Germany, E.M.; Khalimonchuk, O.: Mitochondrial Quality Control Proteases in Neuronal Welfare. Journal of Neuroimmune Pharmacology: The Official Journal of the Society on NeuroImmune Pharmacology 2016; 11: 629–644.

Lin, M.-Y.; Cheng, X.-T.; Tammineni, P.; Xie, Y.; Zhou, B.; Cai, Q.; Sheng, Z.-H.: Releasing Syntaphilin Removes Stressed Mitochondria from Axons Independent of Mitophagy under Pathophysiological Conditions. Neuron 2017; 94: 595-610.e6.

Liu, X.; Weaver, D.; Shirihai, O.; Hajnóczky, G.: Mitochondrial "kiss-and-run": interplay between mitochondrial motility and fusion-fission dynamics. The EMBO journal 2009; 28: 3074–3089.

López-Doménech, G.; Covill-Cooke, C.; Ivankovic, D.; Halff, E.F.; Sheehan, D.F.; Norkett, R.; Birsa, N.; Kittler, J.T.: Miro proteins coordinate microtubule- and actin-dependent mitochondrial transport and distribution. The EMBO journal 2018; 37: 321–336.

Lukyanov, K.A.; Chudakov, D.M.; Lukyanov, S.; Verkhusha, V.V.: Innovation: Photoactivatable fluorescent proteins. Nature Reviews. Molecular Cell Biology 2005; 6: 885–891.

MacAskill, A.F.; Brickley, K.; Stephenson, F.A.; Kittler, J.T.: GTPase dependent recruitment of Grif-1 by Miro1 regulates mitochondrial trafficking in hippocampal neurons. Molecular and Cellular Neurosciences 2009; 40: 301–312.

Maday, S.; Holzbaur, E.L.F.: Autophagosome biogenesis in primary neurons follows an ordered and spatially regulated pathway. Developmental Cell 2014; 30: 71–85.

Maday, S.; Twelvetrees, A.E.; Moughamian, A.J.; Holzbaur, E.L.F.: Axonal transport: cargo-specific mechanisms of motility and regulation. Neuron 2014; 84: 292–309.

Magrané, J.; Cortez, C.; Gan, W.-B.; Manfredi, G.: Abnormal mitochondrial transport and morphology are common pathological denominators in SOD1 and TDP43 ALS mouse models. Human Molecular Genetics 2014; 23: 1413–1424.

Magrané, J.; Sahawneh, M.A.; Przedborski, S.; Estévez, Á.G.; Manfredi, G.: Mitochondrial dynamics and bioenergetic dysfunction is associated with synaptic alterations in mutant SOD1 motor neurons. The Journal of Neuroscience: The Official Journal of the Society for Neuroscience 2012; 32: 229–242.

Mandal, A.; Drerup, C.M.: Axonal Transport and Mitochondrial Function in Neurons. Frontiers in Cellular Neuroscience 2019; 13: 373.

Mandal, A.; Wong, H.-T.C.; Pinter, K.; Mosqueda, N.; Beirl, A.; Lomash, R.M.; Won, S.; Kindt, K.S.; Drerup, C.M.: Retrograde Mitochondrial Transport Is Essential for Organelle Distribution and Health in Zebrafish Neurons. The Journal of Neuroscience: The Official Journal of the Society for Neuroscience 2021; 41: 1371–1392.

Marinković, P.; Godinho, L.; Misgeld, T.: Generation and Screening of Transgenic Mice with Neuronal Labeling Controlled by Thy1 Regulatory Elements. Cold Spring Harbor Protocols 2015a; 875–882.

Marinković, P.; Godinho, L.; Misgeld, T.: Imaging Acute Neuromuscular Explants from Thy1 Mouse Lines. Cold Spring Harbor Protocols 2015b; pdb.prot087692.

Marinkovic, P.; Reuter, M.S.; Brill, M.S.; Godinho, L.; Kerschensteiner, M.; Misgeld, T.: Axonal transport deficits and degeneration can evolve independently in mouse models of amyotrophic lateral sclerosis. Proceedings of the National Academy of Sciences of the United States of America 2012; 109: 4296–4301.

Matsuda, N.; Sato, S.; Shiba, K.; Okatsu, K.; Saisho, K.; Gautier, C.A.; Sou, Y.-S.; Saiki, S.; Kawajiri, S.; Sato, F.; Kimura, M.; Komatsu, M.; Hattori, N.; Tanaka, K.: PINK1 stabilized by mitochondrial depolarization recruits Parkin to damaged mitochondria and activates latent Parkin for mitophagy. The Journal of Cell Biology 2010; 189: 211–221.

McArdle, J.J.; Angaut-Petit, D.; Mallart, A.; Bournaud, R.; Faille, L.; Brigant, J.L.: Advantages of the triangularis sterni muscle of the mouse for investigations of synaptic phenomena. Journal of Neuroscience Methods 1981; 4: 109–115.

Menzies, F.M.; Fleming, A.; Caricasole, A.; Bento, C.F.; Andrews, S.P.; Ashkenazi, A.; Füllgrabe, J.; Jackson, A.; Jimenez Sanchez, M.; Karabiyik, C.; Licitra, F.; Lopez Ramirez, A.; Pavel, M.; Puri, C.; Renna, M.; Ricketts, T.; Schlotawa, L.; Vicinanza, M.; Won, H.; Zhu, Y.; Skidmore, J.; Rubinsztein, D.C.: Autophagy and Neurodegeneration: Pathogenic Mechanisms and Therapeutic Opportunities. Neuron 2017; 93: 1015–1034.

Merzlyak, E.M.; Goedhart, J.; Shcherbo, D.; Bulina, M.E.; Shcheglov, A.S.; Fradkov, A.F.; Gaintzeva, A.; Lukyanov, K.A.; Lukyanov, S.; Gadella, T.W.J.; Chudakov, D.M.: Bright monomeric red fluorescent protein with an extended fluorescence lifetime. Nature Methods 2007; 4: 555–557.

Miani, N.: ANALYSIS OF THE SOMATO-AXONAL MOVEMENT OF PHOSPHOLIPIDS IN THE VAGUS AND HYPOGLOSSAL NERVES. Journal of Neurochemistry 1963; 10: 859–874.

Miesenböck, G.; De Angelis, D.A.; Rothman, J.E.: Visualizing secretion and synaptic transmission with pH-sensitive green fluorescent proteins. Nature 1998; 394: 192–195.

Millecamps, S.; Julien, J.-P.: Axonal transport deficits and neurodegenerative diseases. Nature Reviews. Neuroscience 2013; 14: 161–176.

Miller, K.E.; Sheetz, M.P.: Axonal mitochondrial transport and potential are correlated. Journal of Cell Science 2004; 117: 2791–2804.

Misgeld, T.; Schwarz, T.L.: Mitostasis in Neurons: Maintaining Mitochondria in an Extended Cellular Architecture. Neuron 2017; 96: 651–666.

Misgeld, T.; Kerschensteiner, M.; Bareyre, F.M.; Burgess, R.W.; Lichtman, J.W.: Imaging axonal transport of mitochondria in vivo. Nature Methods 2007; 4: 559–561.

Morris, R.L.; Hollenbeck, P.J.: The regulation of bidirectional mitochondrial transport is coordinated with axonal outgrowth. Journal of Cell Science 1993; 104 (Pt 3): 917–927.

Morris, R.L.; Hollenbeck, P.J.: Axonal transport of mitochondria along microtubules and F-actin in living vertebrate neurons. The Journal of Cell Biology 1995; 131: 1315–1326.

Moughamian, A.J.; Holzbaur, E.L.F.: Dynactin is required for transport initiation from the distal axon. Neuron 2012a; 74: 331–343.

Moughamian, A.J.; Holzbaur, E.L.F.: Synaptic vesicle distribution by conveyor belt. Cell 2012b; 148: 849–851.

Mukherjee, K.; Clark, H.R.; Chavan, V.; Benson, E.K.; Kidd, G.J.; Srivastava, S.: Analysis of Brain Mitochondria Using Serial Block-Face Scanning Electron Microscopy. Journal of Visualized Experiments: JoVE 2016.

Narendra, D.; Tanaka, A.; Suen, D.-F.; Youle, R.J.: Parkin is recruited selectively to impaired mitochondria and promotes their autophagy. The Journal of Cell Biology 2008; 183: 795–803.

Narendra, D.P.; Jin, S.M.; Tanaka, A.; Suen, D.-F.; Gautier, C.A.; Shen, J.; Cookson, M.R.; Youle, R.J.: PINK1 is selectively stabilized on impaired mitochondria to activate Parkin. PLoS biology 2010; 8: e1000298.

Neuspiel, M.; Schauss, A.C.; Braschi, E.; Zunino, R.; Rippstein, P.; Rachubinski, R.A.; Andrade-Navarro, M.A.; McBride, H.M.: Cargo-selected transport from the mitochondria to peroxisomes is mediated by vesicular carriers. Current biology 2008; CB 18: 102–108.

Nguyen, T.N.; Padman, B.S.; Lazarou, M.: Deciphering the Molecular Signals of PINK1/Parkin Mitophagy. Trends in Cell Biology 2016; 26: 733–744.

Nicholls, D.G.; Budd, S.L.: Mitochondria and neuronal survival. Physiological Reviews 2000; 80: 315–360.

Nikić, I.; Merkler, D.; Sorbara, C.; Brinkoetter, M.; Kreutzfeldt, M.; Bareyre, F.M.; Brück, W.; Bishop, D.; Misgeld, T.; Kerschensteiner, M.: A reversible form of axon damage in experimental autoimmune encephalomyelitis and multiple sclerosis. Nature Medicine 2011; 17: 495–499.

Nogales, E.: Structural insights into microtubule function. Annual Review of Biochemistry 2000; 69: 277–302.

Nunnari, J.; Suomalainen, A.: Mitochondria: in sickness and in health. Cell 2012; 148: 1145–1159.

Ochs, S.; Sabri, M.I.; Johnson, J.: Fast transport system of materials in mammalian nerve fibers. Science (New York, N.Y.) 1969; 163: 686–687.

Pagliarini, D.J.; Calvo, S.E.; Chang, B.; Sheth, S.A.; Vafai, S.B.; Ong, S.-E.; Walford, G.A.; Sugiana, C.; Boneh, A.; Chen, W.K.; Hill, D.E.; Vidal, M.; Evans, J.G.; Thorburn, D.R.; Carr, S.A.; Mootha, V.K.: A mitochondrial protein compendium elucidates complex I disease biology. Cell 2008; 134: 112–123.

Palmer, A.E.; Giacomello, M.; Kortemme, T.; Hires, S.A.; Lev-Ram, V.; Baker, D.; Tsien, R.Y.: Ca2+ indicators based on computationally redesigned calmodulin-peptide pairs. Chemistry & Biology 2006; 13: 521–530.

Park, J.; Lee, S.B.; Lee, S.; Kim, Y.; Song, S.; Kim, S.; Bae, E.; Kim, J.; Shong, M.; Kim, J.-M.; Chung, J.: Mitochondrial dysfunction in Drosophila PINK1 mutants is complemented by parkin. Nature 2006; 441: 1157–1161.

Pathak, D.; Sepp, K.J.; Hollenbeck, P.J.: Evidence that myosin activity opposes microtubule-based axonal transport of mitochondria. The Journal of Neuroscience: The Official Journal of the Society for Neuroscience 2010; 30: 8984–8992.

Patterson, G.H.; Lippincott-Schwartz, J.: A photoactivatable GFP for selective photolabeling of proteins and cells. Science (New York, N.Y.) 2002; 297: 1873–1877.

Perkins, G.A.; Frey, T.G.: Recent structural insight into mitochondria gained by microscopy. Micron (Oxford, England: 1993) 2000; 31: 97–111.

Pham, A.H.; McCaffery, J.M.; Chan, D.C.: Mouse lines with photo-activatable mitochondria to study mitochondrial dynamics. Genesis (New York, N.Y.: 2000) 2012; 50: 833–843.

Pilling, A.D.; Horiuchi, D.; Lively, C.M.; Saxton, W.M.: Kinesin-1 and Dynein are the primary motors for fast transport of mitochondria in Drosophila motor axons. Molecular Biology of the Cell 2006; 17: 2057–2068.

Plucińska, G.; Misgeld, T.: Imaging of neuronal mitochondria in situ. Current Opinion in Neurobiology 2016; 39: 152–163.

Plucińska, G.; Paquet, D.; Hruscha, A.; Godinho, L.; Haass, C.; Schmid, B.; Misgeld, T.: In vivo imaging of disease-related mitochondrial dynamics in a vertebrate model system. The Journal of Neuroscience: The Official Journal of the Society for Neuroscience 2012; 32: 16203–16212.

Poole, A.C.; Thomas, R.E.; Yu, S.; Vincow, E.S.; Pallanck, L.: The mitochondrial fusion-promoting factor mitofusin is a substrate of the PINK1/parkin pathway. PloS One 2010; 5: e10054.

Popov, V.; Medvedev, N.I.; Davies, H.A.; Stewart, M.G.: Mitochondria form a filamentous reticular network in hippocampal dendrites but are present as discrete bodies in axons: a three-dimensional ultrastructural study. The Journal of Comparative Neurology 2005; 492: 50–65.

Post, J.N.; Lidke, K.A.; Rieger, B.; Arndt-Jovin, D.J.: One- and two-photon photoactivation of a paGFP-fusion protein in live Drosophila embryos. FEBS letters 2005; 579: 325–330.

Praefcke, G.J.K.; McMahon, H.T.: The dynamin superfamily: universal membrane tubulation and fission molecules? Nature Reviews. Molecular Cell Biology 2004; 5: 133–147.

Rambold, A.S.; Kostelecky, B.; Elia, N.; Lippincott-Schwartz, J.: Tubular network formation protects mitochondria from autophagosomal degradation during nutrient starvation. Proceedings of the National Academy of Sciences of the United States of America 2011; 108: 10190–10195.

Rangaraju, V.; Calloway, N.; Ryan, T.A.: Activity-driven local ATP synthesis is required for synaptic function. Cell 2014; 156: 825–835.

Rintoul, G.L.; Filiano, A.J.; Brocard, J.B.; Kress, G.J.; Reynolds, I.J.: Glutamate decreases mitochondrial size and movement in primary forebrain neurons. The Journal of Neuroscience: The Official Journal of the Society for Neuroscience 2003; 23: 7881–7888.

Russo, G.J.; Louie, K.; Wellington, A.; Macleod, G.T.; Hu, F.; Panchumarthi, S.; Zinsmaier, K.E.: Drosophila Miro is required for both anterograde and retrograde axonal mitochondrial transport. The Journal of Neuroscience: The Official Journal of the Society for Neuroscience 2009; 29: 5443–5455.

Saotome, M.; Safiulina, D.; Szabadkai, G.; Das, S.; Fransson, A.; Aspenstrom, P.; Rizzuto, R.; Hajnóczky, G.: Bidirectional Ca2+-dependent control of mitochondrial dynamics by the

Miro GTPase. Proceedings of the National Academy of Sciences of the United States of America 2008; 105: 20728–20733.

Schindelin, J.; Arganda-Carreras, I.; Frise, E.; Kaynig, V.; Longair, M.; Pietzsch, T.; Preibisch, S.; Rueden, C.; Saalfeld, S.; Schmid, B.; Tinevez, J.-Y.; White, D.J.; Hartenstein, V.; Eliceiri, K.; Tomancak, P.; Cardona, A.: Fiji: an open-source platform for biological-image analysis. Nature Methods 2012; 9: 676–682.

Schnapp, B.J.; Reese, T.S.: Dynein is the motor for retrograde axonal transport of organelles. Proceedings of the National Academy of Sciences of the United States of America 1989; 86: 1548–1552.

Schnapp, B.J.; Vale, R.D.; Sheetz, M.P.; Reese, T.S.: Microtubules and the mechanism of directed organelle movement. Annals of the New York Academy of Sciences 1986; 466: 909–918.

Schneider, M.; Barozzi, S.; Testa, I.; Faretta, M.; Diaspro, A.: Two-photon activation and excitation properties of PA-GFP in the 720-920-nm region. Biophysical Journal 2005; 89: 1346–1352.

Schwarz, T.L.: Mitochondrial trafficking in neurons. Cold Spring Harbor Perspectives in Biology 2013; 5.

Shaner, N.C.; Campbell, R.E.; Steinbach, P.A.; Giepmans, B.N.G.; Palmer, A.E.; Tsien, R.Y.: Improved monomeric red, orange and yellow fluorescent proteins derived from Discosoma sp. red fluorescent protein. Nature Biotechnology 2004; 22: 1567–1572.

Sheng, Z.-H.; Cai, Q.: Mitochondrial transport in neurons: impact on synaptic homeostasis and neurodegeneration. Nature Reviews. Neuroscience 2012; 13: 77–93.

Shigeoka, T.; Jung, H.; Jung, J.; Turner-Bridger, B.; Ohk, J.; Lin, J.Q.; Amieux, P.S.; Holt, C.E.: Dynamic Axonal Translation in Developing and Mature Visual Circuits. Cell 2016; 166: 181–192.

Shim, S.-H.; Xia, C.; Zhong, G.; Babcock, H.P.; Vaughan, J.C.; Huang, B.; Wang, X.; Xu, C.; Bi, G.-Q.; Zhuang, X.: Super-resolution fluorescence imaging of organelles in live cells with photoswitchable membrane probes. Proceedings of the National Academy of Sciences of the United States of America 2012; 109: 13978–13983.

Shimomura, O.; Johnson, F.H.; Saiga, Y.: Extraction, purification and properties of aequorin, a bioluminescent protein from the luminous hydromedusan, Aequorea. Journal of Cellular and Comparative Physiology 1962; 59: 223–239.

Sigal, Y.M.; Zhou, R.; Zhuang, X.: Visualizing and discovering cellular structures with super-resolution microscopy. Science (New York, N.Y.) 2018; 361: 880–887.

Smirnova, E.; Griparic, L.; Shurland, D.L.; van der Bliek, A.M.: Dynamin-related protein Drp1 is required for mitochondrial division in mammalian cells. Molecular Biology of the Cell 2001; 12: 2245–2256.

Smith, A.W.; Smoligovets, A.A.; Groves, J.T.: Patterned two-photon photoactivation illuminates spatial reorganization in live cells. The Journal of Physical Chemistry 2011; A 115: 3867–3875.

Soubannier, V.; McLelland, G.-L.; Zunino, R.; Braschi, E.; Rippstein, P.; Fon, E.A.; McBride, H.M.: A vesicular transport pathway shuttles cargo from mitochondria to lysosomes. Current biology 2012; CB 22: 135–141.

Spillane, M.; Ketschek, A.; Merianda, T.T.; Twiss, J.L.; Gallo, G.: Mitochondria coordinate sites of axon branching through localized intra-axonal protein synthesis. Cell Reports 2013; 5: 1564–1575.

van Spronsen, M.; Mikhaylova, M.; Lipka, J.; Schlager, M.A.; van den Heuvel, D.J.; Kuijpers, M.; Wulf, P.S.; Keijzer, N.; Demmers, J.; Kapitein, L.C.; Jaarsma, D.; Gerritsen, H.C.; Akhmanova, A.; Hoogenraad, C.C.: TRAK/Milton motor-adaptor proteins steer mitochondrial trafficking to axons and dendrites. Neuron 2013; 77: 485–502.

Stark, D.A.; Kulesa, P.M.: An in vivo comparison of photoactivatable fluorescent proteins in an avian embryo model. Developmental Dynamics: An Official Publication of the American Association of Anatomists 2007; 236: 1583–1594.

Stepanova, T.; Slemmer, J.; Hoogenraad, C.C.; Lansbergen, G.; Dortland, B.; De Zeeuw, C.I.; Grosveld, F.; van Cappellen, G.; Akhmanova, A.; Galjart, N.: Visualization of microtubule growth in cultured neurons via the use of EB3-GFP (end-binding protein 3-green fluorescent protein). The Journal of Neuroscience: The Official Journal of the Society for Neuroscience 2003; 23: 2655–2664.

Stowers, R.S.; Megeath, L.J.; Górska-Andrzejak, J.; Meinertzhagen, I.A.; Schwarz, T.L.: Axonal transport of mitochondria to synapses depends on milton, a novel Drosophila protein. Neuron 2002; 36: 1063–1077.

Sun, F.; Zhu, C.; Dixit, R.; Cavalli, V.: Sunday Driver/JIP3 binds kinesin heavy chain directly and enhances its motility. The EMBO journal 2011; 30: 3416–3429.

Suzuki, R.; Hotta, K.; Oka, K.: Transitional correlation between inner-membrane potential and ATP levels of neuronal mitochondria. Scientific Reports 2018; 8: 2993.

Tanaka, Y.; Kanai, Y.; Okada, Y.; Nonaka, S.; Takeda, S.; Harada, A.; Hirokawa, N.: Targeted disruption of mouse conventional kinesin heavy chain, kif5B, results in abnormal perinuclear clustering of mitochondria. Cell 1998; 93: 1147–1158.

Tondera, D.; Grandemange, S.; Jourdain, A.; Karbowski, M.; Mattenberger, Y.; Herzig, S.; Da Cruz, S.; Clerc, P.; Raschke, I.; Merkwirth, C.; Ehses, S.; Krause, F.; Chan, D.C.; Alexander, C.; Bauer, C.; Youle, R.; Langer, T.; Martinou, J.-C.: SLP-2 is required for stress-induced mitochondrial hyperfusion. The EMBO journal 2009; 28: 1589–1600.

Twig, G.; Elorza, A.; Molina, A.J.A.; Mohamed, H.; Wikstrom, J.D.; Walzer, G.; Stiles, L.; Haigh, S.E.; Katz, S.; Las, G.; Alroy, J.; Wu, M.; Py, B.F.; Yuan, J.; Deeney, J.T.; Corkey, B.E.; Shirihai, O.S.: Fission and selective fusion govern mitochondrial segregation and elimination by autophagy. The EMBO journal 2008; 27: 433–446.

Vale, R.D.; Schnapp, B.J.; Reese, T.S.; Sheetz, M.P.: Organelle, bead, and microtubule translocations promoted by soluble factors from the squid giant axon. Cell 1985a; 40: 559–569.

Vale, R.D.; Schnapp, B.J.; Mitchison, T.; Steuer, E.; Reese, T.S.; Sheetz, M.P.: Different axoplasmic proteins generate movement in opposite directions along microtubules in vitro. Cell 1985b; 43: 623–632.

Valente, E.M.; Abou-Sleiman, P.M.; Caputo, V.; Muqit, M.M.K.; Harvey, K.; Gispert, S.; Ali, Z.; Del Turco, D.; Bentivoglio, A.R.; Healy, D.G.; Albanese, A.; Nussbaum, R.; González-Maldonado, R.; Deller, T.; Salvi, S.; Cortelli, P.; Gilks, W.P.; Latchman, D.S.; Harvey, R.J.; Dallapiccola, B.; Auburger, G.; Wood, N.W.: Hereditary early-onset Parkinson's disease caused by mutations in PINK1. Science (New York, N.Y.) 2004; 304: 1158–1160.

Vallee, R.B.; Williams, J.C.; Varma, D.; Barnhart, L.E.: Dynein: An ancient motor protein involved in multiple modes of transport. Journal of Neurobiology 2004; 58: 189–200.

Verburg, J.; Hollenbeck, P.J.: Mitochondrial membrane potential in axons increases with local nerve growth factor or semaphorin signaling. The Journal of Neuroscience: The Official Journal of the Society for Neuroscience 2008; 28: 8306–8315.

Verstreken, P.; Ly, C.V.; Venken, K.J.T.; Koh, T.-W.; Zhou, Y.; Bellen, H.J.: Synaptic mitochondria are critical for mobilization of reserve pool vesicles at Drosophila neuromuscular junctions. Neuron 2005; 47: 365–378.

Wang, L.; Jackson, W.C.; Steinbach, P.A.; Tsien, R.Y.: Evolution of new nonantibody proteins via iterative somatic hypermutation. Proceedings of the National Academy of Sciences of the United States of America 2004; 101: 16745–16749.

Wang, X.; Schwarz, T.L.: The mechanism of Ca2+ -dependent regulation of kinesin-mediated mitochondrial motility. Cell 2009; 136: 163–174.

Wang, X.; Winter, D.; Ashrafi, G.; Schlehe, J.; Wong, Y.L.; Selkoe, D.; Rice, S.; Steen, J.; LaVoie, M.J.; Schwarz, T.L.: PINK1 and Parkin target Miro for phosphorylation and degradation to arrest mitochondrial motility. Cell 2011; 147: 893–906.

Watanabe, W.; Shimada, T.; Matsunaga, S.; Kurihara, D.; Fukui, K.; Shin-Ichi Arimura, S.-I.; Tsutsumi, N.; Isobe, K.; Itoh, K.: Single-organelle tracking by two-photon conversion. Optics Express 2007; 15: 2490–2498.

Waterman-Storer, C.M.; Karki, S.; Holzbaur, E.L.: The p150Glued component of the dynactin complex binds to both microtubules and the actin-related protein centractin (Arp-1). Proceedings of the National Academy of Sciences of the United States of America 1995; 92: 1634–1638.

Weiss, P.; Hiscoe, H.B.: Experiments on the mechanism of nerve growth. The Journal of Experimental Zoology 1948; 107: 315–395.

Wong, M.Y.; Zhou, C.; Shakiryanova, D.; Lloyd, T.E.; Deitcher, D.L.; Levitan, E.S.: Neuropeptide delivery to synapses by long-range vesicle circulation and sporadic capture. Cell 2012; 148: 1029–1038.

Yi, M.; Weaver, D.; Hajnóczky, G.: Control of mitochondrial motility and distribution by the calcium signal: a homeostatic circuit. The Journal of Cell Biology 2004; 167: 661–672.

Youle, R.J.; van der Bliek, A.M.: Mitochondrial fission, fusion, and stress. Science (New York, N.Y.) 2012; 337: 1062–1065.

Zhang, J.; Campbell, R.E.; Ting, A.Y.; Tsien, R.Y.: Creating new fluorescent probes for cell biology. Nature Reviews. Molecular Cell Biology 2002; 3: 906–918.